December 2012

## Geotechnical Solutions for Soil Improvement, Rapid Embankment Construction, and Stabilization of the Pavement Working Platform

# Compaction "Roadeo" Field Demonstration: Roller-Integrated Compaction Monitoring and Subgrade Geosynthetic Reinforcement

SHRP 2 Renewal Project R02

**PROJECT REPORT**

CENTER FOR
CEER
EARTHWORKS ENGINEERING
RESEARCH

IOWA STATE UNIVERSITY
Institute for Transportation

## About the Center for Earthworks Engineering Research

The mission of the Center for Earthworks Engineering Research (CEER) at Iowa State University is to be the nation's premier institution for developing fundamental knowledge of earth mechanics, and creating innovative technologies, sensors, and systems to enable rapid, high quality, environmentally friendly, and economical construction of roadways, aviation runways, railroad embankments, dams, structural foundations, fortifications constructed from earth materials, and related geotechnical applications.

## Disclaimer Notice

The contents of this report reflect the views of the authors, who are responsible for the facts and the accuracy of the information presented herein. The opinions, findings and conclusions expressed in this publication are those of the authors and not necessarily those of the sponsors.

The sponsors assume no liability for the contents or use of the information contained in this document. This report does not constitute a standard, specification, or regulation.

The sponsors do not endorse products or manufacturers. Trademarks or manufacturers' names appear in this report only because they are considered essential to the objective of the document.

## Non-Discrimination Statement

Iowa State University does not discriminate on the basis of race, color, age, religion, national origin, sexual orientation, gender identity, genetic information, sex, marital status, disability, or status as a U.S. veteran. Inquiries can be directed to the Director of Equal Opportunity and Compliance, 3280 Beardshear Hall, (515) 294-7612.

**Technical Report Documentation Page**

| 1. Report No. | 2. Government Accession No. | 3. Recipient's Catalog No. | |
|---|---|---|---|
| **4. Title and Subtitle**<br>Geotechnical Solutions for Soil Improvement, Rapid Embankment Construction, and Stabilization of the Pavement Working Platform<br>**Compaction "Roadeo" Field Demonstration: Roller-Integrated Compaction Monitoring and Subgrade Geosynthetic Reinforcement** | | **5. Report Date**<br>December 2012<br>**6. Performing Organization Code** | |
| **7. Author(s)**<br>David White, Pavana Vennapusa, Jie Han, Barry Christopher, Heath Gieselman, Shiyun Wang, Wayne Rilko, Peter Becker, David Horhota, Sanat Pokharel, and Jitendra Thakur | | **8. Performing Organization Report No.** | |
| **9. Performing Organization Name and Address**<br>Center for Earthworks Engineering Research<br>Institute for Transportation<br>Iowa State University<br>2711 South Loop Drive, Suite 4600<br>Ames, IA 50010-8664 | | **10. Work Unit No. (TRAIS)**<br>**11. Contract or Grant No.** | |
| **12. Sponsoring Organization Name and Address**<br>SHRP 2<br>Transportation Research Board<br>500 Fifth Street, NW<br>Washington, DC 20001 | | **13. Type of Report and Period Covered**<br>Project Report<br>**14. Sponsoring Agency Code**<br>SHRP 2 Project R02 | |
| **15. Supplementary Notes**<br>Visit www.ceer.iastate.edu for color pdfs of this and other research reports. | | | |

**16. Abstract**

This field demonstration project was conducted on the SR9B construction project in Jacksonville, Florida from May 16 to May 19, 2011. A Caterpillar CS74 vibratory smooth drum self-propelled roller weighing about 34,000 pounds was used on the project. The machine was setup with a roller-integrated compaction monitoring (RICM) system. Four test beds (TBs) were constructed and tested using the on-site poorly-graded sand embankment fill (A-3 according to the AASHTO classification system).

TB1 involved constructing six test sections incorporating several different geosynthetic reinforcement materials: biaxial geogrid (BX), geogrid/nonwoven geotextile geocomposite (C30), polypropylene woven fabric (PPWF), and 100 mm or 150 mm geocell (GC) materials, and one control section. TB2 involved compacting a thick loose lift (about 1.2 m deep) in two sections—one with BX geogrid reinforcement and one without reinforcement. TBs 3 and 4 involved mapping project production areas using the RICM roller and selecting test locations based on the color-coded on-board computer display in the roller for in situ testing.

The main objectives of this demonstration project were as follows:

- Evaluate the use of RICM technology with on-board computer display for compacted fill quality control (QC) and quality assurance (QA) testing
- Evaluate compaction influence depth under the RICM roller
- Evaluate differences in engineering properties between different types of geosynthetic and geocell reinforced fill test sections along with unreinforced fill test section using different QC/QA testing methods
- Evaluate differences in the in-ground dynamic stresses under the roller between different test sections
- Provide hands-on experience with RICM technology and various QC/QA testing technologies, and various geosynthetic/geocell reinforcement products to researchers and practitioners

| 17. Key Words | 18. Distribution Statement | | |
|---|---|---|---|
| compacted fill—compaction monitoring—geocell reinforcement—geosynthetic reinforcement—in situ testing—reinforced fills—RICM evaluation | No restrictions. | | |
| **19. Security Classification (of this report)** | **20. Security Classification (of this page)** | **21. No. of Pages** | **22. Price** |
| Unclassified. | Unclassified. | 138 | NA |

**Form DOT F 1700.7 (8-72)** **Reproduction of completed page authorized**

**SHRP 2 PROJECT R02:**
**GEOTECHNICAL SOLUTIONS FOR SOIL IMPROVEMENT, RAPID EMBANKMENT CONSTRUCTION, AND STABILIZATION OF THE PAVEMENT WORKING PLATFORM**

# COMPACTION "ROADEO" FIELD DEMONSTRATION: ROLLER-INTEGRATED COMPACTION MONITORING AND SUBGRADE GEOSYNTHETIC REINFORCEMENT

**PROJECT REPORT**

Prepared for
The Second Strategic Highway Research Program
Transportation Research Board
of
The National Academies

David White, Pavana Vennapusa, Jie Han, Barry Christopher,
Heath Gieselman, Shiyun Wang, Wayne Rilko, Peter Becker, David Horhota,
Sanat Pokharel, and Jitendra Thakur

**DECEMBER 2012**

## ACKNOWLEDGMENT OF SPONSORSHIP

This work was sponsored by Federal Highway Administration in cooperation with the American Association of State Highway and Transportation Officials, and was conducted in the Strategic Highway Research Program, which is administered by the Transportation Research Board of the National Academies.




## SHRP 2 R02

## GEOTECHNICAL SOLUTIONS FOR SOIL IMPROVEMENT, RAPID EMBANKMENT CONSTRUCTION, AND STABILIZATION OF THE PAVEMENT WORKING PLATFORM

## PROJECT RESEARCH TEAM MEMBERS:

### PRINCIPAL INVESTIGATORS


RYAN BERG, RYAN R. BERG & ASSOCIATES
DONALD BRUCE, GEOSYSTEMS, L.P.
BARRY CHRISTOPHER, CONSULTANT
JIM COLLIN, THE COLLIN GROUP, LTD.
GARY FICK, TRINITY CONSTRUCTION
GEORGE FILZ, VIRGINIA TECH
JIE HAN, UNIVERSITY OF KANSAS
JIM MITCHELL, VIRGINIA TECH
VERN SCHAEFER, IOWA STATE UNIVERSITY
DENNIS TURNER, CONSULTANT
LINBING WANG, VIRGINIA TECH
DAVID WHITE, IOWA STATE UNIVERSITY


### STUDENTS/RESEARCHERS


BHAGABAN ACHARYA, UNIVERSITY OF KANSAS
STEVE ADAMCHAK, VIRGINIA TECH
AMANDA BARNGROVER, VIRGINIA TECH
ANDREW BEATTY, IOWA STATE UNIVERSITY
PETER BECKER, IOWA STATE UNIVERSITY
ANIL BHANDARI, UNIVERSITY OF KANSAS
JAMIE BRICKMAN, VIRGINIA TECH
CORRIE CAMPBELL, VIRGINIA TECH
KOLLEEN CARLSON, VIRGINIA TECH
CONRAD CHO, VIRGINIA TECH
RYAN COREY, UNIVERSITY OF KANSAS
ASHLEY DISBURG, IOWA STATE UNIVERSITY
CALEB DOUGLAS, IOWA STATE UNIVERSITY
CRISTIAN DRUTA, VIRGINIA TECH
HEATH GIESELMAN, IOWA STATE UNIVERSITY
MICAH HATCH, VIRGINIA TECH
PETER HUNSINGER, IOWA STATE UNIVERSITY
DEEP KHATRI, UNIVERSITY OF KANSAS
KYLE LAWSON, VIRGINIA TECH
WENJUAN LI, IOWA STATE UNIVERSITY
SHENTING LI, IOWA STATE UNIVERSITY
DANIEL MAINE, VIRGINIA TECH
GEORGE MALOUF, VIRGINIA TECH
CAITLIN MCCARTHY, IOWA STATE UNIVERSITY
JAMES MEYER, IOWA STATE UNIVERSITY
MICHAEL NOLDEN, VIRGINIA TECH
ALEX REEB, VIRGINIA TECH
GARY RIGGINS, VIRGINIA TECH
SARI ABUSHARAR, UNIVERSITY OF KANSAS
KURT SCHIMPKE, VIRGINIA TECH
JOEL SLOAN, VIRGINIA TECH
JITENDRA THAKUR, UNIVERSITY OF KANSAS
BIN TONG, IOWA STATE UNIVERSITY
PAVANA VENNAPUSA, IOWA STATE UNIVERSITY
LEE VANZLER, VIRGINIA TECH
CHADD YEATTS, VIRGINIA TECH

## TABLE OF CONTENTS

## LIST OF FIGURES

## LIST OF TABLES

## ACKNOWLEDGEMENTS

This work was sponsored by Federal Highway Administration in cooperation with the American Association of State Highway and Transportation Officials, and was conducted in the Strategic Highway Research Program, which is administered by the Transportation Research Board of the National Academies.

David Horhota, Sastry Putcha, Todd Britton, Jose Hernando, Jerry Moxley, and Ben Watson from Florida Department of Transportation (DOT) assisted in setting up the project and conducting field testing. Robert Hansgen and Tim Thacker with England-Thims and Miller, Inc. and Don Davis and John Hardin with Archer Western Contractors, Ltd., also assisted in gaining access to the project site and in preparation of the test beds. Caterpillar Inc. provided the roller integrated compaction roller. Allen DeClerk from Caterpillar Inc. provided support with roller operations and assisted in field testing. Professional Reinforcement Solutions (PRS) Mediterranean, Inc., in Israel provided geocells for testing. Dr. Ofer Kief from PRS Mediterranean, Inc., Israel assisted and provided recommendations during installation of geocells. Cheng Li from Iowa State University provided assistance with laboratory testing. All their assistance is greatly appreciated.

## EXECUTIVE SUMMARY

### Project Overview

This field demonstration project was conducted on the SR9B construction project in Jacksonville, Florida from May 16 to May 19, 2011. A Caterpillar CS74 vibratory smooth drum self-propelled roller weighing about 34,000 pounds was used on the project. The machine was setup with a roller-integrated compaction monitoring (RICM) system. Four test beds (TBs) were constructed and tested using the on-site poorly-graded sand embankment fill (A-3 according to the AASHTO classification system).

TB1 involved constructing six test sections incorporating several different geosynthetic reinforcement materials: biaxial geogrid (BX), geogrid/nonwoven geotextile geocomposite (C30), polypropylene woven fabric (PPWF), and 100 mm or 150 mm geocell (GC) materials, and one control section. TB2 involved compacting a thick loose lift (about 1.2 m deep) in two sections—one with BX geogrid reinforcement and one without reinforcement. TBs 3 and 4 involved mapping project production areas using the RICM roller and selecting test locations based on the color-coded on-board computer display in the roller for in situ testing.

Field testing involved obtaining RICM measurements during the compaction/mapping process, and point tests including the following: dynamic cone penetrometer (DCP) test, static cone penetrometer test (CPT), static plate load test (PLT), falling weight deflectometer (FWD) test, light weight deflectometer (LWD), nuclear gauge (NG), and sand cone density test. In addition, all test sections of TB1 were instrumented with piezoelectric earth pressure cells (EPCs) to monitor in-ground total vertical and horizontal stresses before, during, and after compaction.

The main objectives of this demonstration project were as follows:

a) Evaluate the use of RICM technology with on-board computer display for compacted fill quality control (QC) and quality assurance (QA) testing
b) Evaluate compaction influence depth under the RICM roller
c) Evaluate differences in engineering properties between different types of geosynthetic and geocell reinforced fill test sections along with unreinforced fill test section using different QC/QA testing methods
d) Evaluate differences in the in-ground dynamic stresses under the roller between different test sections
e) Provide hands-on experience with RICM technology and various QC/QA testing technologies, and various geosynthetic/geocell reinforcement products to researchers and practitioners

Objective (a) was achieved from selecting QC/QA test locations using the computer display unit mounted in the roller and evaluating correlations between point test measurements and RICM measurements in TBs 3 and 4. Objective (b) was achieved by conducting CPT and DCP testing before and after compaction on TBs 1 and 2. Objectives (c) and (d) were achieved using testing conducted using different QC/QA point test methods and EPC measurements on TB 1. Objective (e) was achieved by conducting an open house of the Iowa

State University geotechnical mobile laboratory and RICM roller on the last day of the field project, which was attended by representatives from the Florida DOT, the SHRP 2 R02 project manager and research team members, Caterpillar, consultants and researchers from Iowa State University and the University of Kansas. Some of the attendees operated the RICM roller and new in situ QC/QA spot testing methods and received hands-on experience.

**Key Findings and Conclusions**

Some of the key findings from this study are as follows:

- Color-coded display with 100% coverage of compaction area was effective in selecting “soft” and “stiff” areas for spot testing.
- RICM measurements generally were better correlated with LWD and DCP-CBR spot test measurements, than with nuclear gauge density measurements.
- The MDP*-RICM measurements were influenced by the direction of travel. This is because the MDP* measurements represent the mechanical performance of the whole roller, which are affected by the roller-soil interaction at the front drum and the rear tires, and the results are only reported at the center of the drum. The offset distance for MDP* measurements is observed to be about 2.60 m behind the drum center. This is an important aspect to further evaluate because it directly affects how QC/QA test measurements should be obtained to conduct calibration tests and establish target values for acceptance.
- The CMV-RICM measurements were also influenced by the direction of travel. The offsetting occurs because the CMV at a given point indicates an average value over a roller travel length corresponding to a measurement interval of about 0.5 sec.
- TB3 surfaced with RAP over natural sand, and TB4 compacted sand in the road embankment area, revealed differences in average CMV and MDP* measurements.
- TB1 showed that on average MDP* increases with increasing vibration amplitude.
- Results of in situ spot test measurements and RICM measurements from TB1 constructed with different reinforcements (BX, GC100, GC150, C30, and PPWF) and a control section, revealed the following:
  - MDP* after compaction on layer 1: On average MDP* (a = 0.90 mm) was about 1.07 times higher in the geocell sections compared to the control section. The BX section average MDP*(a = 0.90 mm) was about the same, while the C30 and PPWF sections average MDP* (a = 0.90 mm) were about 0.90 to 0.95 times the control section average MDP* (a = 0.90 mm). Similar trends were observed for MDP* measurements obtained using a = 1.80 mm setting.
  - MDP* after compaction on layer 2 in BX, C30, and PPWF sections: The C30 section average MDP*(a = 0.90 mm) was about the same, while the BX and PPWF sections average MDP* (a = 0.90 mm) were about 0.94 to 0.95 times the control section average MDP* (a = 0.90 mm). Similar trends were observed for MDP* measurements obtained using a = 1.80 mm setting.
  - In contrary to the MDP* measurements, CMV measurements were generally lower in the reinforced sections than in the control section with the exception

of measurements in the GC100 section. BX section showed the lowest ratio values compared to all other reinforced sections.

- On average, the GC100 and GC150 sections resulted in the same dry unit weights while the BX, C30, and PPWF sections resulted in slightly lower (about 0.97 to 0.99) dry unit weights than the control section.
- LWD modulus values in the C30 section were the lowest, while LWD modulus values in the GC150 section were the highest of all test sections. On average, LWD modulus at surface in all reinforced sections (except in C30 section) were about 1.1 to 1.6 times higher than in the control section.
- LWD modulus values obtained in the excavation were higher (by about 1.2 to 1.4 times) than the measurements obtained at the surface, illustrating the influence of lateral confinement on modulus in sandy soils.
- Cyclic plate load tests were conducted in GC150, GC100, and BX sections. The test in GC150 section showed the lowest permanent deformation (4.1 mm) and the BX section showed the highest permanent deformation (5.6 mm) at the end of 10 cycles. The test in GC150 section produced the highest modulus (E = 160 MPa) for the 10th loading cycle while the test in the GC100 section showed the lowest modulus (E = 125 MPa).
- CPT and DCP test profiles revealed the compaction influence depth (i.e., the depth up to which there is some change in soil properties after compaction) varied from about 0.9 m to 1.8 m under the CS74 RICM roller.

**Recommendations for Future Work**

This field demonstration project was originally intended to evaluate different compaction methods for transportation applications including rapid impact compaction (RIC), impact roller (IR) compaction, and various RICM technologies. However, due to budget limitations and lack of IR and RIC equipment availability at the time of this project, only one RICM technology was used in this demonstration. Future demonstration projects should focus on developing pilot studies for the various RIC, IR, and RICM technologies to better define their benefits relating to construction cost, time, efficiency, and effectiveness in consistently obtaining design properties for different material types (granular and non-granular) and subsurface conditions (i.e., lift thicknesses, stable versus unstable foundation layers).

Conventional in situ spot testing methods should be used to document soil density, strength, and stiffness properties and obtain detailed field notes (keeping track of time and cost) to develop comparison information. The information obtained from such demonstration projects will also contribute substantially to earthworks operations for civil infrastructure, as compaction is a common an important element of many infrastructure components. Information obtained from these demonstration projects will also directly contribute to improving the selection and guidance system developed as part of the SHRP 2 R02 project.

# CHAPTER 1. INTRODUCTION

This section of the report provides a brief review of the broader SHRP 2 R02 research effort that made this project possible and some of the field demonstration project details. At the end of this chapter is a brief overview of how the results of this report are organized.

## 1.1 BACKGROUND

Although in existence for several decades, many geoconstruction technologies face both technical and non-technical obstacles preventing broader utilization in transportation infrastructure projects. The research team for Second Strategic Highway Research Program (SHRP 2) Project R02, *Geotechnical Solutions for Soil Improvement, Rapid Embankment Construction, and Stabilization of the Pavement Working Platform,* is investigating the state of practices of transportation project engineering, geotechnical engineering, and earthwork construction to identify and assess methods to advance the use of geoconstruction technologies. Such technologies are often underutilized in current practice, and they offer significant potential to achieve one or more of the SHRP 2 Renewal objectives, which are rapid renewal of transportation facilities, minimal disruption of traffic, and production of long-lived facilities. Project R02 encompasses a broad spectrum of materials, processes, and technologies within geotechnical engineering and geoconstruction that are applicable to one or more of the following "elements" of construction (as defined in the project scope): (I) new embankment and roadway construction over unstable soils; (II) roadway and embankment widening; and (III) stabilization of pavement working platforms.

Recently, the SHRP 2 R02 research team completed a comprehensive review of literature, a detailed assessment of several technical obstacles that interfere with more widespread use, and evaluation of mitigation strategies/action items in terms of benefit-to-cost (B/C) ratio for each of the element III technologies. Three compaction technologies: Rapid Impact Compaction (RIC), Intelligent Compaction (IC), and High Energy Impact Roller (IR), received high B/C ratio. One of the major obstacles for wide-spread implementation of RIC, IC, and IR technologies was identified as lack of well-documented and accessible case histories with benefits related to construction cost, time, efficiency, and effectiveness in consistently obtaining design properties, using these technologies compared to traditional compaction methods. Conducting "Compaction Roadeo" field demonstration projects was identified as an effective mitigation strategy to overcome this obstacle. This report is the first such project demonstration conducted. A discussion of the need for additional demonstration projects is described later in this report.

## 1.2 "COMPACTION ROADEO" FIELD DEMONSTRATION PROJECT

The "Compaction Roadeo" field demonstration project was originally intended to develop detailed case history information for different material and subsurface conditions (i.e., lift thicknesses, etc.) comparing the relative compaction efficiency, time, and cost using the different compaction methods (RIC, IR, RICM, in comparison with traditional methods) in conjunction with detailed in situ testing. However, due to budget limitations and lack of IR

and RIC equipment availability at the time of this project, only RICM technology was used in this demonstration project.

A Caterpillar CS74 vibratory smooth drum self-propelled RICM roller weighing about 34,000 lb was used on this project. In addition to using RICM, several different geosynthetic products including biaxial geogrid (BX), geogrid/nonwoven geotextile geocomposite (C30), polypropylene woven fabric (PPWF)), and 100 mm or 150 mm geocell (GC) materials, were used as reinforcement in compacted fill to evaluate differences in soil strength/stiffness characteristics. Geosynthetic reinforcement and geocell confinement in pavement systems are two separate technologies that are also part of SHRP 2 R02 element III technologies.

This field demonstration project was conducted on the SR9B construction project in Jacksonville, Florida (Figure 1) from May 16 to May 19, 2011. Field testing involved construction and testing of four test beds (TBs) on the project site with poorly-graded sand embankment fill (A-3 according to the AASHTO classification system). The main objectives of this demonstration project were to:

a) evaluate the use of RICM technology with on-board computer display for compacted fill quality control (QC) and quality assurance (QA) testing,
b) evaluate compaction influence depth under the RICM roller,
c) evaluate differences in engineering properties between different types of geosynthetic and geocell reinforced fill test sections along with unreinforced fill test section using different QC/QA testing methods,
d) evaluate differences in the in-ground dynamic stresses under the roller between different test sections, and
e) provide hands-on experience with RICM technology and various QC/QA testing technologies, and various geosynthetic/geocell reinforcement products to researchers and practitioners.

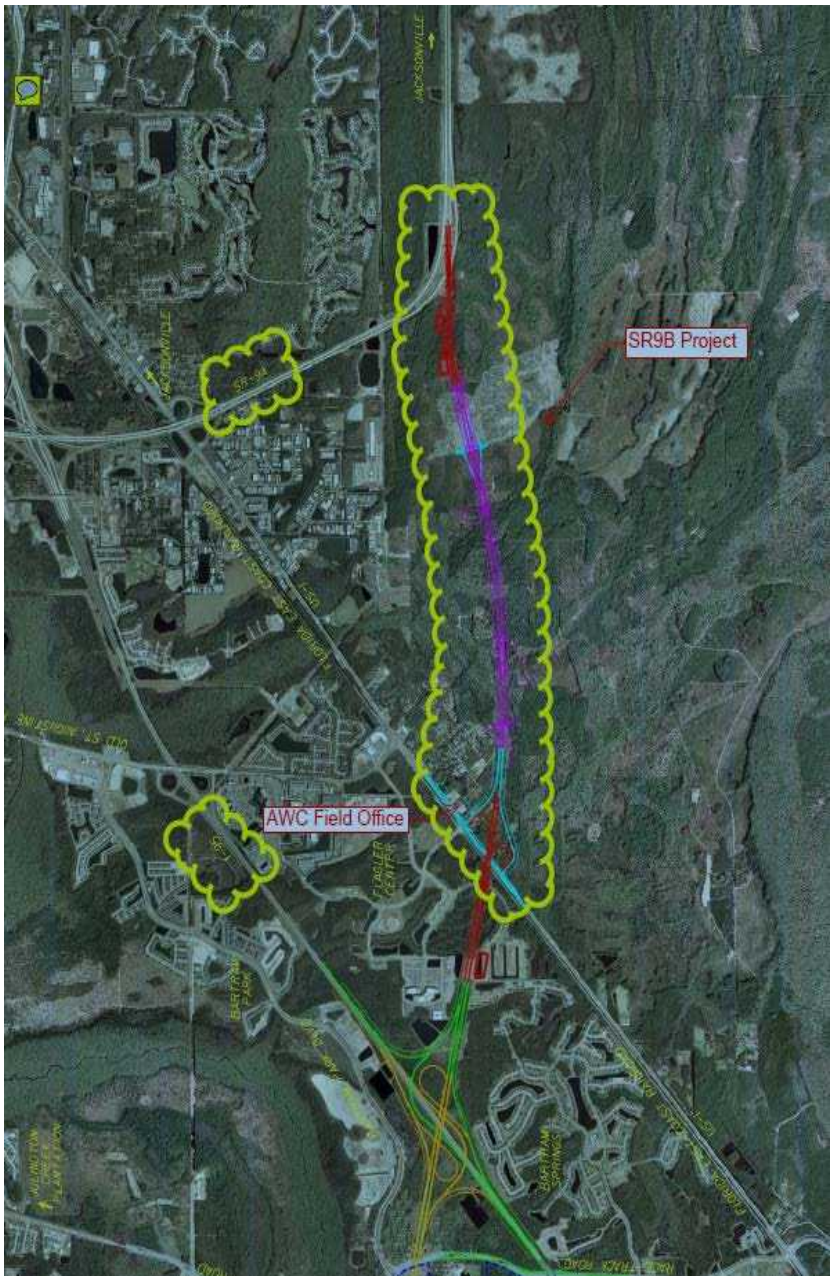


**Figure 1. Location of the SR9B project in Jacksonville, Florida (courtesy of FDOT)**

Objective (a) was achieved by obtaining RICM measurements along with various in situ QC/QA test measurements in four TBs. Two TBs consisted of one-dimensional calibration test areas that are about 6.2 m wide x 25 to 75 m long, while the remaining two TBs consisted of production areas that are about 10 to 12.5 m wide x 65 to 95 m long. In situ QC/QA testing consisted of light weight deflectometer (LWD) tests and static plate load tests (PLTs) to determine elastic modulus, dynamic cone penetrometer (DCP) tests to determine California bearing ratio (CBR) profiles, static cone penetrometer tests (CPTs) to determine cone tip resistance and skin friction profiles (using FDOT equipment), and nuclear gauge and sand cone tests to determine dry unit weight and moisture content. In addition, vibration

monitoring under roller vibratory compaction was conducted by obtaining peak particle velocities using FDOT seismographs.

Objective (b) was achieved by conducting CPT and DCPs before and after compaction on two test beds with different layer thicknesses. Objective (c) was achieved by conducting various in situ tests described above in conjunction with RICM measurements over side-by-side test sections with no reinforcement (control) and with different geosynthetic reinforcements and geocells. Objective (d) was achieved by instrumenting the soil layers in each side-by-side test section with calibrated piezoelectric total earth pressure cells to monitor horizontal and vertical total stresses before, during, and after compaction. Objective (e) was achieved through conducting an Iowa State University geotechnical mobile laboratory open house and field demonstrations of RICM along with various in situ testing equipment for practitioners, Florida DOT personnel, and researchers.

This report is organized into seven chapters. Chapter 2 presents an overview of the technologies used in this demonstration project. Chapter 3 describes the laboratory and in situ test methods used as part of this project. Chapter 4 presents the laboratory test results, and Chapter 5 presents the in situ test results. Chapter 6 presents the key findings and conclusion from this study, and Chapter 7 presents some recommendations for future demonstration projects.

# CHAPTER 2. TECHNOLOGY DESCRIPTIONS

This chapter provides background information of the three technologies used as part of this demonstration project: (a) roller-integrated compaction monitoring (i.e., continuous compaction control, and intelligent compaction), (b) geosynthetic reinforcement in pavement systems, and (c) geocell confinement in pavement systems. Additional information regarding these technologies can be found in the respective Comprehensive Technology Summary (CTS) documents of each technology.

## 2.1 ROLLER-INTEGRATED COMPACTION MONITORING

Roller-integrated compaction monitoring (RICM) is the recording and color coded real-time display of integrated measurement parameter values on rollers including, but not limited to, roller operation parameters, global positioning based position, roller-ground interaction parameter values (e.g. ground stiffness), temperature, and/or moisture content. Intelligent Compaction (IC) and continuous compaction control (CCC) technologies fall under the umbrella of RICM. IC technologies consist of machine-integrated sensors and control systems that provide a record of drum-soil interaction (an indicator of ground stiffness conditions) and automatically adjust vibration amplitude and/or frequency and/or speed using drum feedback during the compaction process. Most of the IC technologies are vibratory based systems applied to self-propelled smooth drum rollers. IC technologies have also been applied to vibratory double drum asphalt compactors and self-propelled padfoot machines. Without the automatic feedback control (AFC) system, the technology is commonly referred to as "continuous compaction control" (CCC). IC and CCC vibratory roller systems have evolved over the past 30 years to include a variety of different measurement techniques and global positioning system (GPS) based documentation systems.

There are at least ten roller-integrated compaction monitoring systems/parameters documented in the literature: Compaction Meter Value (CMV), Oscillometer Value (OMV), Continuous Compaction Value (CCV), Omega value, roller-determined Stiffness ($k_s$), Vibration Modulus ($E_{VIB}$), Alfa ($\alpha$) value, Machine Drive Power (MDP), Onboard Density Measuring System (ODMS), and Intelligent Asphalt Compaction Analyzer (IACA). All measurement parameters are well defined in the literature. A brief description of each parameter is provided below.

- Compaction Meter Value (CMV) is an index parameter (measure of non-linearity) computed as the ratio of drum acceleration amplitude of the first harmonic divided by the acceleration amplitude at the fundamental (eccentric excitation) frequency. This value requires only the measurement of vertical drum acceleration. This measurement system was evaluated as part of this "field demonstration project and additional details of this measurement technology are provided in the following sub-section of this report.
- Oscillometer Value (OMV) is an index parameter obtained from the amplitude of the horizontal acceleration of the drum center from an accelerometer mounted on the bearing plate in horizontal direction. The OMV reflects the horizontal force

transferred from the drum to the soil and hence the horizontal stiffness of the soil surface under dynamic loading.

- Continuous Compaction Value (CCV) is also an index parameter similar to CMV. However, in addition to the fundamental and first harmonic, CCV uses the first sub-harmonic and higher-order harmonics. CMV and CCV are determined via frequency-domain analysis and require 5-10 cycles of vibration data per CMV and CCV data point.
- The Omega value is determined by integrating the drum force transmitted to the soil and drum displacement time history over two cycles of vibration. An accelerometer provides the drum acceleration and an encoder records the position of the rotating eccentric.
- Roller-determined stiffness ($k_s$), vibratory modulus ($E_{VIB}$) and alfa ($\alpha$) values are derived by determining drum displacement, estimating the soil force, and using a dynamic model to calculate stiffness. Soil stiffness is determined as the ratio of soil force to maximum drum displacement. To determine an elastic modulus of the soil, a continuum contact model of the drum/soil is required and a relationship between a cylinder oscillating on an elastic half space is used.
- Machine drive power (MDP) relates to the soil properties controlling drum sinkage and uses the concepts of rolling resistance and sinkage to determine the stresses acting on the drum and the energy necessary to overcome the resistance to motion. This measurement system was also evaluated as part of this field demonstration project and additional details of this measurement technology are provided in the following sub-section of this report.
- On-board density-measuring system (ODMS) empirically estimates the density of an asphalt mixture mat by relating the drum accelerations, fundamental frequency, modulus (estimated) of the underlying layer, temperature of the mix, and thickness of the mat.
- Intelligent asphalt compaction analyzer (IACA) uses accelerometer data, mat temperature data, and measured density data over a calibration area, and processes the data through an artificial neural network classifier to predict the density of the asphalt mix.

Different types of in situ testing methods have been used to correlate with RICM measurements and can be broadly categorized into the following:

- Penetration tests.
- Static plate load tests.
- Dynamic plate load tests.
- Small-strain modulus tests.
- Moisture/Density tests.
- In situ soil sampling.
- Elevation monitoring.
- Proof rolling.

RICM can itself also be used for QC/QA, if properly implemented. It must be noted that using roller compaction measurements obtained in automatic feedback control (i.e., IC) can influence the correlations as the roller measurement values are influence by changes in

amplitude, frequency and roller speed. Literature review indicates that IC/CCC measurements provide a measure of soil stiffness or modulus and generally do not correlate well with density measurements. Some existing specifications (developed by ISSMGE, German, Sweden, and Austria highway authorities) recommend using static or dynamic plate load tests and not using density measurements for QC/QA in conjunction with CCC. Some research studies (e.g., Mooney et al. 2010) indicated that performing multivariate regression analysis using moisture and/or underlying layer variations as parameters would improve correlations between density and CCC measurements. The empirical relationships between CCC measurements and in situ test measurements are significantly influenced by the roller size, vibration amplitude and frequency, velocity, soil type, and stratigraphy underlying the soil being compacted. Therefore, the use of roller monitoring requires careful calibration. The associated relationships developed during calibration must be strictly adhered to during subsequent site measurement.

Application of the RICM technology is fairly broad because it applies to compaction of fill material, which could be considered a component of all three SHRP 2 Elements. The technology helps achieve SHRP 2 Renewal objectives 1 (Rapid Renewal of Transportation Facilities) and 3 (Production of Long-Lived Facilities), by potentially improving the compaction efficiency and quality. The impact of implementation of this technology to meet the needs of SHRP 2 Renewal Objective 2 (Minimal Disruption of Traffic) is less.

Four national level workshops (White 2008, White and Vennapusa 2009, White and Vennapusa 2010a, 2010b) and a workshop at the 2010 Transportation Research Board meeting were recently conducted to serve as a platform for manufacturers, state/federal agencies, and academicians for collaboration and exchange of ideas, experiences, and research results. Simple tools for selecting a RICM technology and machine size, establishing machine target values, data archiving and analysis protocols, limited project scale information/case histories (mostly limited to only test sections), and training field personnel are identified as some of the key implementation obstacles during these workshops. Field demonstration projects comparing conventional approaches to RICM approaches would be a strategy to overcome some of the implementation obstacles. This "Compaction Roadeo" field demonstration project is an attempt to mitigate some of these implementation obstacles. Caterpillar CS74 vibratory smooth drum roller equipped with CMV/RMV and MDP measurement systems integrated with GPS measurements is used in this study (Figure 2). Brief descriptions of these measurement systems are provided in the following sections and a summary of the CS74 roller features is provided in Table 1.

### 2.1.1 Compaction Meter Value (CMV) And Resonant Meter Value (RMV)

CMV is a dimensionless compaction parameter developed by Geodynamik that depends on roller dimensions, (i.e., drum diameter and weight) and roller operation parameters (e.g., frequency, amplitude, speed), and is determined using the dynamic roller response (Sandström 1994). It is calculated using Eq. 1, where C is a constant (300), $A_{2\Omega}$ = the acceleration of the first harmonic component of the vibration, $A_{\Omega}$ = the acceleration of the fundamental component of the vibration (Sandström and Pettersson 2004). Correlation studies relating CMV to soil dry unit weight, strength, and stiffness are documented in the

literature (e.g., Floss et al. 1983, Samaras et al. 1991, Brandl and Adam 1997, Thompson and White 2008, White and Thompson 2008).

$$CMV = C \cdot \frac{A_{2\Omega}}{A_{\Omega}} \tag{1}$$

RMV provides an indication of the drum behavior (e.g. continuous contact, partial uplift, double jump, rocking motion, and chaotic motion) and is calculated using Eq. 2, where $A_{0.5\Omega}$ = subharmonic acceleration amplitude caused by jumping (the drum skips every other cycle). It is important to note that the drum behavior affects the CMV measurements (Brandl and Adam 1997) and therefore must be interpreted in conjunction with the RMV measurements (Vennapusa et al. 2010). More discussion on effect of drum behavior on CMV measurements is provided later in this report.

$$RMV = C \cdot \frac{A_{0.5\Omega}}{A_{\Omega}} \tag{2}$$


**Figure 2. CS74 vibratory smooth drum roller with on-board computer display shown in the insert**

**Table 1. Summary features of the RICM roller used on the project**

| Feature | Description |
|---|---|
| Make/Model | Caterpillar CS74 |
| Drum Type | Smooth drum |
| Drum Geometry | 2.13 m (7.0 ft) wide and 1.524 m (5.0 ft) diameter |
| Weight at Drum | 10,150 kg (22,377 lb) |
| Maximum Centrifugal Force at $f$ = 30 Hz | 332 kN (74,600 lb) at 1.80 mm amplitude<br>166 kN (37,200 lb) at 0.90 mm amplitude |
| Frequency ( $f$ ) | 30 Hz |
| Amplitude ($a$) Settings | Static, 0.90 mm (low amplitude), and 1.80 mm (high amplitude) |
| RICM-MV | MDP* (shown as CCV in the output), and Geodynamik CMV and RMV |
| Display Software | AccuGrade™ office |
| GPS coordinates | Based on local arbitrary coordinates at the base station |
| Output Documentation | Date/Time, Location (Northing/Easting/Elevation of left and right ends of the roller drum), Speed, CCV, CMV, RMV, Frequency, Amplitude (theoretical), Direction (forward/ backward), Vibration (On/Off) |
| Data frequency | About every 0.2 m at the center of the drum<br>(for a nominal $v$ = 4 km/h) |
| Output Export File | *.csv |
| Automatic Feedback Control (AFC)[a] | No |

Notes: [a]AFC mode involves automatic adjustment of vibration amplitude and/or frequency during compaction. MDP* is different than MDP – see text for further description.

### 2.1.2 Machine Drive Power (MDP) Value

MDP technology relates mechanical performance of the roller during compaction to the properties of the compacted soil. Detailed background information on the MDP system is provided by White et al. (2005). Controlled field studies documented by White and Thompson (2008), Thompson and White (2008), and Vennapusa et al. (2009) verified that MDP values are empirically related to soil compaction characteristics (e.g., density, stiffness, and strength). MDP is calculated using Eq. 3:

$$MDP = P_g - Wv\left(Sin\alpha + \frac{A'}{g}\right) - (mv + b) \quad (3)$$

where MDP = machine drive power (kJ/s), $P_g$ = gross power needed to move the machine (kJ/s), W = roller weight (kN), A' = machine acceleration ($m/s^2$), g = acceleration of gravity

($m/s^2$), α = slope angle (roller pitch from a sensor), *v* = roller velocity (m/s), and m (kJ/m) and b (kJ/s) = machine internal loss coefficients specific to a particular machine (White et al. 2005). MDP is a relative value referencing the material properties of the calibration surface, which is generally a hard compacted surface (MDP = 0 kJ/s). Positive MDP values therefore indicate material that is less compact than the calibration surface, while negative MDP values indicate material that is more compacted than the calibration surface (i.e. less roller drum sinkage). The MDP values obtained from the machine used in this study were recalculated to range between 1 and 150 and these re-scaled values are referred to as MDP* in this report. While the original MDP values decrease in increasing compaction, the MDP* values increase with increasing compaction.

## 2.2 GEOSYNTHETIC REINFORCEMENT IN PAVEMENT SYSTEMS

Geosynthetics have been used in pavement systems at the interface between subgrade and base as subgrade improvement or restraint, within unbound granular bases as base reinforcement, and below overlays as interlayer to increase bearing capacity and reduce rutting, fatigue cracking, cracking due to heaving, and reflective cracking. Different types of geosynthetic reinforcements have been used in pavement systems depending on the type of level of improvement desired (Berg et al. 2000): (a) nonwoven or woven geotextiles, (b) extruded or knitted or woven geogrids, and (c) geo-composites. Design of geosynthetics for subgrade improvement has been based on the concepts of local bearing capacity failure and an increase of bearing capacity by the use of geosynthetics. A tensioned membrane effect is sometimes considered in the design; however, its effect is minimal unless an excessive rut depth is allowed. The design methods developed so far are empirical or semi-empirical and have been used for many projects. Subgrade improvement is commonly used for soft subgrade with CBR less than 3. The acceptance of the state DOTs to use subgrade improvement is relatively high. Recent research has demonstrated that geosynthetics can also minimize expansive soil problems by placing geosynthetic reinforcement above subgrade. A few projects for this application have been completed so far.

Design of geosynthetics for base reinforcement has been conducted by extending the AASHTO 1993 Design Guide including the benefits of geosynthetics. Three design parameters, Traffic Benefit Ratio (TBR), Bearing Capacity Ratio (BCR), and Layer Coefficient Ratio (LCR), have been proposed to consider the benefits of geosynthetics. The purposes of geosynthetics used as base reinforcement are to reduce the required base thickness and prolong pavement life. In the past few years, great efforts have been made to develop a mechanistic-based design method for this application. Methods have been adopted, and are still being developed, by AASHTO, FHWA, and the geosynthetic industry. Base reinforcement has been used for low to medium strength subgrade CBR up to 8 with noticeable benefits to varying degrees.

Geosynthetics used below overlays act as stress relief, waterproofing, and/or reinforcement layer. Research has been completed that demonstrates the benefits of geosynthetics in reducing reflective cracking. This application has been used in the field, however, with mixed results. Quality control during the installation of a geosynthetic interlayer is crucial to the performance of this technology. Guidelines for incorporating a geosynthetic interlayer in

asphalt overlays are available from the Texas Transportation Institute (Cleveland et al. 2002) and FHWA (Holtz et al. 2008). However, no well accepted design method has been developed to date.

Geosynthetic reinforcement in pavement systems technology does not apply to Element 1 (New Embankment construction over Unstable Soils) or Element 2 (Embankment Widening) but does apply to Element 3 (Stabilization of Pavement Working Platforms) because it is used to provide a stable foundation and reinforce pavement structure. Placement of geosynthetics is relatively fast and easy and the benefits from geosynthetics are realized immediately; therefore, this technology is suitable for rapid renewal of transportation facilities. Traffic disruption is not an issue because geosynthetics are only used for new construction, not rehabilitation. This technology can produce long-lived facilities and this is potentially the most significant benefit of this technology.

Despite many documented benefits, very few states consider the use of geosynthetics for base reinforcement as standard practice. A number of agencies are or have considered their use on an experimental basis. However, the majority of states have not used geosynthetics for base reinforcement. The main reasons for the states not to use this technology are (1) lack of an acceptable method to evaluate the differences among different products, (2) the lack of an acceptable design method, and (3) the lack of information regarding whether there is a cost benefit for this technology.

Three types of geosynthetics are used in this study: (a) biaxial (BX) geogrid (Figure 3), (b) geogrid/nonwoven geotextile geocomposite (C30) (Figure 4), and (c) polypropylene woven fabric (PPWF) (Figure 5). A summary of key features of these products is provided in Table 2.

**Figure 3. Pictures of BX geogrid used in this study**

**Figure 4. Pictures of C30 geogrid/nonwoven geotextile geocomposite used in this study**

**Figure 5. Pictures of PPWF geotextile used in this study**

**Table 2. Summary features of geosynthetic products used in this study (from manufacturers)**

| Feature | Products | | |
|---|---|---|---|
| | **BX Geogrid** | **C30 Geogrid/Nonwoven Geotextile Geocomposite** | **PPWF** |
| Product Description | Biaxial Geogrid – coated polyester | Polypropylene (PP) welded biaxial geogrid with PP needle-punched non-woven geotextile | Polypropylene woven fabric (black) |
| Aperture Dimensions | 25 x 25 mm | 32 x 32 mm | Apparent opening size = 0.425 mm |
| *Tensile Strength/Modulus* | | | |
| Ultimate Tensile Strength | 36.5 kN/m* | 30 kN/m* | 890 N** |
| Tensile strength at 2% Strain | 7.3 kN/m* | 10 kN/m* | N/A |
| Tensile strength at 5% strain | 14.6 kN/m* | 24 kN/m* | N/A |

*Strength properties were the same in both machine and cross machine directions

**According to ASTM D4632

## 2.3 GEOCELL REINFORCEMENT IN PAVEMENT SYSTEMS

Geocell is one of the geosynthetic products used primarily for soil confinement. It was originally developed by the US Army Corps of Engineers in the 1970s for quick construction of unpaved roads with cohesionless soil. Like other geosynthetic products, geocell is usually made from polymeric materials by welding, sewing, or bodkin bars. Currently, high-density poly-ethylene (HDPE) and novel polymeric alloy (NPA) types of geocells are commonly being used. For convenient transportation, most geocell products have a foldable three-dimensional geometry (often honeycomb shaped after stretched). During construction, geocell has to be first stretched to the desired width and fixed to a leveled surface. A layer of geotextile is often placed under the geocell to separate the infill material from the underlying soil. The infill material is then poured into the pockets of the geocell (Figure 6) and compacted to the desired density. Today, HDPE and NPA geocells have been successfully used to reinforce base/subbase and subgrade layers in unpaved roads and some paved roads. Sometimes, geogrids or geotextiles are also used to make the pocket like geocell and used to confine the soils.

Geocell is often placed at the bottom of the base/subbase or on the top of the subgrade layer. It can provide lateral confinement to infill material and thus increase the stiffness and shear strength of the reinforced soils. As a result, the wheel load will be distributed to a wider area on the underlying soft layers, and the rutting of the road (caused by the permanent deformation of the base course and subgrade soils) after a certain number of wheel passes will be reduced. The design method for geocell confinement is still under development. Currently there is no widely accepted design method available for geocell-reinforced roads.

Geocell confinement technology is applicable to SHRP 2 Element 1 (New Embankment and Roadway Construction over Unstable Soils), Element 2 (Roadway and Embankment Widening), and Element 3 (Stabilization of Pavement Working Platforms). Geocell confinement is suitable to reinforce a wide variety of unbound pavement materials. Sands and gravels are improved more with geocells than any other geosynthetics. Installation of geocell is typically slower than planar geosynthetic reinforcement. Geocell is typically more costly than planar geosynthetic reinforcement if aggregate is used. However, it can be more cost-effective when sand or rounded gravel is used. Main obstacles for implementation of this technology include: (a) lack of a design method, (b) well-developed QC/QA methods, and (c) well-documented case histories and (d) difficulties during compaction.

Geocells made of polymeric nano-composite alloy (NPA) were used in this project. The NPA geocells are nano-composite alloy of polyester/polyamide nano-fibers, dispersed in polyethylene matrix. The NPA is characterized by flexibility at low temperatures similar to high density polyurethane (HDPE) with elastic behavior similar to engineering thermoplastic. It combines the ductility of HDPE with the dimensional stability and creep resistance of polyester. This NPA geocell has a lower thermal expansion coefficient ($\leq$80 ppm/$^{o}$C) and higher tensile stiffness and strength than typical HDPE geocells. The geocell strips were ultrasonically spot-welded uniformly across each cell joint. Geocells with 150 mm (GC150) and 100 mm (GC100) cell heights with wall thickness of about 1.1 mm were used in this study. A summary of key features of the geocell products is provided in Table 3. The

interconnected geocells had individual internal cell size of 205 mm x 235 mm when expanded to a near circular shape. Pictures of geocell product before and after stretching are shown in Figure 6 and Figure 7, respectively.

**Figure 6. 150 mm Geocell (GC150) shipped product before expanding**

**Figure 7. Placement of infill material into geocells**

**Table 3. Summary of key features of geocell products used in this study (from product manufacturer**

| Feature | Products | |
|---|---|---|
| | **GC150** | **GC100** |
| Product ID | PRS-330-150-76P | PRS-330-100-76P |
| Material | polymeric nano-composite alloy | |
| Cell Height | 150 mm | 100 mm |
| Cell Cross-Sectional Dimensions (Expanded) | 250 x 210 mm | |
| Cell Distance between Weld Seams | 330 mm (±2.5%) | |
| Number of cells/$m^2$ | 40 | |
| Section Size (Expanded) | 2.5 x 8.0 m (±3%) | |
| Section Weight | 23.6 kg | 35.9 kg |
| Short-Term Strength at Yield | >21.5 kN/m | |
| Long-Term Resistance to Permanent Deformations (allowed strength for 50 year design) | >8.0 kN/m | |
| Creep Reduction Factor (for 50 year design) | <2.7 kN/m | |
| Coefficient of Thermal Expansion | <80 ppm/$^oC$ | |
| Tensile Strength | 20.9 MPa | |
| Elastic Modulus | 350 MPa at 2% strain | |

# CHAPTER 3. TEST METHODS

This chapter describes the laboratory and field testing methods and procedures followed in this study. The Iowa State University geotechnical mobile laboratory was used to conduct all the testing. For tests where an American Standard for Testing and Materials (ASTM) standard was followed, that standard is simply referenced. Any deviations from the ASTM standard procedures are briefly described. For test methods where no ASTM standard is available or not followed, appropriate references are cited or the test procedure followed is briefly described.

## 3.1 LABORATORY TEST METHODS

### 3.1.1 Soil Classification Tests

Particle-size analysis tests were conducted on the samples collected from field in accordance with ASTM C136-06 "*Standard test method for sieve analysis of fine and coarse aggregates"*. Atterberg limit tests (i.e., liquid limit—LL, plastic limit—PL, and plasticity index—PI) were performed in accordance with ASTM D4318-10 "*Standard test methods for liquid limit, plastic limit, and plasticity index of soils*" using the dry preparation method. Using the results from particle size analysis and Atterberg limits tests, the samples were classified using the unified soil classification system (USCS) in accordance with ASTM D2487-10 *"Standard Practice for Classification of Soils for Engineering Purposes (Unified Soil Classification System)"* and American Association of State Highway and Transportation Officials (AASHTO) classification system in accordance with ASTM D3282-09 "*Standard Practice for Classification of Soils and Soil-Aggregate Mixtures for Highway Construction Purposes"*. Specific gravity tests were conducted in accordance with ASTM C128-07a "*Standard Test Method for Density, Relative Density (Specific Gravity), and Absorption of Fine Aggregate"*.

### 3.1.2 Soil Compaction Tests

Two laboratory compaction tests were used to determine the relationship between dry density and moisture content for the soils obtained from the field:

- Standard Proctor compaction test in accordance with ASTM D698-07 "*Standard test methods for laboratory compaction characteristics of soil using standard effort*".
- Maximum and minimum index density tests using a vibratory table in accordance with ASTM D4253-00 "*Standard test methods for maximum index density and unit weight of soil using a vibratory table*" and D4254-00 "*Standard test methods for minimum index density and unit weight of soils and calculation of relative density*". The test standards require conducting tests on oven-dry material. In addition to this, compaction tests were conducted by incrementally increasing the moisture content of the material by approximately 2% for each test.

## 3.2 IN SITU TEST METHODS

Six different in situ testing methods were used in this study to evaluate the in situ soil engineering properties: (a) Zorn light weight deflectometer (LWD) setup with 300 mm diameter plate to determine elastic modulus ($E_{LWD}$), (b) cyclic plate load test (PLT) to determine elastic initial/reload modulus and permanent deformation characteristics, (c) dynamic cone penetrometer (DCP) to determine California bearing ratio (CBR), (d) static cone penetrometer test (CPT) to measure cone tip resistance ($q_t$) and skin friction ($f_s$), (e) Troxler nuclear gauge (NG) to measure moisture content ($w$) and dry unit weight ($\gamma_d$), (f) sand cone density testing to measure $w$ and $\gamma_d$, (g) vibration monitoring testing to monitor peak particle velocities (vibrations) during vibratory compaction of fill material, and (h) real-time kinematic (RTK) global positioning system (GPS). Total earth pressure cells (EPCs) were installed in soil layers to monitor total horizontal and vertical stresses before, during, and after vibratory compaction. Descriptions of each of the procedures followed for these tests and measurement parameters are provided below.

### 3.2.1 Light Weight Deflectometer

LWD tests were performed following manufacturer recommendations (Zorn 2003) and the $E_{LWD}$ values were determined using Eq. 4, where E = elastic modulus (MPa), $d_0$ = measured maximum plate deflection (mm), $\eta$ = Poisson's ratio (0.4), $\sigma_0$ = applied contact stress (MPa), r = radius of the plate (mm), F = shape factor depending on stress distribution (assumed as 8/3) (see Vennapusa and White 2009).

$$E = \frac{(1-\eta^2)\sigma_0 r}{d_0} \times F \quad \textbf{(4)}$$

A picture of the Zorn 300 mm LWD used in this study is shown in Figure 8.

**Figure 8. LWD testing using Zorn 300 mm diameter plate**

### 3.2.2 Plate Load Test

PLT's were conducted by applying a load on 300 mm diameter plate against a 62kN (14000 lb) capacity reaction force for 10 loading/unloading cycles. A maximum load of about 29 kN (6500 lb) was applied for 9 loading cycles and a maximum load of about 53 kN (12000 lb) was applied for 1 loading cycle. The applied load was measured using a 90-kN load cell and deformations were measured using three 50-mm linear voltage displacement transducers (LVDTs). The load and deformation readings were continuously recorded during the test using a data logger. The elastic modulus (E) values were determined from Eq. 4 using deflection values at 0.1 and 0.2 MPa applied contact stresses. Permanent deformation values were also determined at the end of each loading/unloading cycle. A picture of the PLT setup used in this study is shown in Figure 9.


**Figure 9. Static plate load testing (PLT) setup using freightliner, reaction beam, and 300 mm diameter steel plate, and 3 deflection sensors**

### 3.2.3 Dynamic Cone Penetrometer

DCP tests (Figure 10) were performed in accordance with ASTM D6951-03 *"Standard Test Method for Use of the Dynamic Cone Penetrometer in Shallow Pavement Applications"* to determine dynamic cone penetration index (DPI) and calculate CBR using Eq. 5.

$$\text{CBR} = \frac{292}{\text{DPI}^{1.12}} \quad \textbf{(5)}$$

The DCP test results are presented in this report as DPI or CBR with depth profiles, or weighted average CBR measurements for a given layer. For e.g., results reported as $CBR_{Base}$ represent weighted average CBR for the thickness equal to the thickness of the base layer. Weighted average is calculated using Eq. 6, where $CBR_i$ = CBR of $i^{th}$ layer and Hi = is the thickness of the $i^{th}$ layer.

$$CBR_{Base} \text{ or } CBR_{Subgrade} = \frac{(CBR_i \times H_i) + (CBR_{i+1} \times H_{i+1}) + ....(CBR_n \times H_n)}{\sum H_n} \quad \textbf{(5)}$$

**Figure 10. DCP testing**

### 3.2.4 Cone Penetration Test

CPTs were conducted by FDOT personnel. Tests were conducted using a cone with $60^o$ taper angle and 10 $cm^2$ area to measure tip resistance ($q_t$) and sleeve friction ($f_s$). Tests were conducted at a nominal penetration rate of 2 cm/s. A picture of the FDOT's CPT equipment used in this study is shown in Figure 11.

**Figure 11. Static cone penetration testing (CPT)**

### 3.2.5 Nuclear Gauge

A calibrated Troxler nuclear gauge (NG) was used to measure moisture content (w) and dry unit weight ($\gamma_d$) of the fill material. NG tests were conducted by FDOT personnel. Moisture content measurements obtained from NG were compared with oven-dry moisture content measurements from one test bed and the results are described in Chapter 4. A picture of the Troxler NG used in this study is provided in Figure 12.

### 3.2.6 Sand Cone Test

Sand cone density testing was performed in accordance with ASTM D1556-07 *"Standard Test Method for Density and Unit Weight of Soil in Place by the Sand Cone Method"*. Testing was conducted in sections with geocells to determine density of the infill material within the geocell. Material excavated from the geocell was used to determine moisture content using oven dry method. A picture of the sand cone density testing setup is shown in Figure 13.

**Figure 12. Troxler nuclear gauge used for moisture and density testing**

**Figure 13. Sand cone testing used for moisture and density determination**

### 3.2.7 Vibration Monitor

An Instantel Series III Minimate Plus$^{TM}$ vibration monitor seismograph was used to monitor peak particle velocities (PPVs) at several locations away from the roller during vibratory compaction of fill materials. Vibration monitoring was conducted by FDOT personnel.

### 3.2.8 Real-Time Kinematic Global Positioning System

RTK-GPS system was used to obtain spatial coordinates (x, y, and z) of in situ test locations. A Trimble SPS 881 receiver was used with base station correction provided from a Trimble SPS851 established on site. According to the manufacturer, this survey system is capable of horizontal accuracies of < 10 mm and vertical accuracies < 20 mm. The GPS mounted on the RICM roller also utilized the base station to provide the corrected measurements.

**Figure 14. Hand-held Trimble SPS881 GPS receiver**

### 3.2.9 Earth Pressure Cells

Piezoelectric EPCs with a measurement range of 0-600 kPa and 0-1000 kPa were used in this study to measure the total horizontal ($\sigma_h$) and total vertical ($\sigma_v$) stresses in the soil before, during, and after compaction. The EPC's used in this study were of 100 mm diameter and 10 mm thick piezoelectric sensors made of two stainless steel plates welded together and fill with de-aired hydraulic fluid. The EPC's were calibrated prior to installation using a specially fabricated calibration chamber by placing the cells in compacted poorly-graded ASTM silica sand. The EPC calibrations were also performed by applied a constant stress at various temperatures to obtain temperature correction factors. A picture of the EPC calibration device is shown in Figure 16 and a detailed description of the device is provided in White et al. 2008. The EPC's were placed in one test bed in a sand subgrade layer. The EPC's were embedded in a thin layer of ASTM silica sand used during calibration.

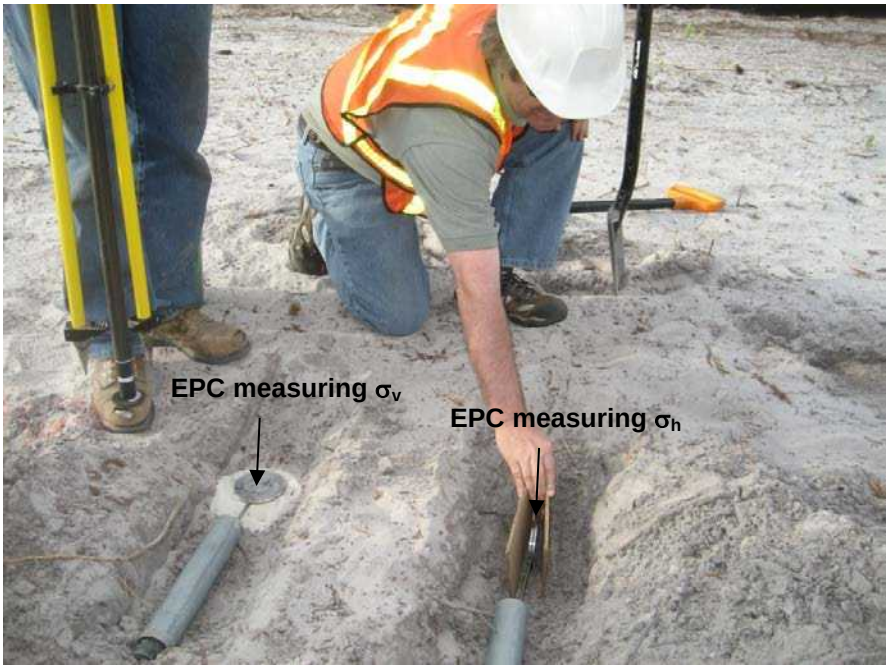


**Figure 15. EPC installation in the sand base layer to measure vertical and horizontal in-ground total stresses**

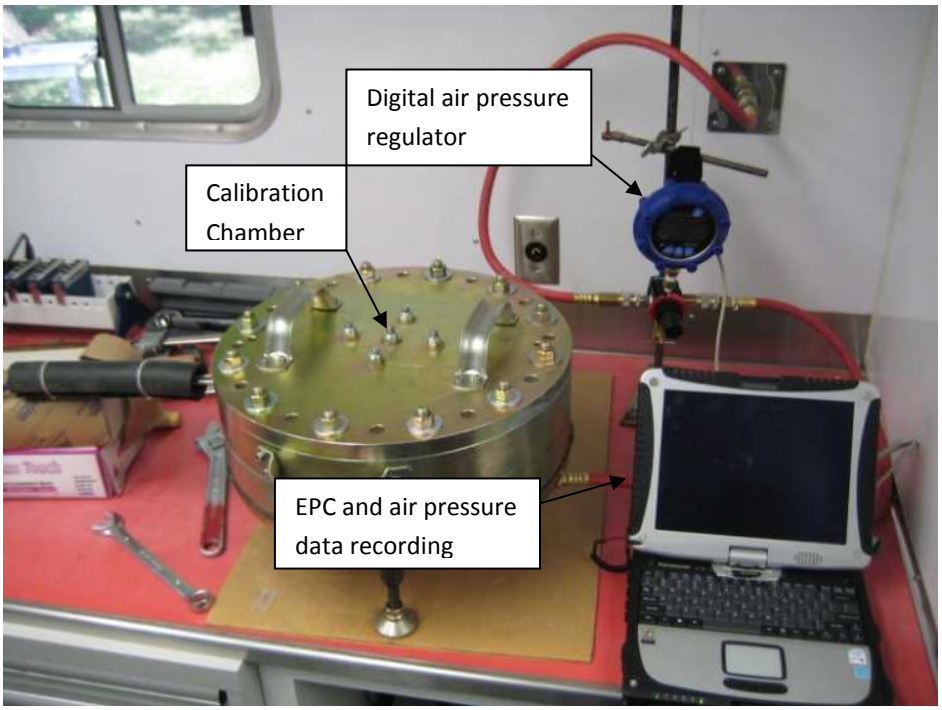


**Figure 16. Complete setup of the EPC calibration process (from White et al. 2008)**

# CHAPTER 4. LABORATORY TEST RESULTS

Two soil samples were collected from the field and tested in the laboratory as part of this project. The two soil samples are identified as gray existing sand base and brown sand fill. A summary of laboratory test results (i.e., laboratory compaction test, grain-size analysis test, Atterberg limits test, soil classification, and specific gravity results) is provided in Table 4. Also included in Table 4 are laboratory classification test results and resilient modulus ($M_r$) provided by FDOT on brown sand fill material.

## 4.1 CLASSIFICATION TEST RESULTS

Grain-size distribution curves from particle-size analysis tests on the two materials collected by ISU and FDOT test results are shown in Figure 17. The two materials collected by ISU and results by FDOT showed similar grain-size distribution. The materials were non-plastic. Based on the particle-size analysis test results the materials are classified as poorly-graded sand (SP) according to the USCS and A-3 according to the AASHTO classification system.

## 4.2 LABORATORY COMPACTION TEST RESULTS

Moisture versus dry unit weight relationships obtained from standard and modified Proctor tests and vibratory compaction tests are shown in Figure 18. Standard Proctor compaction test results provided by FDOT are also shown in Figure 18.

The FDOT Proctor test results showed a slightly higher maximum dry unit weight ($\gamma_{dmax}$ = 15.58 kN/m$^3$ (99.2 pcf)) than the ISU Proctor test results ($\gamma_{dmax}$ = 15.23 kN/m3 (97.0 pcf)), on the brown sand fill material. Both FDOT and ISU testing showed similar optimum moisture content ($w_{opt}$ = 16.5%) for the brown sand fill material. Standard Proctor moisture-dry unit weight relationships for both gray and brown sand materials exhibited a “bulking” phenomenon at a moisture content of about 4.0%, where the dry unit weights of the materials were low. The moisture-dry unit weight curves were slightly different on the dry side of optimum for the gray and brown sand materials, but the $w_{opt}$ and $\gamma_{dmax}$ were about the same.

Vibratory laboratory compaction test results indicated a $\gamma_{dmax}$ = 15.93 kN/m$^3$ (101.4 pcf) for gray sand and $\gamma_{dmax}$ = 15.56 kN/m$^3$ (99.1 pcf) for brown sand materials at oven-dry moisture contents. The moisture-dry unit weight relationships exhibited a “bulking” phenomenon at *w* = 1.6% and 2.6% for brown and gray sand materials, respectively, where the dry unit weight of the materials were low.

**Table 4. Summary of laboratory test results**

| Parameter | ISU Testing | | Brown Sand Fill – FDOT Testing |
|---|---|---|---|
| | Gray Existing Sand Base | Brown Sand Fill | |
| *Grain-Size Analysis Results* | | | |
| Gravel Content (%) (> 4.75mm) | 0 | 0 | 0 |
| Sand Content (%) (4.75mm – 75μm) | 97 | 97 | 98 |
| Silt + Clay Content (%) (<75μm) | 3 | 3 | 2 |
| $D_{10}$ (mm) | 0.094 | 0.095 | 0.096 |
| $D_{30}$ (mm) | 0.156 | 0.159 | 0.157 |
| $D_{60}$ (mm) | 0.190 | 0.191 | 0.196 |
| Coefficient of Uniformity, $c_u$ | 2.02 | 2.01 | 2.04 |
| Coefficient of Curvature, $c_c$ | 1.36 | 1.38 | 1.31 |
| *Atterberg Limits Test Results* | | | |
| Liquid Limit, LL (%) | Non-Plastic | Non-Plastic | Non-Plastic |
| Plasticity Index, PI (%) | | | |
| *AASHTO Classification* | A-3 | A-3 | A-3 |
| *USCS Classification* | SP | SP | SP |
| *USCS Soil Description* | Poorly-graded sand | | |
| *Specific Gravity, $G_s$* | 2.63 | 2.61 | Not provided |
| *Standard Proctor Test Results (ASTM D698)* | | | |
| Maximum dry unit weight, $\gamma_{dmax}$ (kN/m$^3$) | 15.28 | 15.23 | 15.58 |
| Optimum moisture content, $w_{opt}$ (%) | 16.5 | 16.5 | 16.5 |
| *Relatively density test (ASTM D4253/D4254)* | | | |
| Minimum dry unit weight, $\gamma_{dmax}$ (kN/m$^3$) (oven-dry) | 12.72 | 12.22 | |
| Maximum dry unit weight, $\gamma_{dmax}$ (kN/m$^3$) (oven-dry) | 15.93 | 15.56 | — |
| *Resilient Modulus ($M_r$) Test Results (Provided by FDOT)* | | | |
| $M_r$ at 75.8 kPa bulk stress (MPa) [$\gamma_d$ = 15.74 kN/m$^3$ and $w$ = 14.9%] | — | — | 83.5 |

In situ dry unit weight and moisture content test results from ISU test beds and FDOT QA testing are shown on Figure 18 along with the standard Proctor test results. The in situ test results from ISU test beds on brown sand fill materials indicated relative compaction (RC) values in the range of 97% to 106% with an average of about 100%, with reference to the ISU standard Proctor $\gamma_{dmax}$. The in situ moisture contents were in the range of 2.6% to 7.7%, which was about 13.9% to 8.8%, dry of ISU standard Proctor $w_{opt}$. FDOT QA test results indicated RC values in the range of 100% to 103% with an average of about 102%, with

reference to the FDOT standard Proctor $\gamma_{dmax}$. The in situ moisture contents were in the range of 4.7% to 11.1%, which was about 11.8% to 5.4%, dry of FDOT standard Proctor $w_{opt}$.

In situ dry unit weight and moisture content test results are also compared with the laboratory vibratory compaction test results in Figure 18. Relative density ($D_r$) is calculated for the in situ test results in accordance with ASTM D4253/4254. The in situ $D_r$ of the brown fill material in ISU test beds varied from about 82% to 113% with an average of about 93%. FDOT QA testing indicated that the in situ $D_r$ varied from about 102% to 112% with an average of about 107%.

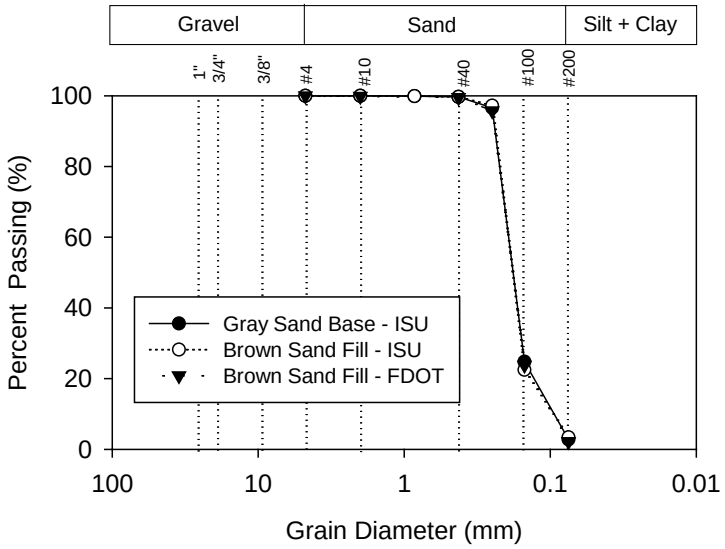


**Figure 17. Grain size distribution curves of material used on the project**

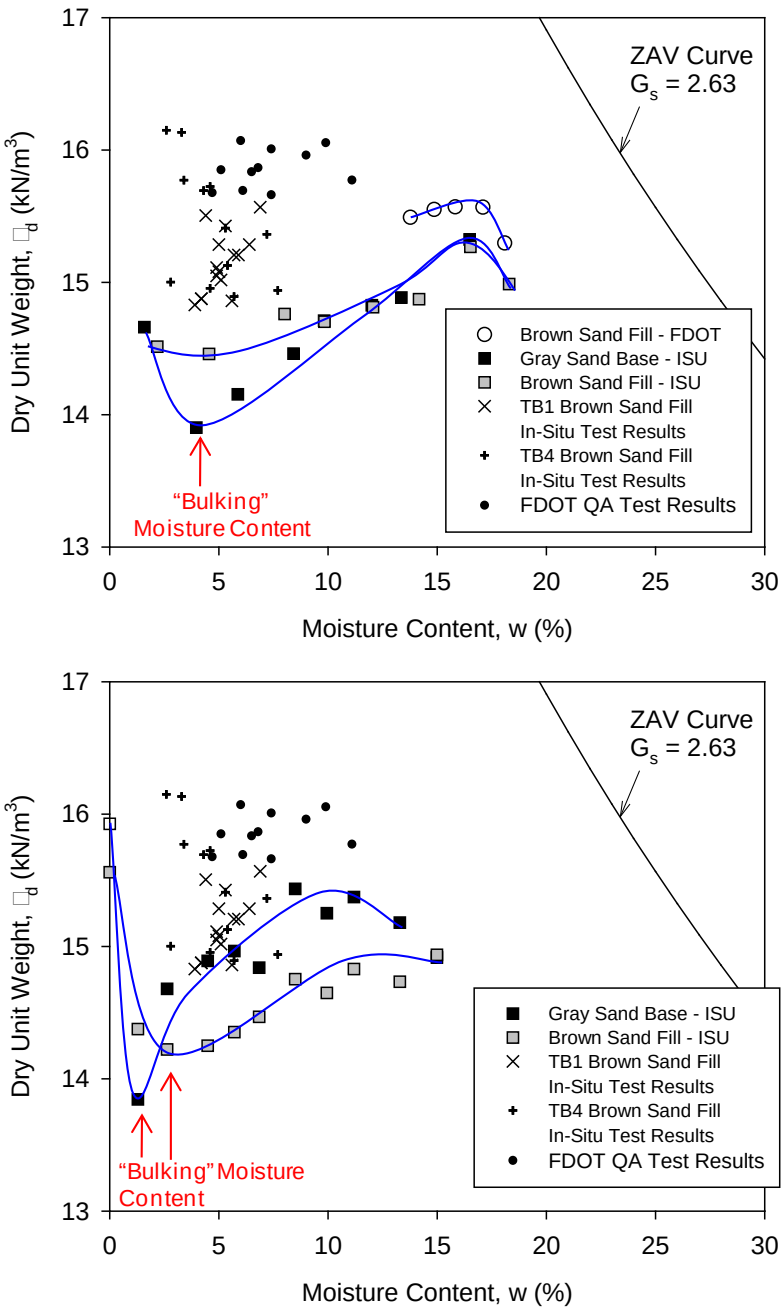


**Figure 18. Laboratory moisture density results from standard Proctor test (top) and vibratory relative density compaction test (bottom) in comparison with field moisture density results**

## CHAPTER 5. IN SITU TEST RESULTS

This chapter presents in situ test results obtained from TBs studied as part of this project. A summary description of all TBs is provided below followed by detailed test results and analysis from each test bed.

### 5.1 DESCRIPTION OF TEST BEDS

A total of four TBs were studies as part of this field project. TBs 1 and 2 consisted of calibration test areas that are about 6.2 m wide x 25 to 75 m long, while TBs 3 and 4 consisted of production areas that are about 10 to 12.5 m wide x 65 to 95 m long. A summary of each test bed conditions and construction operations is provided in Table 5. TBs 1 and 2 are located outside the SR9B road alignment, while TBs 3 and 4 production areas are located within the SR9B project alignment.

**Table 5. Summary of test bed conditions and construction operations**

<table>
<tr><th>Date</th><th>TB</th><th>Soil Stratigraphy</th><th>Compaction passes</th></tr>
<tr><td rowspan="6">05/16 to 05/18</td><td>1-1(50)*(BX)</td><td>1 to 2 layers of brown sand fill over existing gray sand base.</td><td rowspan="6">Layer 1 (5/17):<br>1-4: Low amp[1]; 5: High amp[1]<br>6: High amp[1]; 7-10: Low amp[2]<br>Layer 2 (5/17):<br>1-4: Low amp[1]; 5: High amp[1]<br>6: Static[1]; 7-10: Low amp[2]<br>4 water truck passes[2]; 11-12: Low amp[2]; 13: Low amp[1]; 14-15: High amp[1]; 16: Low amp[1]<br>Layer 2 (5/18):<br>17: Static[1]; 18: Low amp[2]; 19: High amp[1]</td></tr>
<tr><td>1-2(50)* (GC150)</td><td rowspan="2">1 layer of brown sand fill over existing gray sand base.</td></tr>
<tr><td>1-3(50)* (GC100)</td></tr>
<tr><td>1-4(12)* (C30)</td><td rowspan="2">1 to 2 layers of brown sand fill over existing gray sand base.</td></tr>
<tr><td>1-4(38)* (PPWF)</td></tr>
<tr><td>1-5(50)*(Control)</td><td>1 layer of brown sand fill over existing gray sand base.</td></tr>
<tr><td rowspan="2">05/18</td><td>2-1</td><td>About 1.2 m thick loose lift with BX grid placed at about 100 mm below surface.</td><td rowspan="2">1-12: High amp[1]</td></tr>
<tr><td>2-2</td><td>About 1.2 m thick loose lift.</td></tr>
<tr><td>05/16</td><td>3</td><td>30 to 120 mm thick recycled asphalt surfacing over sand subgrade (haul road)</td><td>1: Static; 2: Low amp; 3: Low amp; 4: High amp; 5: Static</td></tr>
<tr><td>05/18</td><td>4</td><td>Brown sand fill (compacted)</td><td>1: Static; 2: Low amp; 3: High amp; 4: Static</td></tr>
<tr><td colspan="4">*No roller passes on the existing gray sand base and the number in the parenthesis indicates the length of each section in feet; [1]Direction of travel is west to east; [2]Direction of travel is east to west.</td></tr>
</table>

### 5.2 TB1 – CALIBRATION TEST AREA

#### 5.2.1 TB Construction and In Situ Testing

The test bed included a test area of about 6.2 m wide x 75 m long where brown sand fill material was placed over the existing gray sand base layer as shown in Figure 19. The test

area was first divided in to six test sections as shown in Figure 20, labeled as shown below depending on the type of reinforcement (geotextile/geocell) placed over the existing sand layer:

1. 1-1(50) BX — BX geogrid
2. 1-2(50) GC150 — geocell with 150 mm cell height
3. 1-3(50) GC100 — geocell with 100 mm cell height
4. 1-4(12) C30 — geogrid/nonwoven geocomposite
5. 1-4(38) PPWF — Polypropylene woven fabric
6. 1-5(50) Control — section with no reinforcement

LWD, DCP, CPT, and NG in situ tests were conducted in each test section. GPS coordinates of the in situ test locations on the existing sand base layer are shown in Figure 20. LWD tests were conducted at the surface of the sand base layer and in an excavation at a depth of about 150 mm below surface. The tests in the excavation were intended to evaluate the influence of confinement on the elastic modulus values. DCP tests were conducted to a depth of about 0.9 m below surface and CPTs were conducted to a depth of about 4 m below surface. NG tests were conducted at surface with 300 mm probe penetration. Piezo-electric EPCs were installed in each test section to measure total $\sigma_h$ and $\sigma_v$. The EPCs were placed at about 75 mm below the surface and the two sensors in each section were placed at about 300 to 500 mm apart. The GPS coordinates of the EPCs are shown in Figure 20 and its location in each test section are shown in a cross-sectional view in Figure 21.

BX, C30, and PPWF geosynthetic products, and GC150 and GC100 geocell products were placed on top of the existing sand base layer (Figure 22 to Figure 27). Brief descriptions of the installation procedures are provided below.

The BX geogrid was supplied in a 3.5 m wide roll. The geogrid was unrolled along the width transverse to the direction of compaction operations. Five BX geogrid segments were placed along the total length of the BX section and each geogrid segment was overlapped and connected using zip ties (Figure 22).

Short rebar stakes were used as pegs to install the geocells. The pegs were installed at spacing of about 250 mm in the wheel direction and about 420 mm in the transverse direction corresponding to a seam length of 250 mm in the wheel direction and length of two cells across the wheel direction (Figure 23). A string was used to align peg locations and borders. The geocells were placed on the natural subgrade and were stretched out in a near circular pattern (Figure 24) as recommended by Pokharel (2010). The end cells of the geocell panels were set over the rebar stakes. A 5.2 m x 4.4 m panel was formed when the geocell was fully expanded and stacked down. Three panels were laid out for each 15 m test section. All adjacent panels were made flushed with each other and connected together using a heavy-duty pneumatic stapler along the length. Per manufacturer's recommendation, five stitches of stainless steel staples for were used GC150 and three for the GC100 at each connection along the height of the geocells to match the weld strength of the ultrasonic weld. The cells were then filled with the infill materials (Figure 25) and the rebar stakes were taken out before

compaction to avoid puncturing the roller tires. A minimum of 7.5 cm top cover of the infill material was maintained in all sections to avoid damage to geocell sections from compaction. The C30 geogrid/nonwoven geocomposite was supplied in a 3.0 m roll. The roll was cut to the required length and was placed on the test section (Figure 26). The PPWF was supplied in a 4 m wide roll. The fabric was unrolled along the test section length (Figure 27).

Fill layer 1 was placed on top of each test section using a bucket loader (Figure 28 to Figure 30). The compacted layer thickness of the fill layer 1 varied from about 130 mm to 200 mm. The fill layer was compacted using the RICM roller for 10 roller passes. Details on the operation settings for each pass are provided in Table 5. LWD testing was conducted after pass 1 and pass 10 at the surface.

Fill layer 2 was placed on the C30 section, and partially on BX and PPWF sections as shown in Figure 21. Another layer of geotextile was placed below fill layer 2 in each of these test sections as illustrated in Figure 21. The thickness of the fill layer 2 varied from about 100 to 150 mm. The test bed was compacted after fill layer 2 was placed using 16 roller passes on 5/17/11 and 3 roller passes on 5/18/11. Details on the operation settings for each pass are provided in Table 5.

In situ test locations on fill layer 2 is shown on Figure 21. LWD and DCP tests were conducted after pass 16 at all test points. LWD tests were conducted at surface, and in excavations at depths of about 50 to 70 mm and at about 90 to 180 mm below surface (Figure 31). DCPs were conducted to a depth of about 0.9 m below the surface. CPTs and NG tests were conducted at all test points after pass 19. CPTs were conducted to a depth of about 4 m below surface. NG tests were conducted using 300 mm probe penetration depth. NG tests were also conducted using the back-scattering method to compare with oven-dry moisture contents obtained from samples collected from the NG test locations. PLTs were conducted at three test locations (with one test location each in BX, GC150, and GC100 sections).

FDOT conducted vibration monitoring tests by positioning the seismograph at 7.6 m and 30.5 m away from the middle of the GC100 test section, when roller vibratory compaction passes were made using low amplitude (a = 0.90 mm) and high amplitude (a = 1.80 mm) settings.

**Figure 19. Existing sand base layer – TB1**

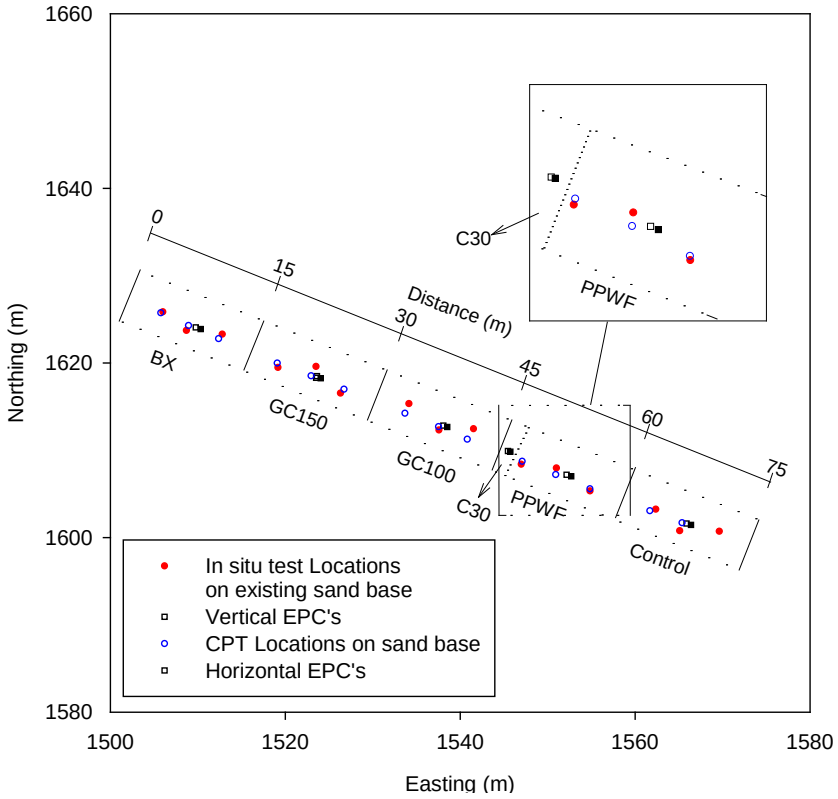


**Figure 20. Plan view of TB1 with GPS in situ test locations and locations of EPC's**

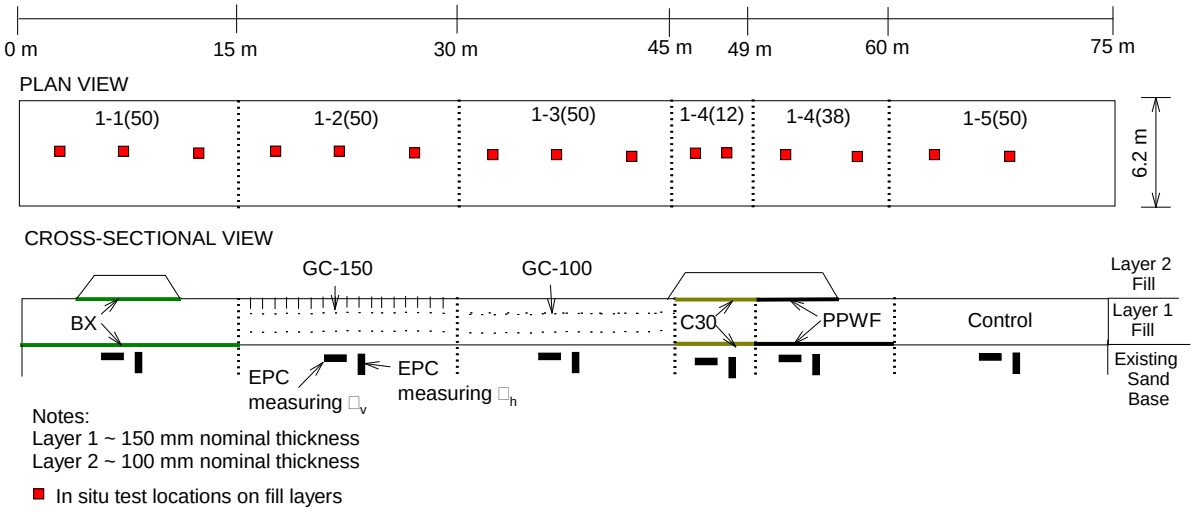


**Figure 21. Plan and cross-sectional views of TB1**

**Figure 22. Biaxial (BX) geogrid placed on the sand base layer – TB1**

**Figure 23. Rebars or pegs installed in transverse and wheel directions to aid in stretching the geocells – TB1**

**Figure 24. Stretching the geocells – TB1**


**Figure 25. GC150 and GC100 installed on the sand base layer – TB1**

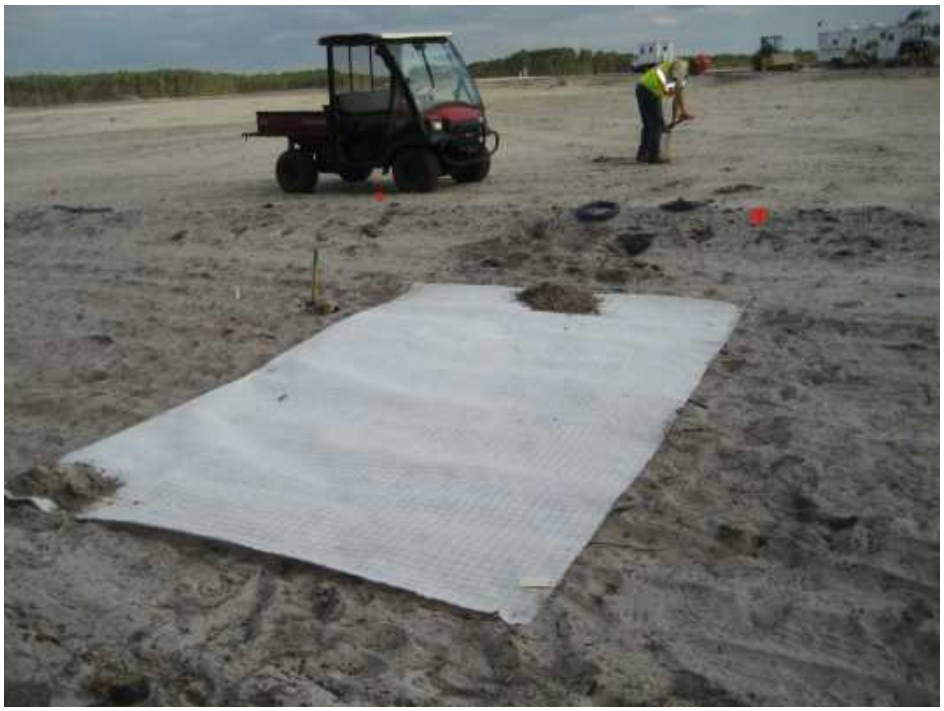

**Figure 26. Geocomposite C-30 placed on the sand base layer – TB1**

**Figure 27. Woven fabric (PPWF) placed on the sand base layer – TB1**

**Figure 28. Fill layer 1 placement on BX geogrid section – TB1**

**Figure 29. Fill layer 1 placement on GC150 section – TB1**

**Figure 30. Fill layer 1 placement on PPWF section – TB1**

**Figure 31. LWD testing on surface (left) and in excavation (right) – TB1**

### 5.2.2 RICM Measurements

MDP* and CMV measurements obtained from passes 1 to 10 on layer 1 are shown in Figure 32 and Figure 33, respectively. Similarly, MDP* and CMV measurements obtained from passes 1 to 19 after layer 2 is placed in portions of the TB (as illustrated in Figure 21) are shown in Figure 34 and Figure 35, respectively. The roller direction of travel corresponding to each compaction pass is shown on these figures.

MDP* and CMV measurements shown in Figure 32 and Figure 33 indicate that these measurements generally increased with increasing pass up to pass 4. No significant change is observed in the MDP* and CMV measurements obtained using a = 0.90 mm setting beyond pass 4. Results indicate that MDP* measurements are influenced by the vibration settings—for example, pass 6 static setting MDP* measurements were higher than pass 4 a = 0.90 mm setting and pass 5 a = 1.80 mm setting MDP* measurements (Figure 32). CMV measurements are also influenced by the vibration settings—for example, pass 5 a = 1.80 mm setting CMV measurements were higher than pass 4 or 7 a = 0.90 mm setting CMV measurements (Figure 32 and Figure 35).

Results also indicate that both MDP* and CMV RICM measurements are influenced by the roller direction of travel. This is illustrated in more detail in Figure 36 for MDP* obtained from passes 4 and 7 using a = 0.90 mm setting. The MDP* data is reported at the center of the drum. However, the MDP* measurements represent the mechanical performance of the whole roller, which are affected by the roller-soil interaction at the front drum and the rear tires. To assess the amount of influence the front drum versus the rear tire has on the MDP* measurements, the data obtained from passes 4 and 7 (with a = 0.90 mm settings) were

repositioned to match the sharp transitions or peaks observed along the TB (Figure 36). The offset distance for repositioning was observed to be about 2.60 m behind the drum center. It must be noted that this offset calculation inherently assumes that the subsurface conditions under the full length of the roller are the same in both directions of travel when the drum is positioned at a point. This clearly is not true given the fact that each section along this TB has distinctly different reinforcement system. For example, if the roller is traveling from left to right (0 m to 75 m) and the drum center is positioned at 30 m (BX/GC150 transition) the rear tire would be in the BX section. In contrary, if the roller is traveling from right to left (75 m to 0 m) the rear tire would be in the GC150 section. Further research is warranted to clearly identify/characterize the relative influence of the front drum versus the rear tires on MDP* measurements. This is an important aspect to further evaluate because it directly affects how QC/QA test measurements should be obtained to conduct calibration tests and establish target values for acceptance.

The influence of roller direction of travel on CMV measurements is illustrated in Figure 37. Using a similar procedure explained above for MDP* measurements, the offset distance for CMV measurements was obtained as 0.9 m. Unlike MDP* measurements, the CMV measurements are purely based on drum/soil interaction with minimal influence of rear tires. However, the offsetting occurs because the CMV at a given point indicates an average value over a roller travel length of about 0.5 sec (Geodynamik ALFA-030, undated). The roller travel speed for passes 4 and 7 was about 5.0 km/h; therefore, the travel distance in 0.5 sec was about 0.7 m, which is very close to the calculated 0.9 m offset distance.

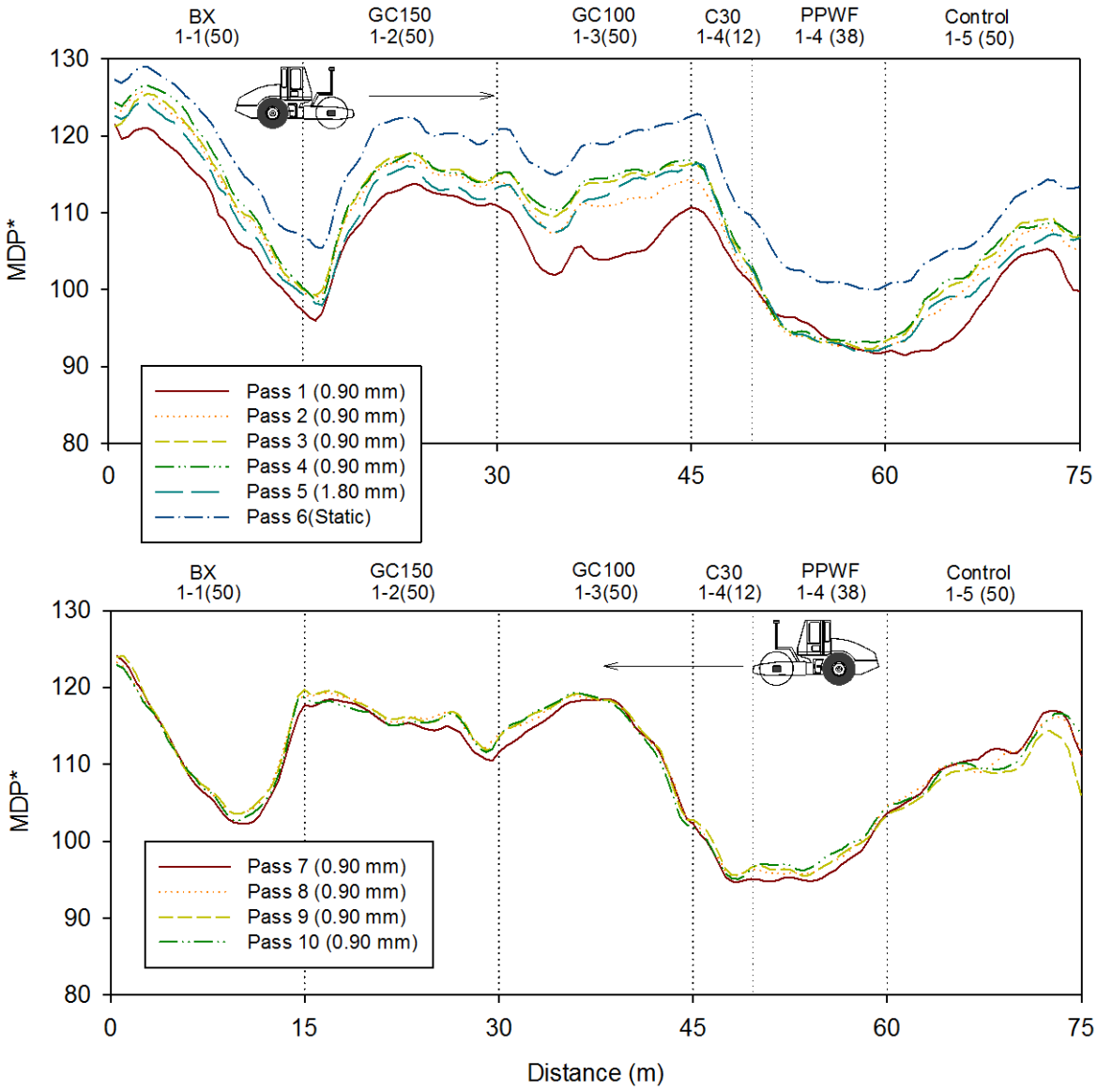


**Figure 32. Roller-integrated MDP* measurements for passes 1 to 10 on layer 1 – TB1**

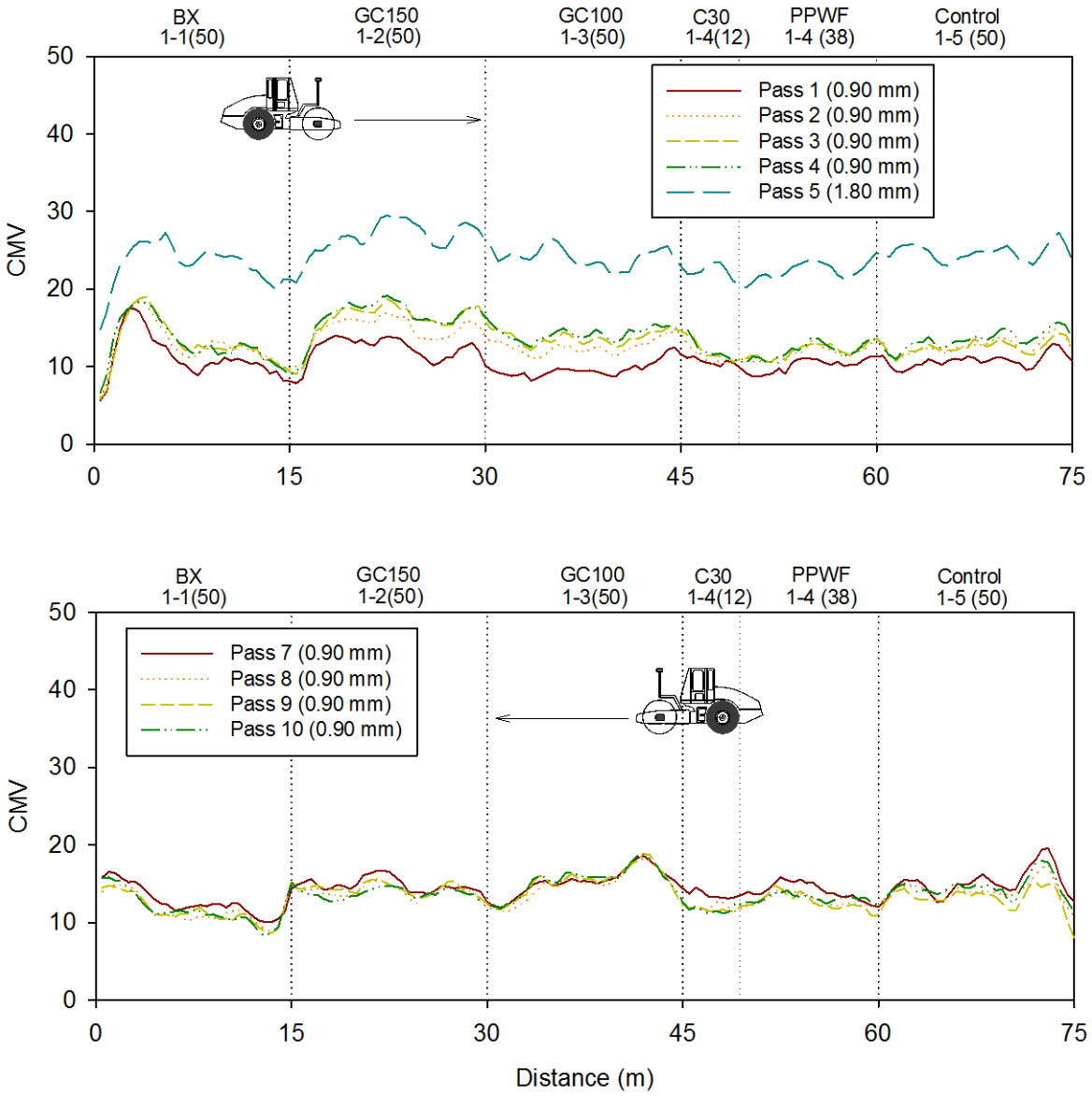


**Figure 33. Roller-integrated CMV measurements for passes 1 to 10 on layer 1 – TB1**

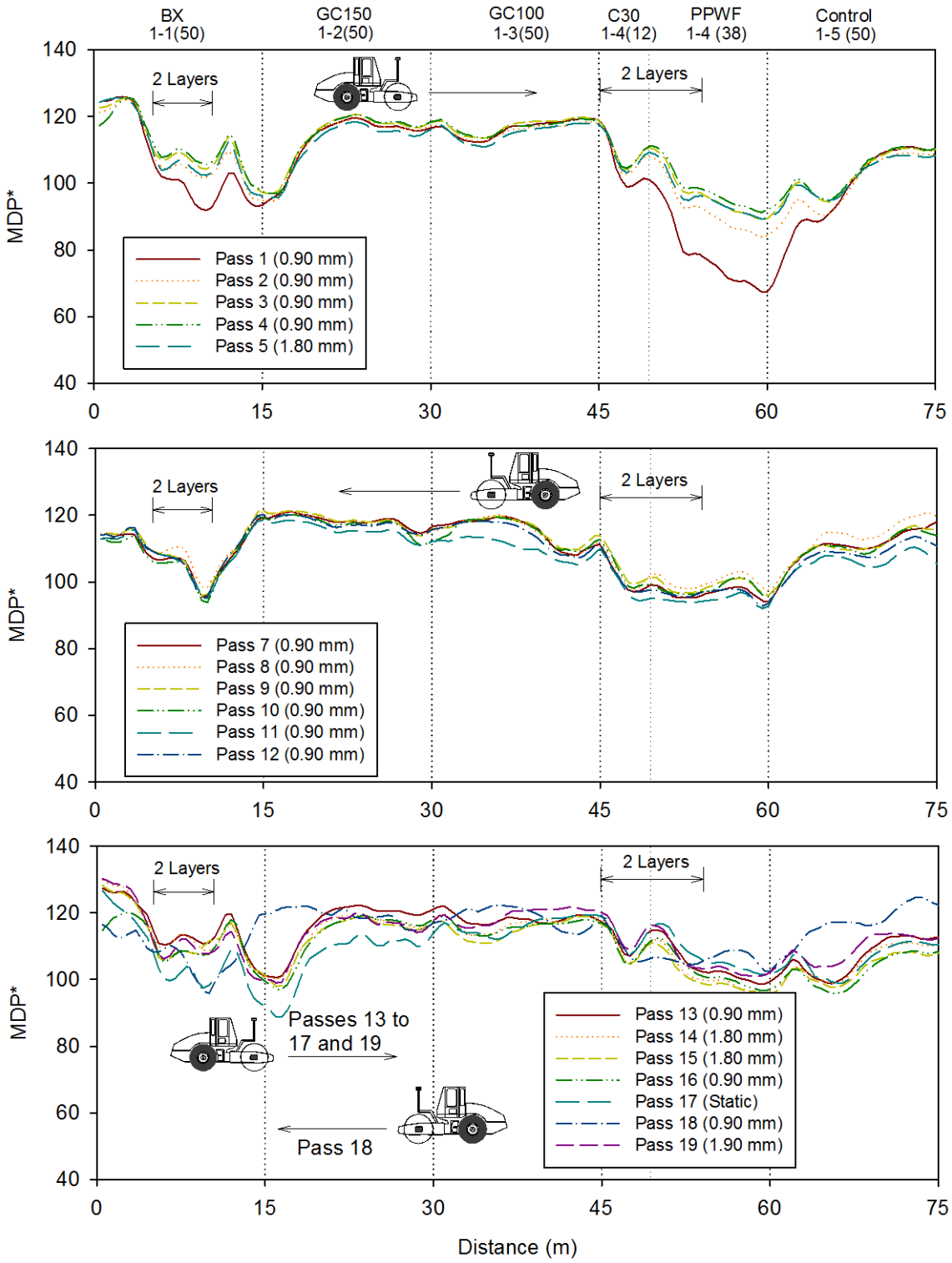


**Figure 34. Roller-integrated MDP* measurements for passes 1 to 19 after placement on layer 2 – TB1**

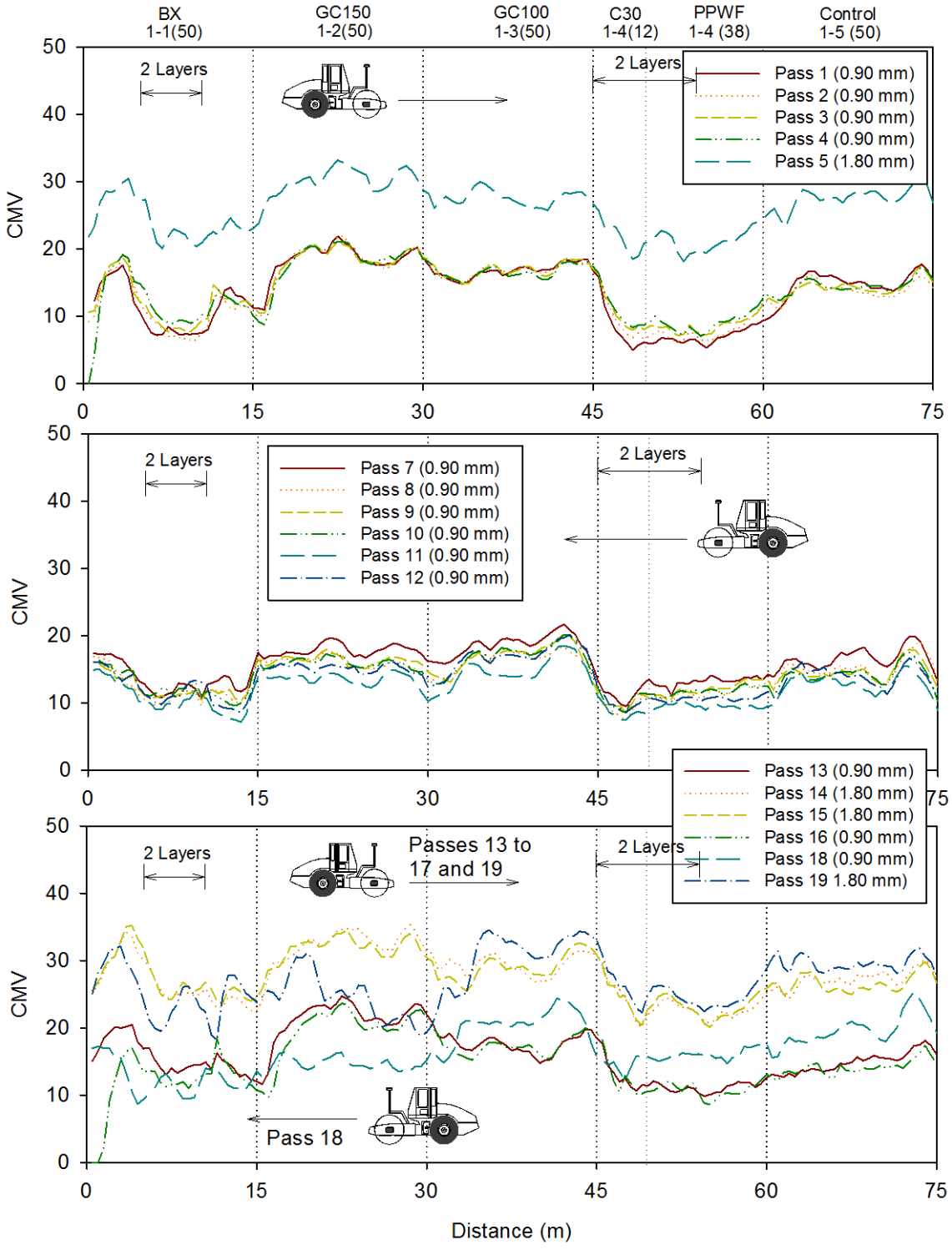


**Figure 35. Roller-integrated CMV measurements for passes 1 to 19 after placement on layer 2 – TB1**

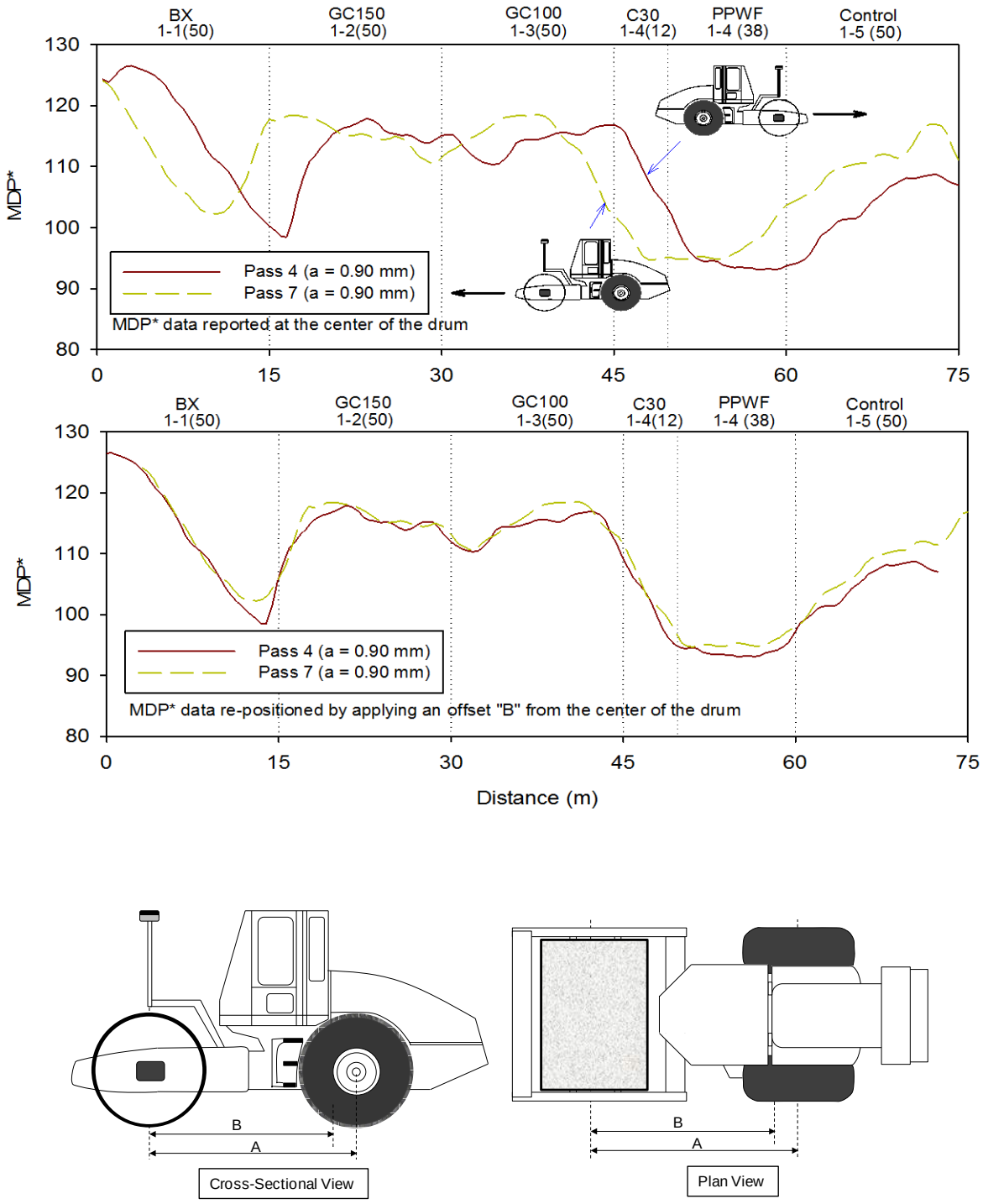


A = 2.90 m = Length between wheel bases
B = 2.60 m = Offset length used to adjust MDP* position depending on the direction of travel

**Figure 36. MDP* measurements for passes 4 and 7 (layer 1) before and after offsetting the measurements positions and a roller schematic showing the measurement offset position**

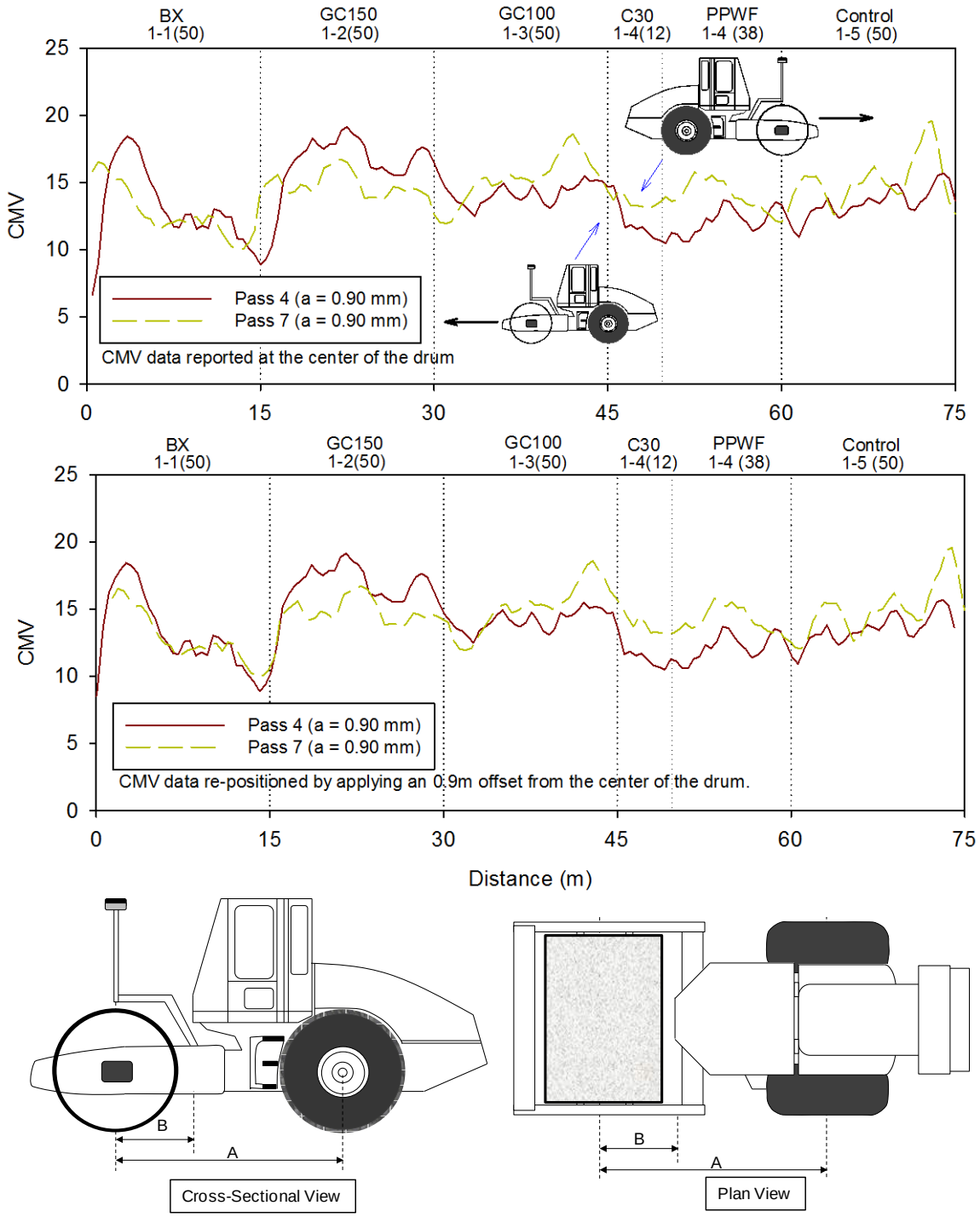


**Figure 37. CMV measurements for passes 4 and 7 (layer 1) before and after offsetting the measurements positions and a roller schematic showing the measurement offset position**

Change in the average MDP* and CMV in each section with increasing pass count are presented in Figure 38 and Figure 39. The average values for each section are calculated after offsetting the measurements as discussed above. The average MDP* and CMV values for final a = 0.90 mm and 1.80 mm passes on layers 1 and 2 are shown as bar chart plots in Figure 40. These average values for each section are also summarized in Table 6 and Table 7 along with a ratio of measurements in the reinforced and the control (unreinforced) sections for comparison. Some key observations from these comparisons are as follows:

- MDP* after compaction on layer 1: The average MDP* (a = 0.90 mm) was about 1.07 times higher in the geocell sections compared to the control section. The BX section average MDP*(a = 0.90 mm) was about the same, while the C30 and PPWF sections average MDP* (a = 0.90 mm) were about 0.90 to 0.95 times lower than the control section average MDP* (a = 0.90 mm). Similar trends were observed for MDP* measurements obtained using a = 1.80 mm setting.
- MDP* after compaction on layer 2 in BX, C30, and PPWF sections (note that BX and PPWF sections were only partially filled with 2 layers): The C30 section average MDP*(a = 0.90 mm) was about the same, while the BX and PPWF sections average MDP* (a = 0.90 mm) were about 0.94 to 0.95 times lower than the control section average MDP* (a = 0.90 mm). Similar trends were observed for MDP* measurements obtained using a = 1.80 mm setting.
- In contrary to the MDP* measurements, CMV measurements were generally lower in the reinforced sections than in the control section with the exception of measurements in the GC100 section. The BX section showed the lowest ratio values compared to all other reinforced sections.

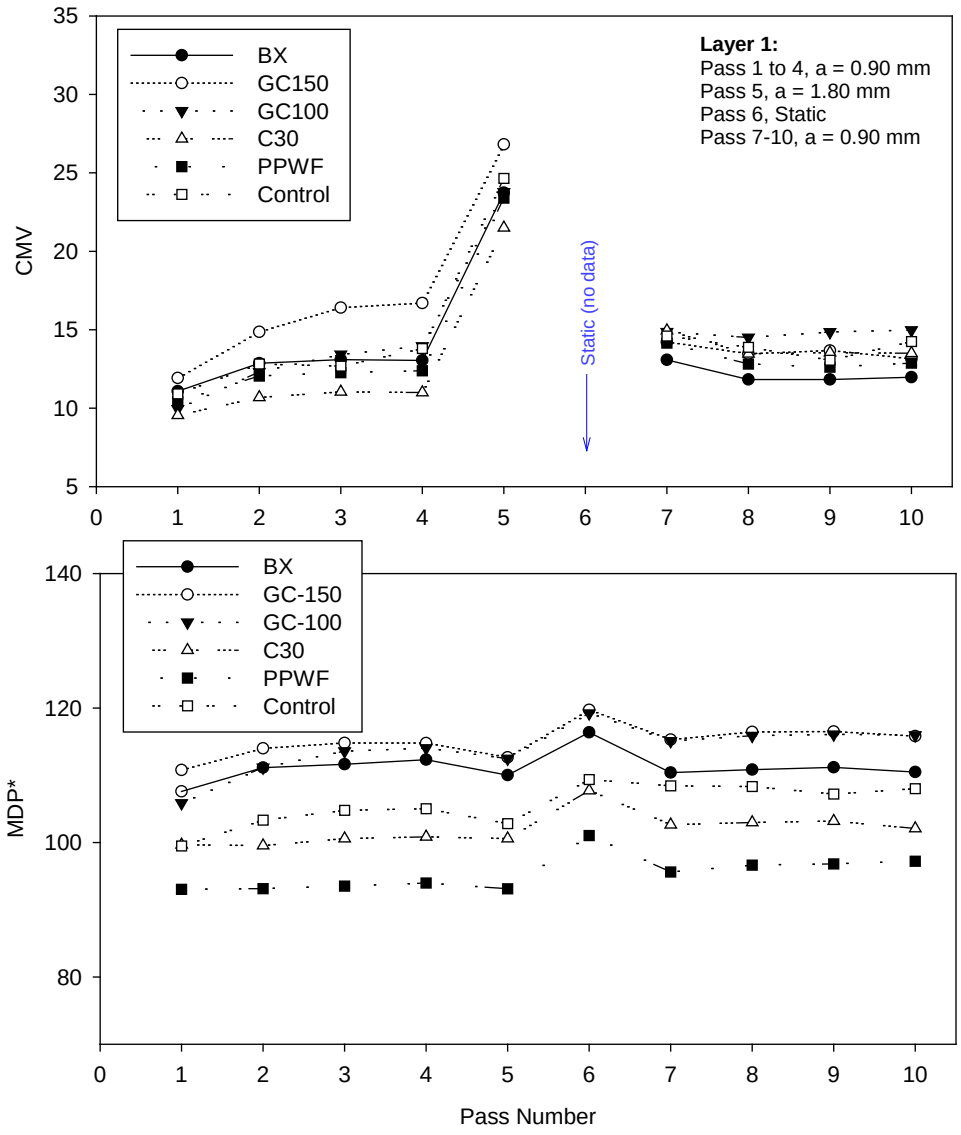


**Figure 38. Change in average MDP* and CMV measurements in each section with increasing pass count – TB1**

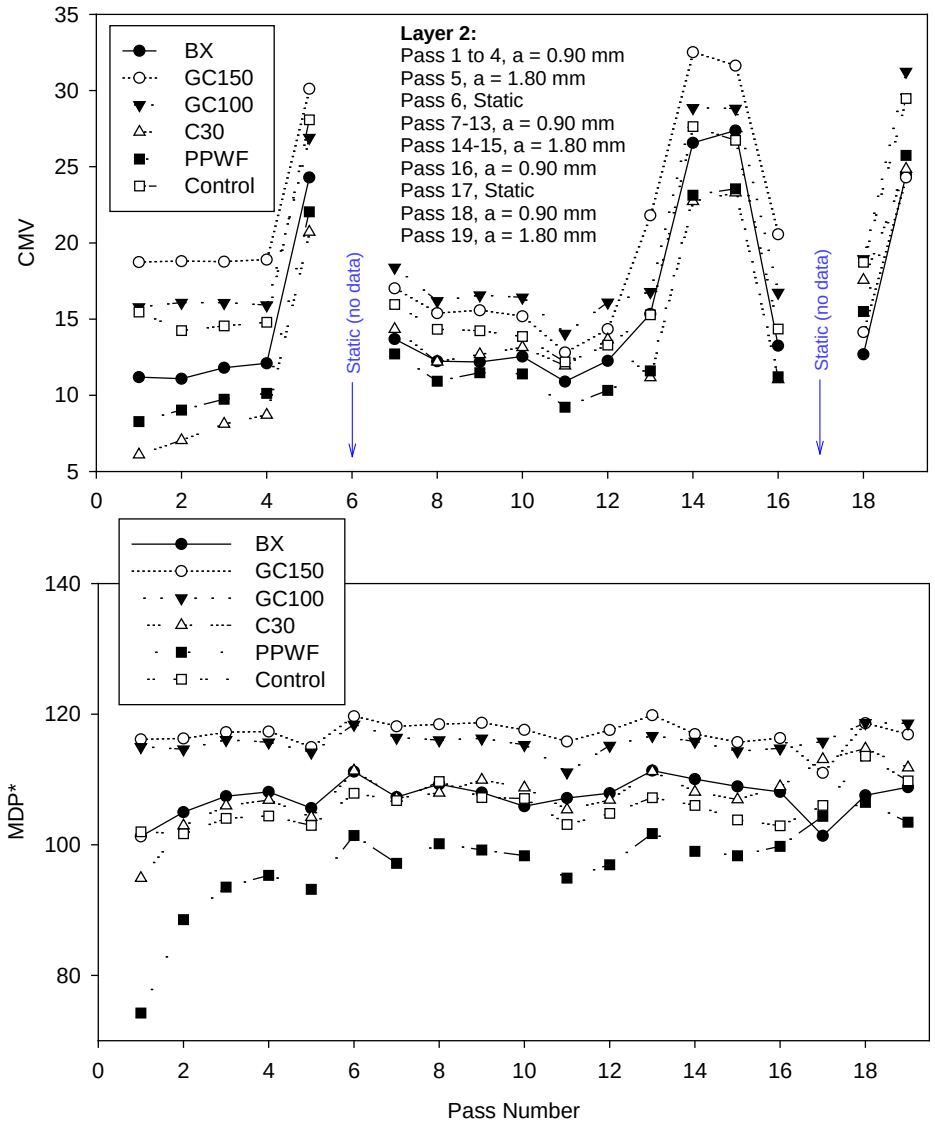


**Figure 39. Change in average MDP* and CMV measurements in each section with increasing pass count – TB1**

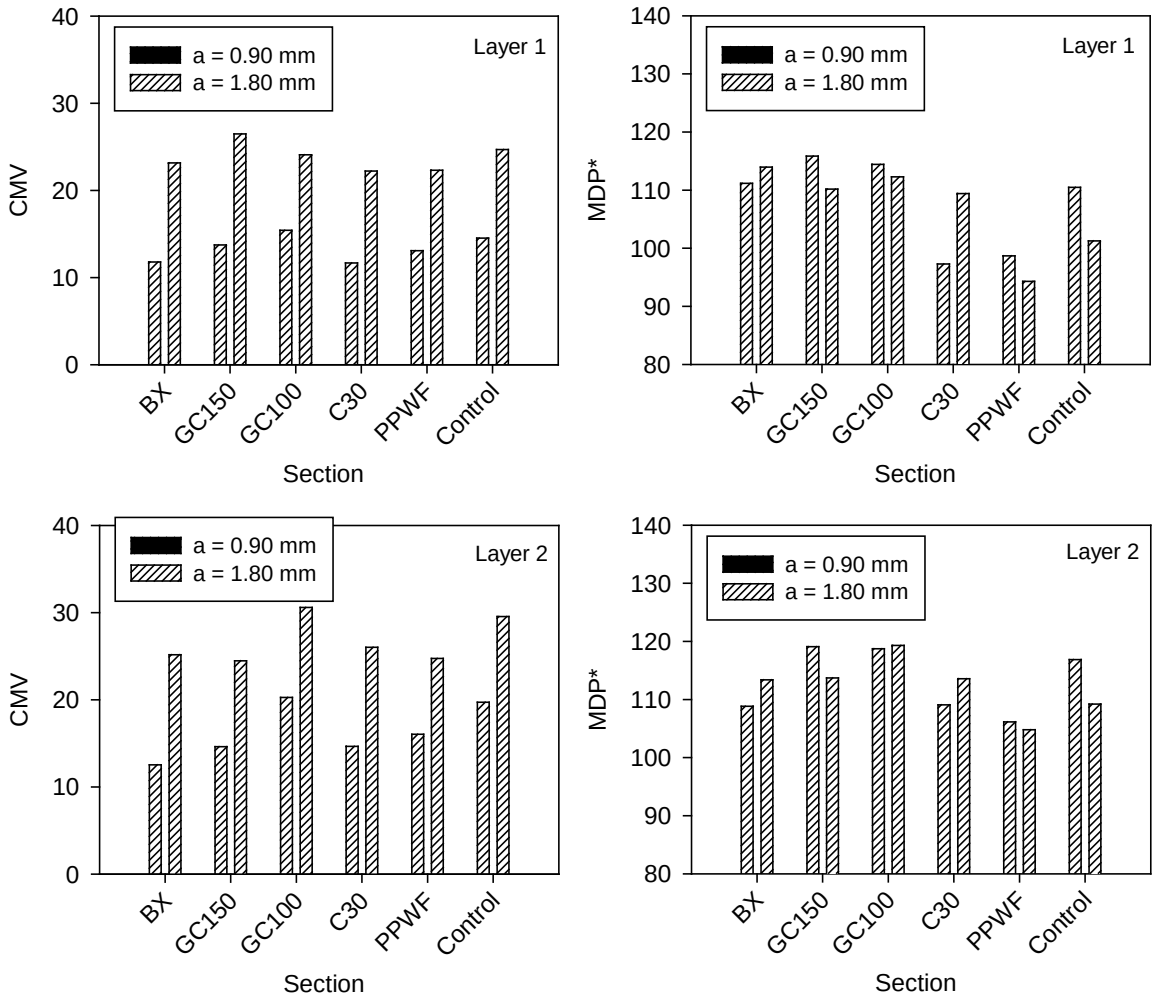


**Figure 40. Comparison of average CMV and MDP* measurements obtained using a = 0.90 mm (pass 10 for layer 1 and pass 18 for layer 2) and a = 1.80 mm (pass 5 for layer 1 and pass 19 for layer 2) settings between different sections on layer 1 and after placement of layer 2 – TB1 (note that final pass made using these settings were used in determining the average values)**

**Table 6. Comparison of average RICM and in situ test measurements between the test sections after compacting layer 1**

| Measurement | Section | | | | | |
|---|---|---|---|---|---|---|
| | **BX** | **GC150** | **GC100** | **C30** | **PPWF** | **Control** |
| *Average Measurements Per Test Section* | | | | | | |
| MDP* (a = 0.90 mm) | 110.5 | 115.8 | 116.0 | 102.1 | 97.2 | 108.0 |
| MDP* (a = 1.80 mm) | 110.0 | 112.7 | 112.5 | 100.6 | 93.1 | 102.8 |
| CMV (a = 0.90 mm) | 12.0 | 13.2 | 15.0 | 13.5 | 12.9 | 14.2 |
| CMV (a = 1.80 mm) | 23.7 | 26.8 | 23.8 | 21.5 | 23.4 | 24.6 |
| $E_{LWD}$ (MPa) | 18.5 | 28.1 | 21.3 | 17.3 | 20.7 | 17.2 |
| *Ratio of Reinforced Test Section and Control Section Measurements* | | | | | | |
| MDP* (a = 0.90 mm) | 1.02 | 1.07 | 1.07 | 0.95 | 0.90 | 1.00 |
| MDP* (a = 1.80 mm) | 1.07 | 1.10 | 1.09 | 0.98 | 0.91 | 1.00 |
| CMV (a = 0.90 mm) | 0.85 | 0.93 | 1.06 | 0.95 | 0.91 | 1.00 |
| CMV (a = 1.80 mm) | 0.96 | 1.09 | 0.97 | 0.87 | 0.95 | 1.00 |
| $E_{LWD}$ (MPa) (Pass 10) | 1.08 | 1.63 | 1.24 | 1.01 | 1.20 | 1.00 |

**Table 7. Comparison of average RICM and in situ test measurements between the test sections after compacting layer 2**

| Measurement | Section | | | | | |
|---|---|---|---|---|---|---|
| | **BX** | **GC150** | **GC100** | **C30** | **PPWF** | **Control** |
| *Average Measurements Per Test Section* | | | | | | |
| MDP* (a = 0.90 mm) | 107.6 | 118.6 | 118.7 | 114.7 | 106.5 | 113.6 |
| MDP* (a = 1.80 mm) | 108.8 | 116.9 | 118.6 | 111.8 | 103.5 | 109.8 |
| CMV (a = 0.90 mm) | 12.7 | 14.2 | 19.0 | 17.6 | 15.5 | 18.7 |
| CMV (a = 1.80 mm) | 24.5 | 24.3 | 31.3 | 24.9 | 25.8 | 29.5 |
| $E_{LWD}$ (MPa) at surface | 24.7 | 34.2 | 29.4 | 21.1 | 27.7 | 22.9 |
| $E_{LWD}$ (MPa) at about 50 to 70 mm below surface | 30.0 | 46.2 | 36.0 | 27.1 | 33.0 | 30.0 |
| E (MPa) after 10 load cycles | 36.3 | 43.3 | 38.4 | No Measurements | | |
| Perm. Def. after 10 load cycles (mm) | 5.6 | 4.1 | 4.9 | | | |
| $\gamma_d$ (kN/m$^3$) | 14.86 | 15.26 | 15.33 | 15.03 | 15.08 | 15.29 |
| *Ratio of Reinforced Test Section and Control Section Measurements* | | | | | | |
| MDP* (a = 0.90 mm) | 0.95 | 1.04 | 1.04 | 1.01 | 0.94 | 1.00 |
| MDP* (a = 1.80 mm) | 0.99 | 1.06 | 1.08 | 1.02 | 0.94 | 1.00 |
| CMV (a = 0.90 mm) | 0.68 | 0.76 | 1.02 | 0.94 | 0.83 | 1.00 |
| CMV (a = 1.80 mm) | 0.83 | 0.82 | 1.06 | 0.84 | 0.87 | 1.00 |
| $E_{LWD}$ (MPa) at surface (Pass 16) | 1.08 | 1.49 | 1.28 | 0.92 | 1.21 | 1.00 |
| $E_{LWD}$ (MPa) at about 50 to 70 mm below surface (Pass 16) | 1.00 | 1.54 | 1.20 | 0.90 | 1.10 | 1.00 |
| $\gamma_d$ (kN/m$^3$) (Pass 19) | 0.97 | 1.00 | 1.00 | 0.98 | 0.99 | 1.00 |

### 5.2.3 In Situ Test Measurements

LWD modulus measurements obtained from each test section on the existing sand base layer, on layer 1 after passes 1 and 10, and on layers 1 and 2 after pass 16 are shown in Figure 41. The average LWD modulus for each test section and the ratio of average LWD modulus in reinforced and control sections are summarized in Table 6 and Table 7. LWD modulus values in the C30 section were the lowest, while LWD modulus values in the GC150 section were the highest of all test sections. On average, LWD modulus at surface in all reinforced sections (except in C30 section) were about 1.1 to 1.6 times higher than in the control section. LWD modulus values obtained in the excavation were higher (by about 1.2 to 1.4 times) than the measurements obtained at the surface, illustrating the influence of lateral confinement on modulus in sandy soils.

Dry unit weight and moisture content results obtained from NG tests on the existing sand base, and layers 1 or 2 after pass 19 are shown in Figure 42. Dry unit weight and moisture content results obtained from sand cone tests on GC150 and GC100 sections are also shown in Figure 42. NG test results on the existing sand base layer indicate that the relative compaction varied from about 88% to 102% with an average of about 97% and the moisture contents varied from about 4.5% to 12.8% dry of optimum with an average of about 9.7% dry of optimum, with reference to standard Proctor test results. NG test results on the fill layers indicate that the relative compaction varied from about 97% to 102% with an average of about 99% and the moisture contents varied from about 9.6% to 12.6% dry of optimum with an average of about 11.3% dry of optimum, with reference to standard Proctor test results. Average dry unit weight in each test section and ratios of average dry unit weight in the reinforced and Control sections for fill layers are shown in Table 7. On average, the GC100 and GC150 sections resulted in same dry unit weights while the BX, C30, and PPWF sections resulted in slightly lower (about 0.97 to 0.99) dry unit weights than the Control section.

Sand cone test dry unit weight results generally showed slightly higher values than NG test dry unit weight results, with the exception of one test location in the GC100 test section. Based on sand cone test results, the relative compaction of the sand fill material in the GC100 and GC150 test sections varied from about 99% to 104% with an average of about 102%, with reference to standard Proctor test results. As explained earlier in the test methods section of this report, it must be noted that the sand cone tests were conducted to determine the dry unit weight of the material within the geocell by excavating any material above the geocell (Figure 13). On the other hand, NG tests were conducted at the surface without any excavation (Figure 12) and therefore, some differences between NG and sand cone tests must be expected.

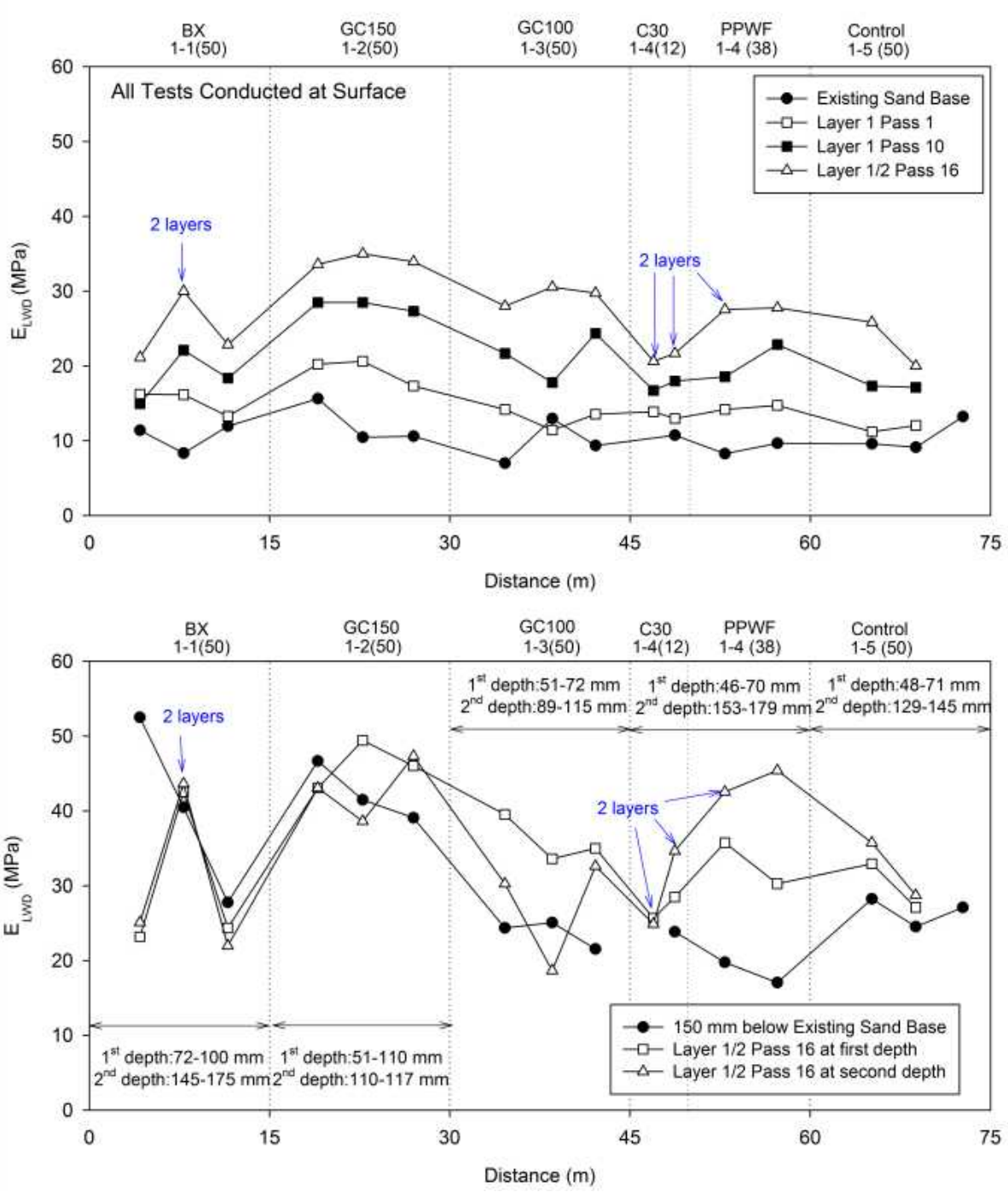


**Figure 41. LWD modulus test results on existing sand base and fill layers (tests conducted in excavation) – TB1**

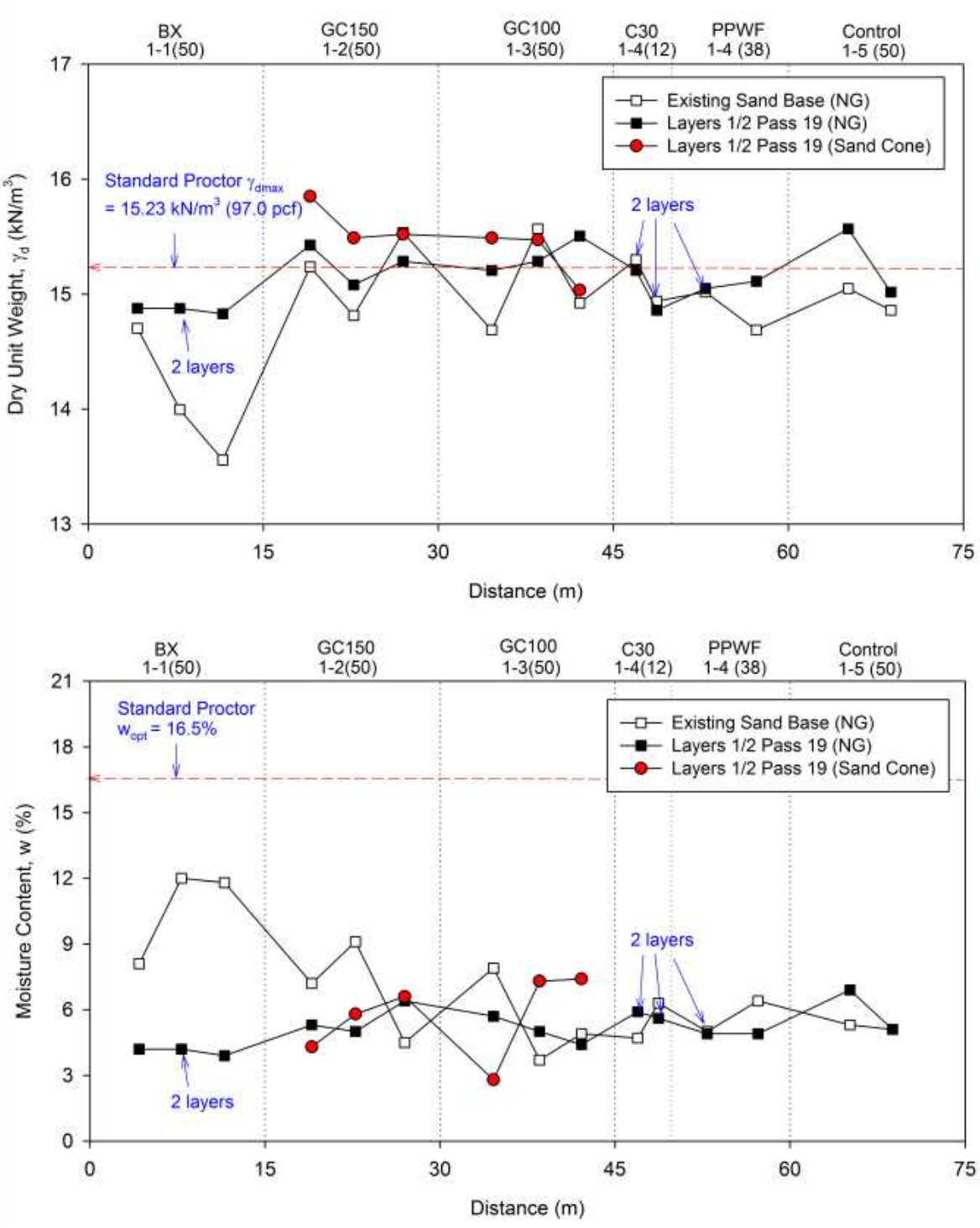


**Figure 42. In situ dry unit weight and moisture content test results on fill layer 1 – TB1**

To validate moisture content measurements obtained from NG, bag samples were obtained from each NG test location to determine oven-dry moisture contents. Results comparing the NG moisture contents and oven-dry moisture contents are shown in Figure 43, which show that on average the NG moisture contents were about 0.93 times the oven-dry moisture contents.

PLT results for ten loading and unloading cycles with plate contact results versus deflection measurements from the BX, GC150, and GC100 test sections are shown in Figure 44. Permanent deformation at the end of each loading/unloading cycle and elastic modulus determined for each loading cycle (for contact stress range = 200 to 400 kPa) are shown in Figure 45 and Figure 46, respectively. Also shown in Figure 46 is modulus of subgrade reaction, *k*, for each loading cycle. The test in GC150 section showed the lowest permanent deformation (4.1 mm) and the BX section showed the highest permanent deformation (5.6 mm) at the end of 10 cycles. The modulus values generally increased with increasing loading cycles, but the rate of increase decreased after 5 loading cycles. The test in GC150 section showed the highest modulus (E = 161 MPa) for the $10^{th}$ loading cycle while the test in the GC100 section showed the lowest modulus (E = 125 MPa).

A comparison of the average LWD modulus, PLT modulus and modulus of subgrade reaction (for $1^{st}$ loading cycle), PLT permanent deformation (at the end of 10 loading/unloading cycles), NG dry unit weight, and NG moisture content measurements between different sections on layers 1 or 2 is shown in Figure 47.

CPT profiles showing cone tip resistance ($q_t$), sleeve friction ($f_s$), friction ratio ($F_r$), SPT blow count ($N_{60}$), and soil identification for tests conducted on the existing sand layer and on fill layers 1 or 2 (after pass 19) are shown in Figure 48 to Figure 53. Tests conducted in each test section are grouped in each figure. Similarly, DCP test profiles showing DPI, CBR, and cumulative blows for tests conducted on the existing sand layer and on fill layers 1 or 2 (after pass 19) are shown in Figure 54 to Figure 59. The CPT and DCP profiles were primarily conducted to evaluate the compaction influence depth, i.e., the depth up to which the soil properties are affected due to vibratory compaction at the surface. The DCP profiles show at least some level of increase in CBR down to the termination depth of about 0.9 m below surface at all test locations. Change in $q_t$ and $N_{60}$ values are presented in Figure 60 and Figure 61, respectively. Test measurements obtained from each test section are grouped in these figures. The $q_t$ and $N_{60}$ profiles generally showed improvements up to a depth of about 0.9 m to 1.8 m. No obvious differences could be discerned in the CPT/DCP profiles between the test sections.

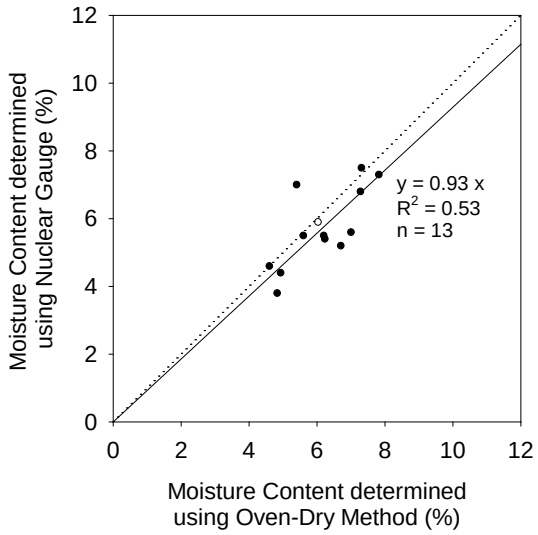


**Figure 43. Comparison between moisture determined using nuclear gauge and oven-dry methods – TB1**

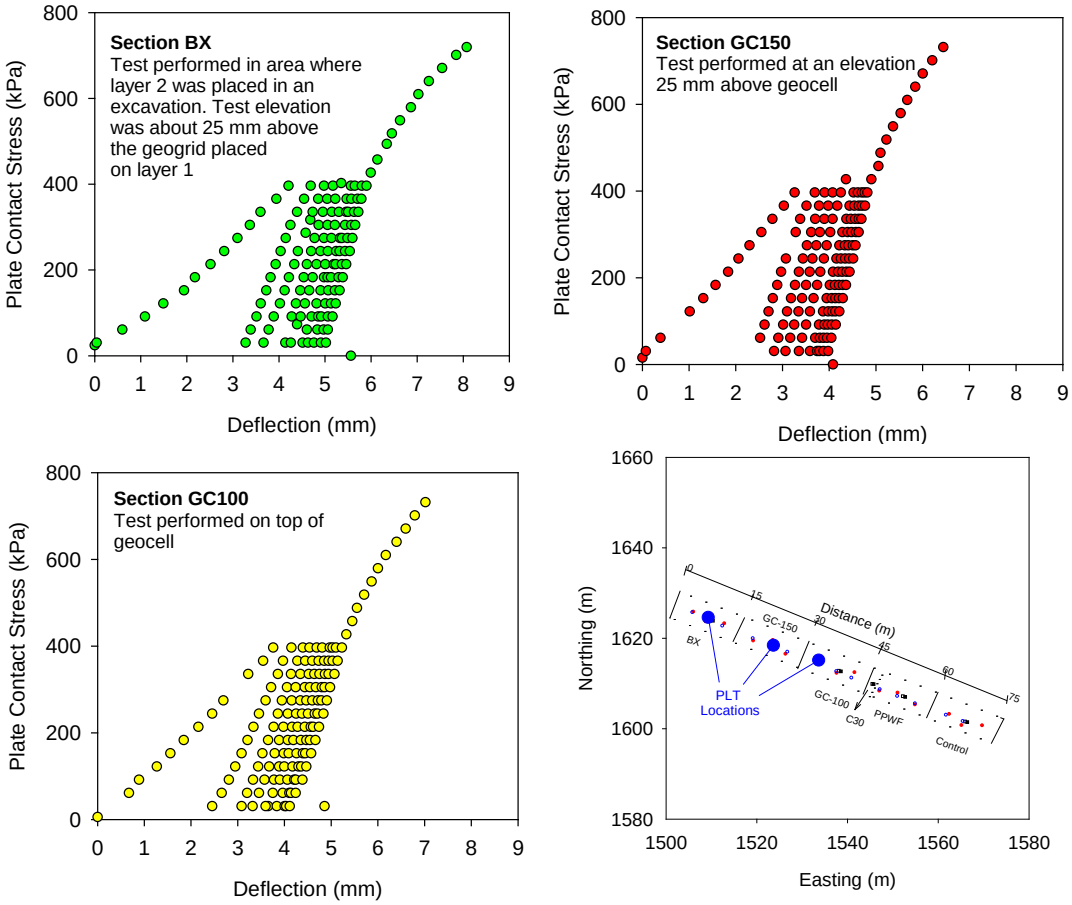


**Figure 44. PLT contact stress versus deflection results at three test locations and location of PLTs – TB1**

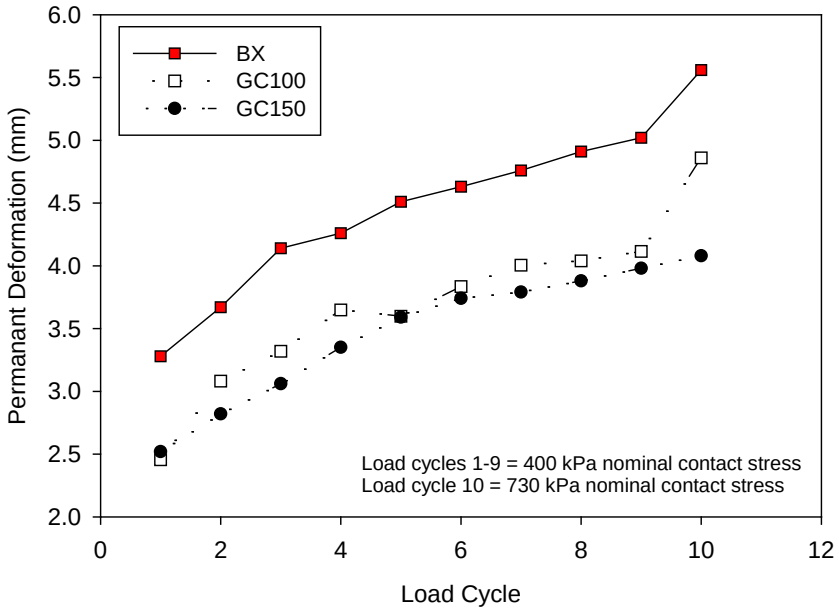


**Figure 45. Permanent deformation versus static PLT load cycle at three test locations – TB1**

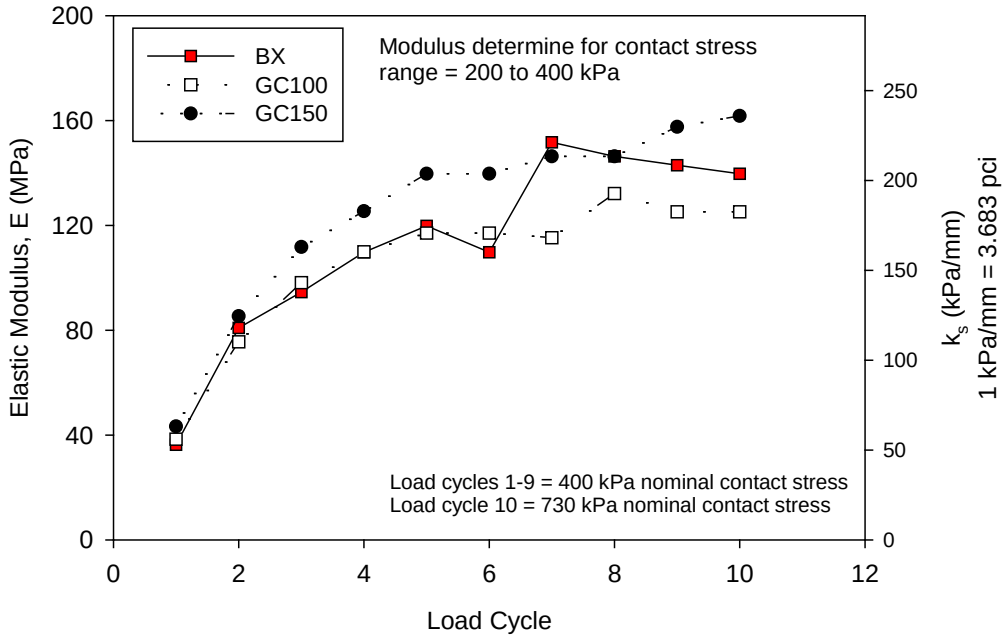


**Figure 46. Elastic modulus/modulus of subgrade reaction versus static PLT load cycle at three test locations – TB1**

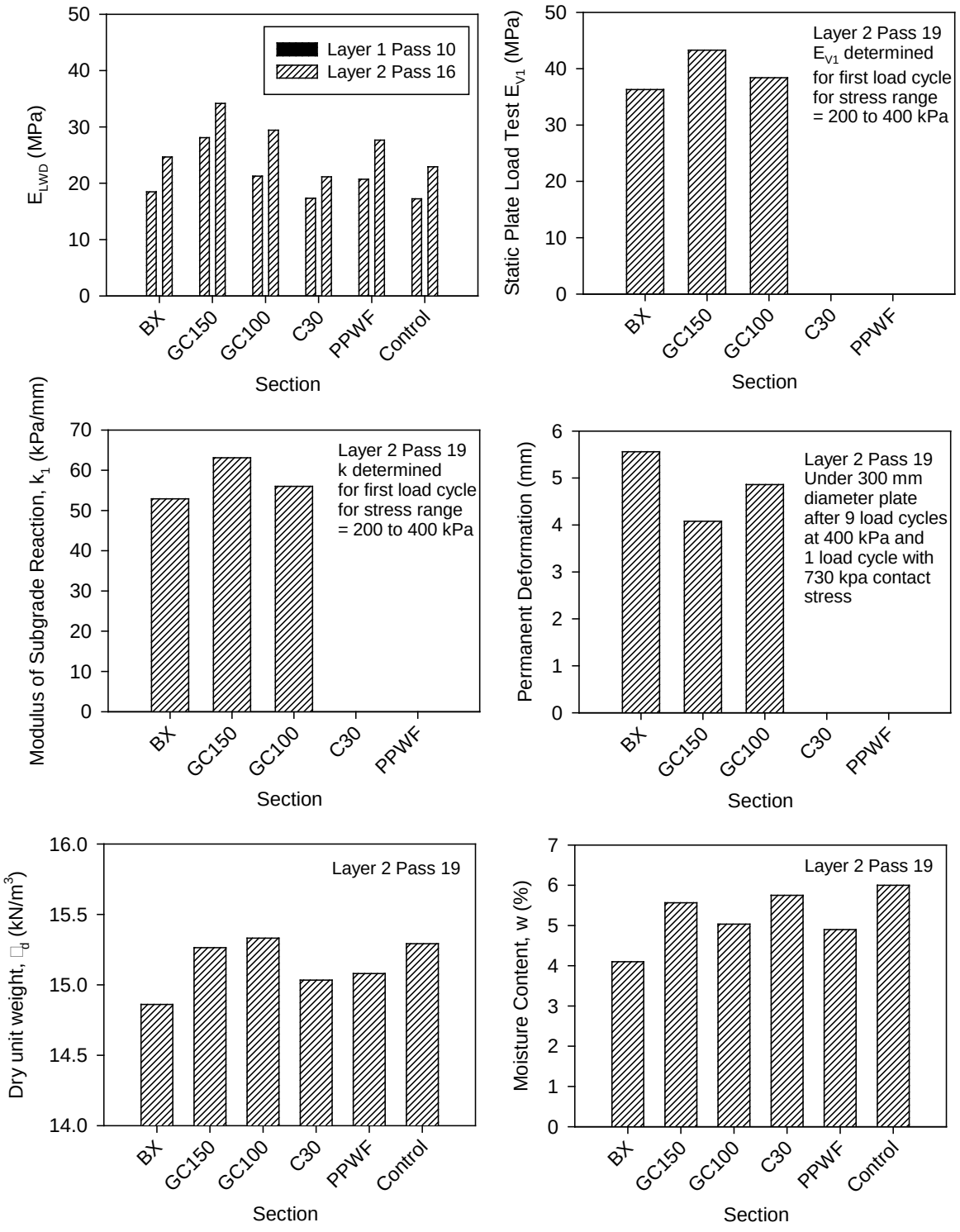


**Figure 47. Comparison of average in situ measurements between different sections on layer 1 and after placement of layer 2 – TB1**

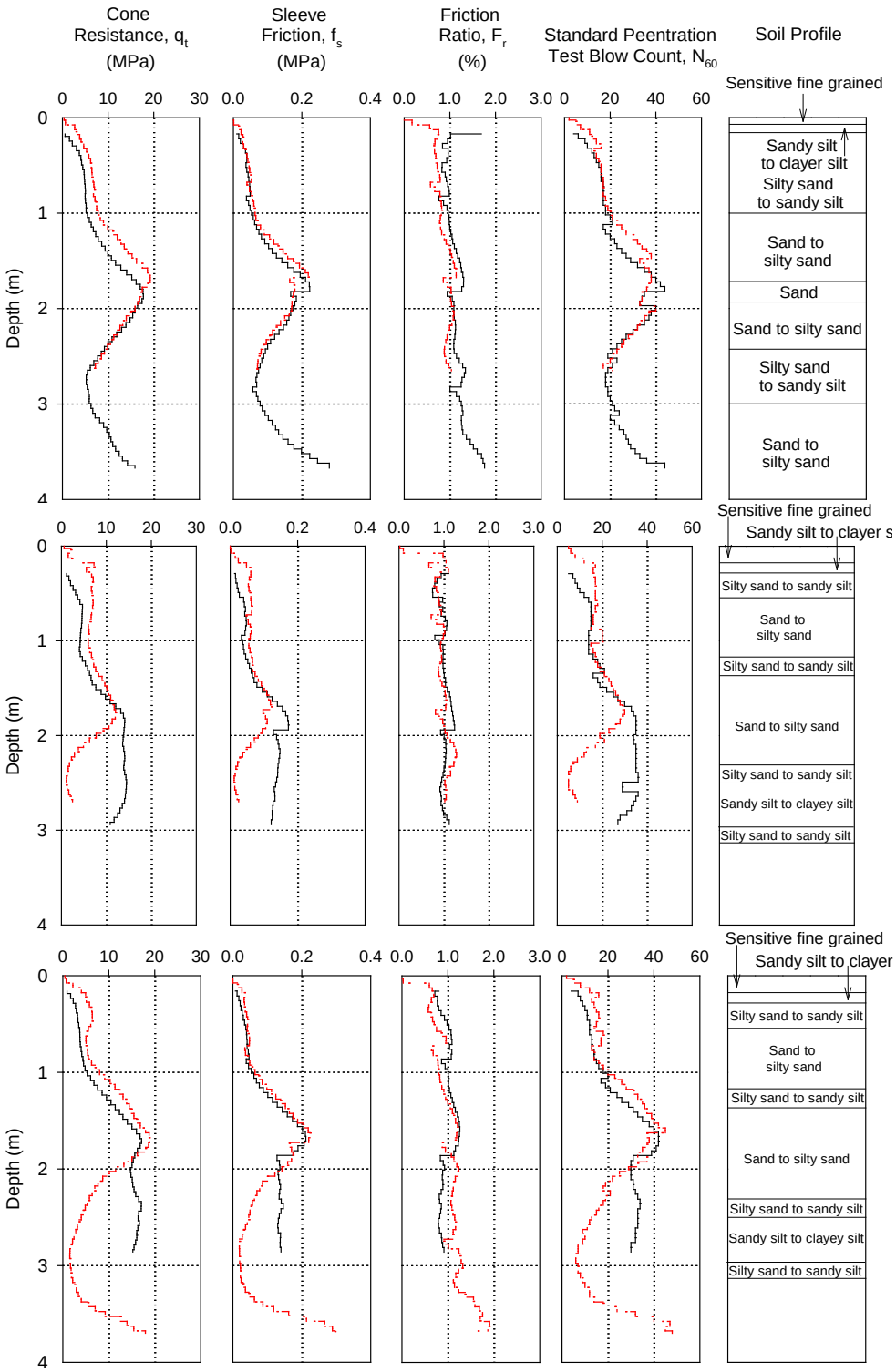


**Figure 48. CPT profiles at three test locations in 1-1(50) BX section (solid line represents test on the existing sand base, dashed line represents test after Pass 19) – TB1**

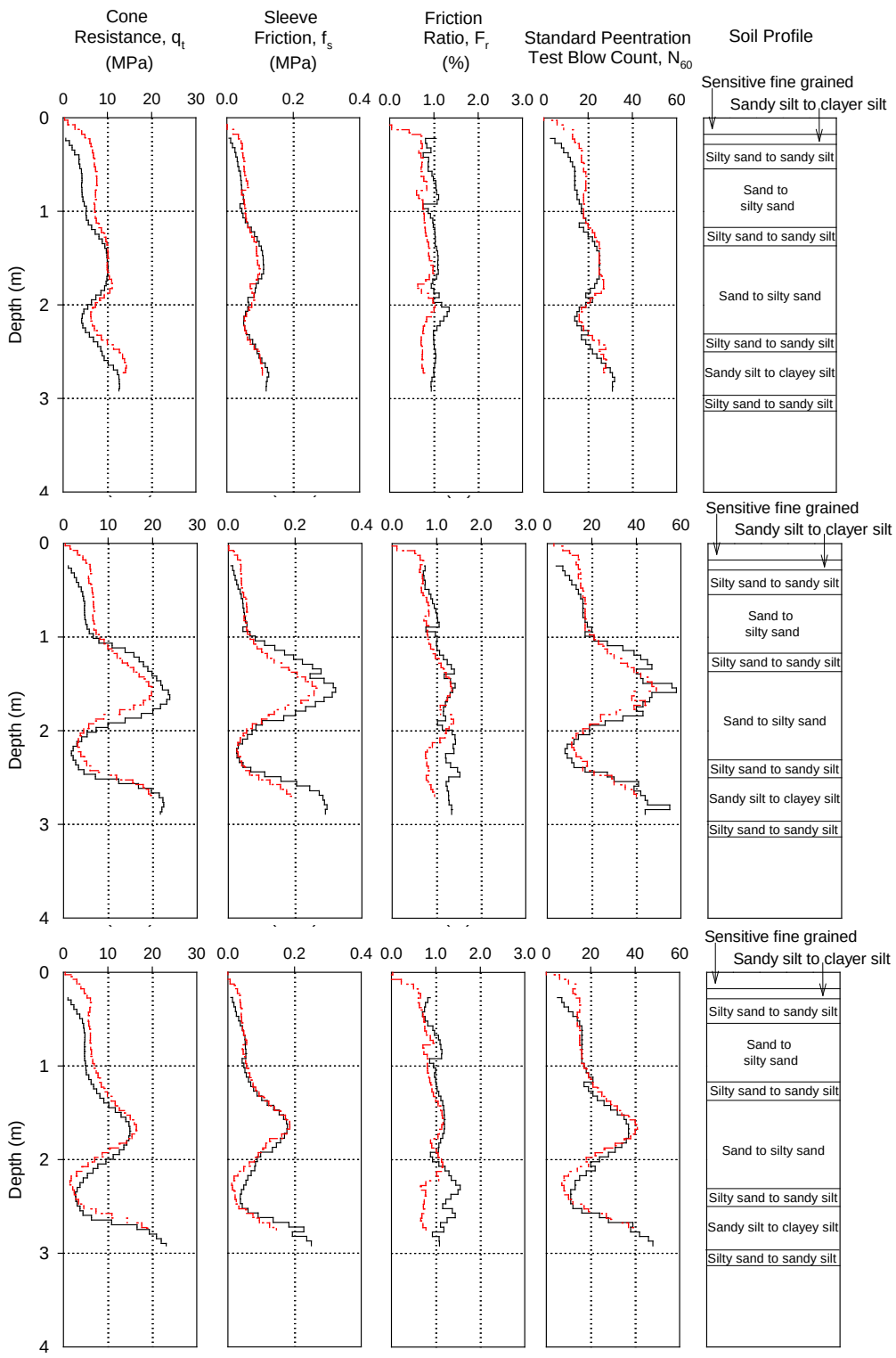


**Figure 49. CPT profiles at three test locations in 1-2(50) GC150 section (solid line represents test on the existing sand base, dashed line represents test after Pass 19) – TB1**

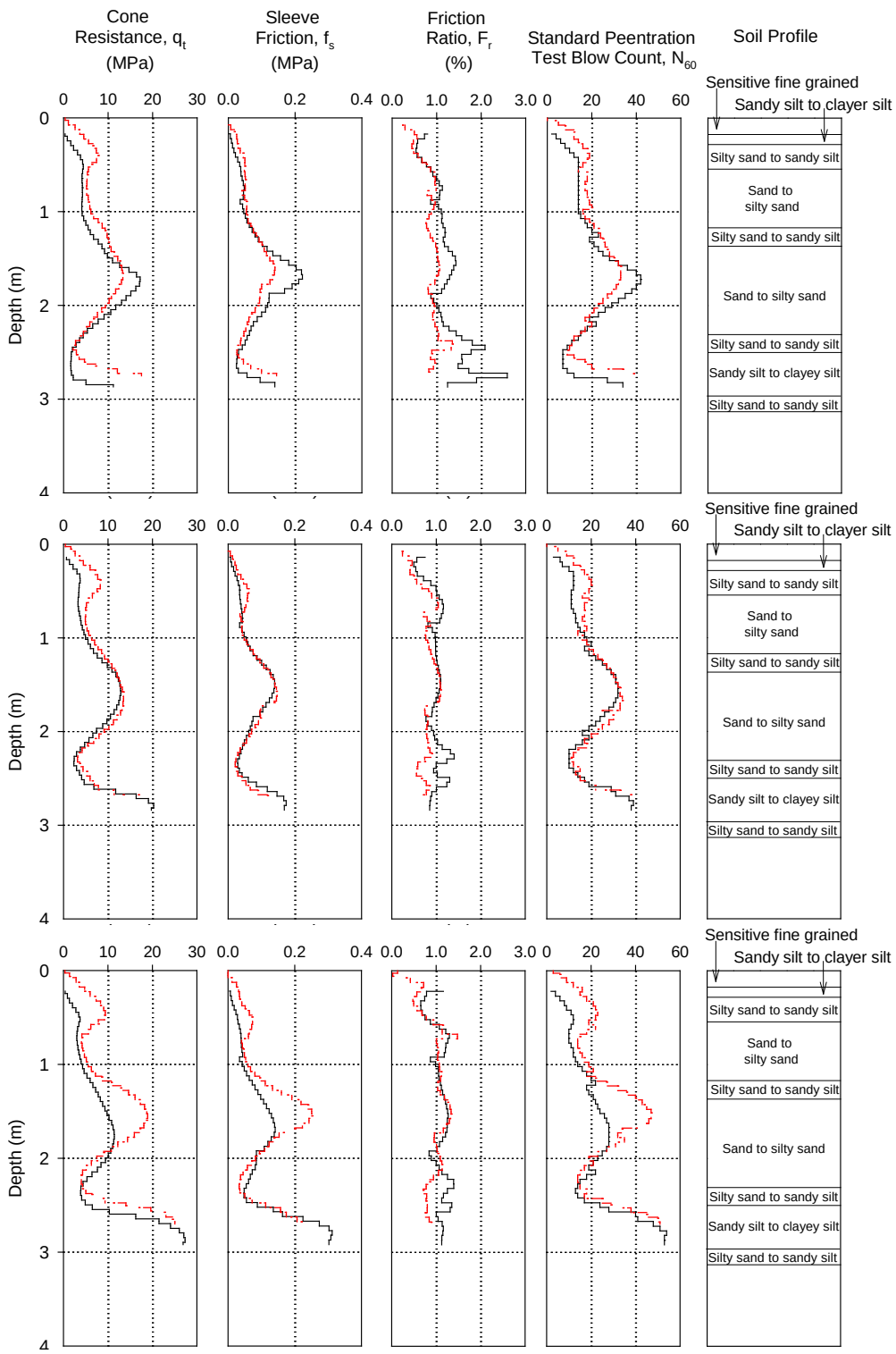


**Figure 50. CPT profiles at three test locations in 1-3(50) GC100 section (solid line represents test on the existing sand base, dashed line represents test after Pass 19) – TB1**

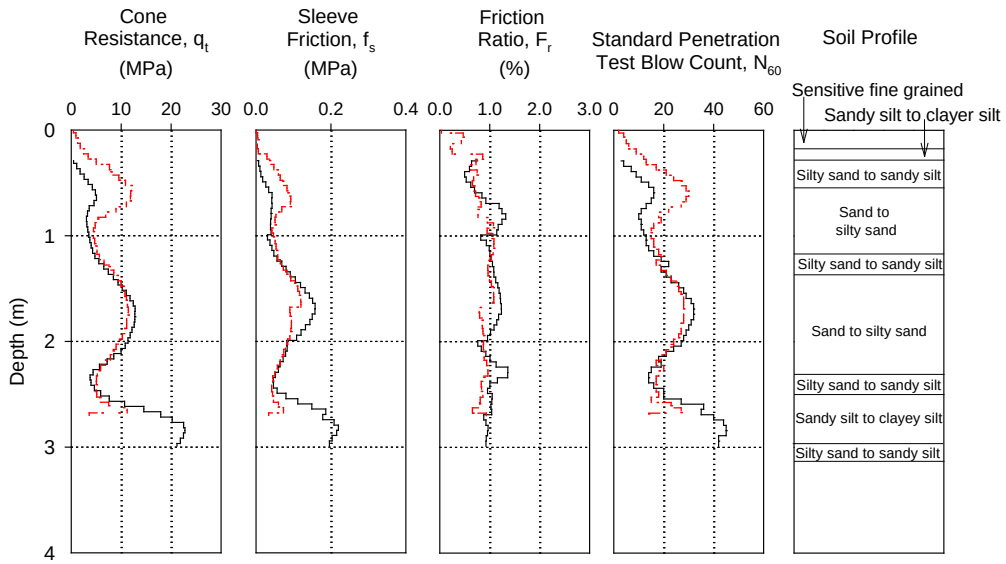


**Figure 51. CPT profiles at one test locations in 1-4(12) C30 section (solid line represents test on the existing sand base, dashed line represents test after Pass 19) – TB1**

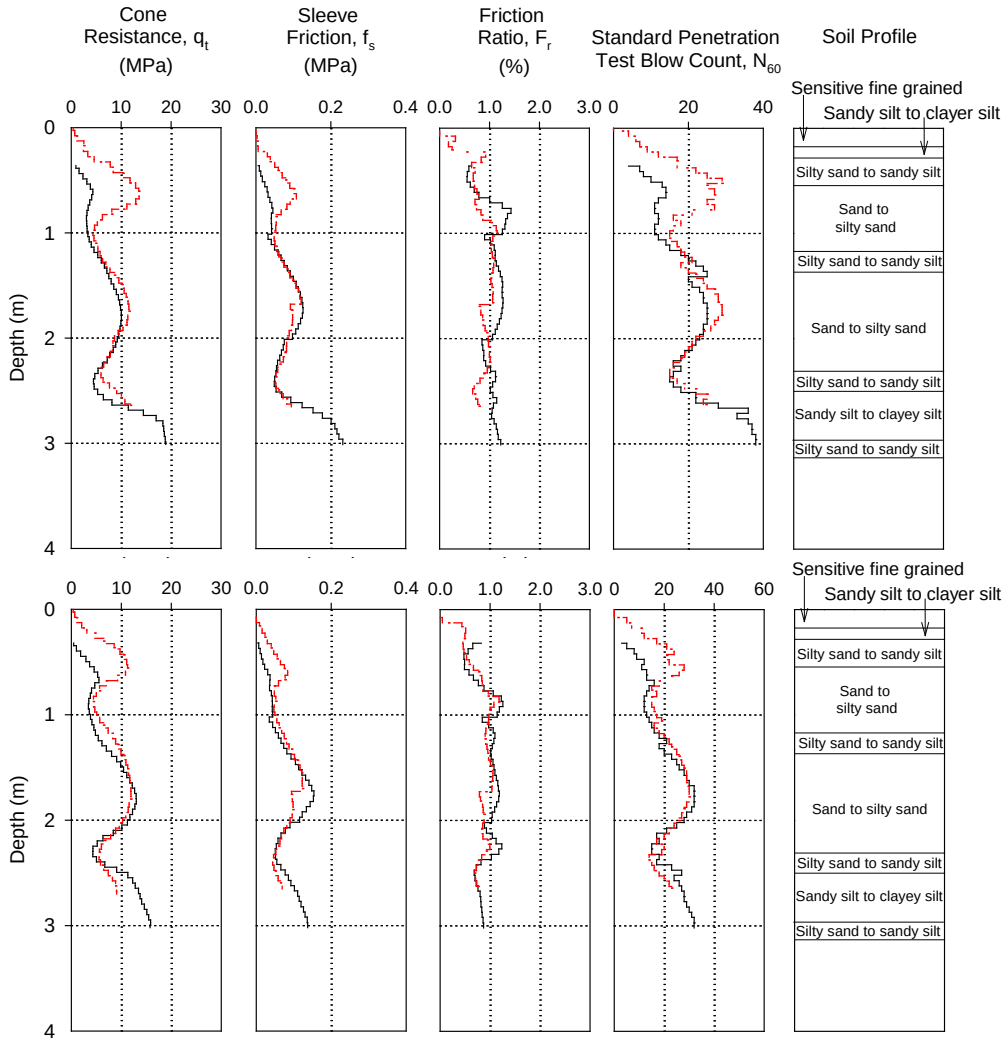


**Figure 52. CPT profiles at two test locations in 1-4(38) PPWF section (solid line represents test on the existing sand base, dashed line represents test after Pass 19) – TB1**

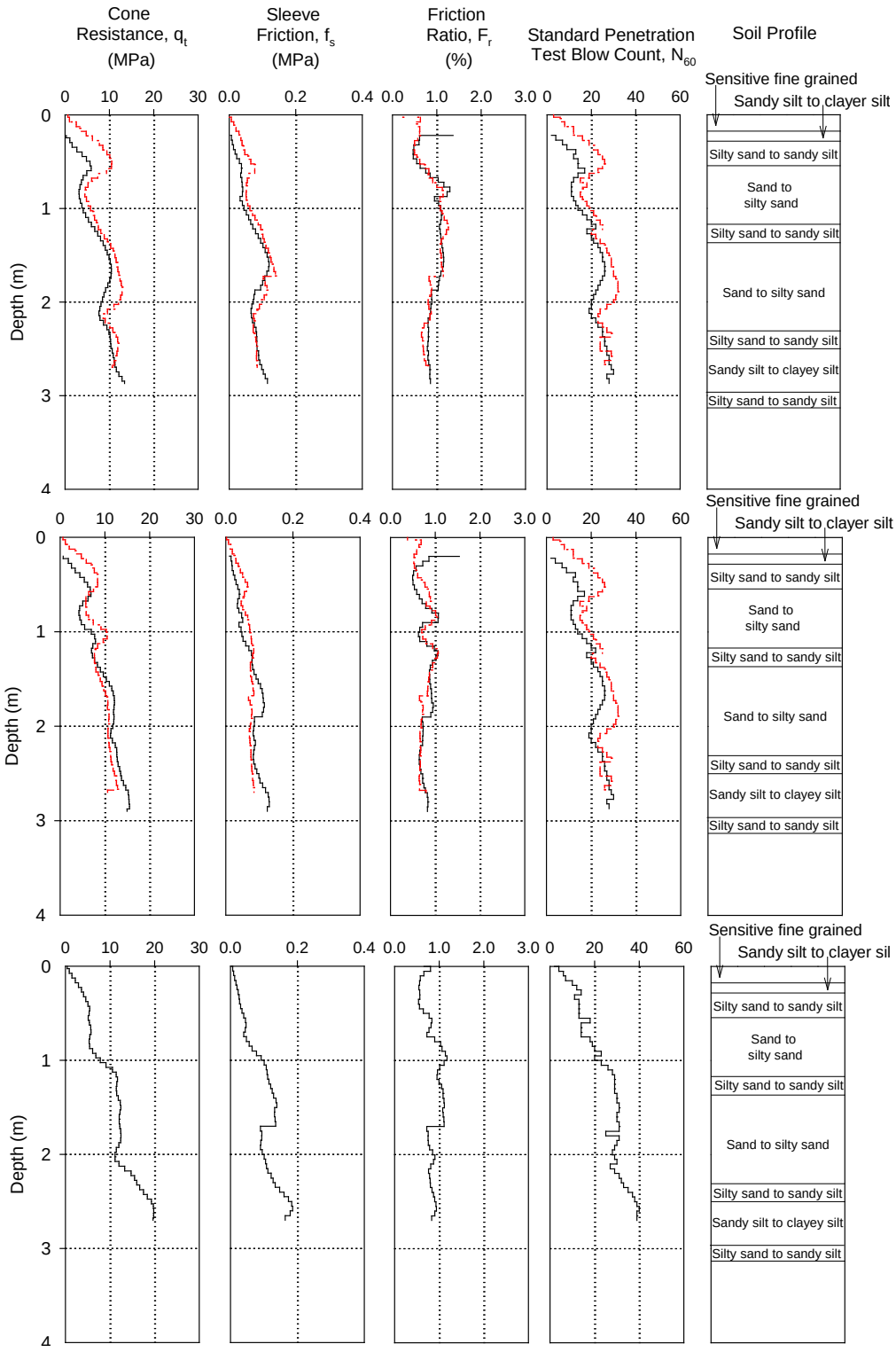


**Figure 53. CPT profiles at three test locations in 1-5(50) control section (solid line represents test on the existing sand base, dashed line represents test after Pass 19) – TB1**

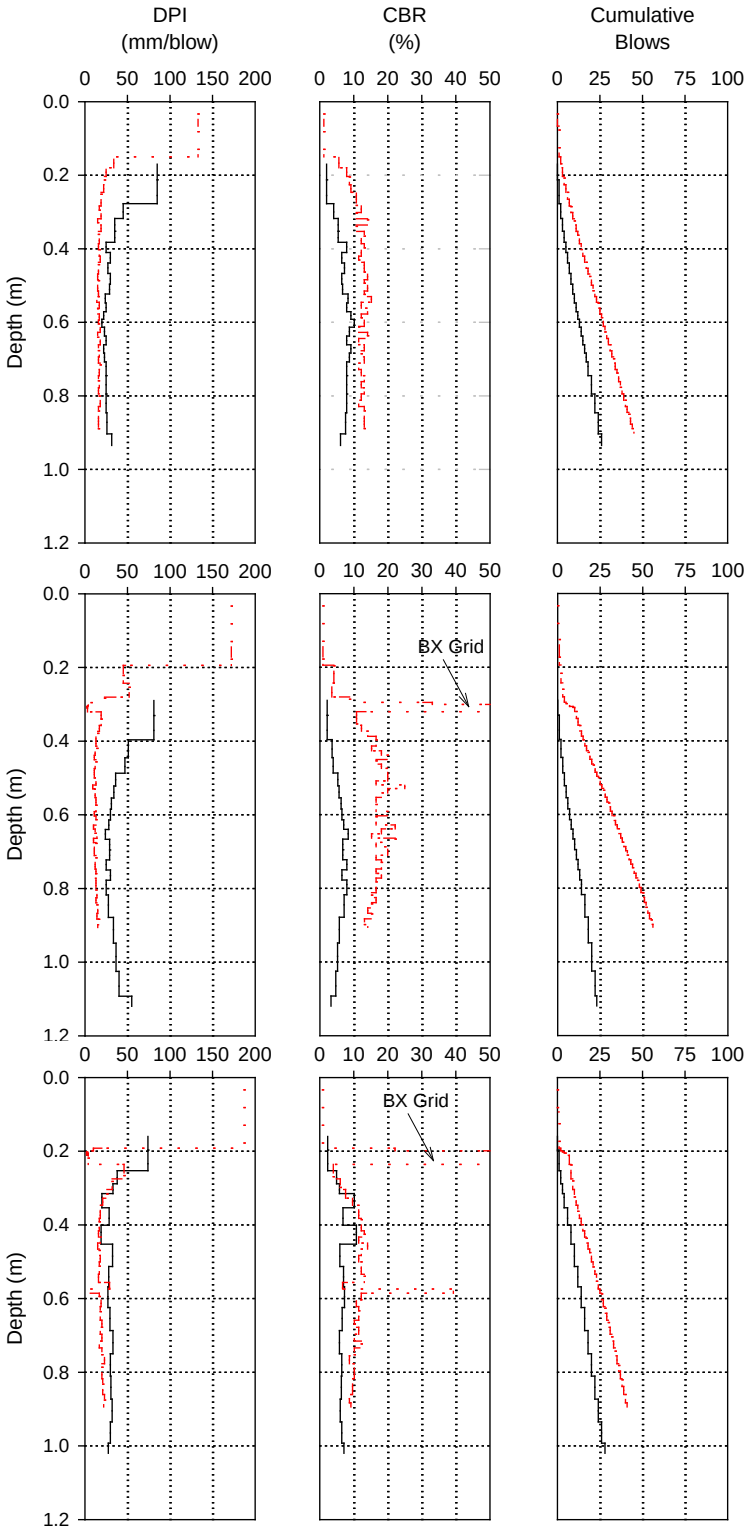


**Figure 54. DCP profiles at three test locations in 1-1(50) BX section (solid line represents test on the existing sand base, dashed line represents test after Pass 19) – TB1**

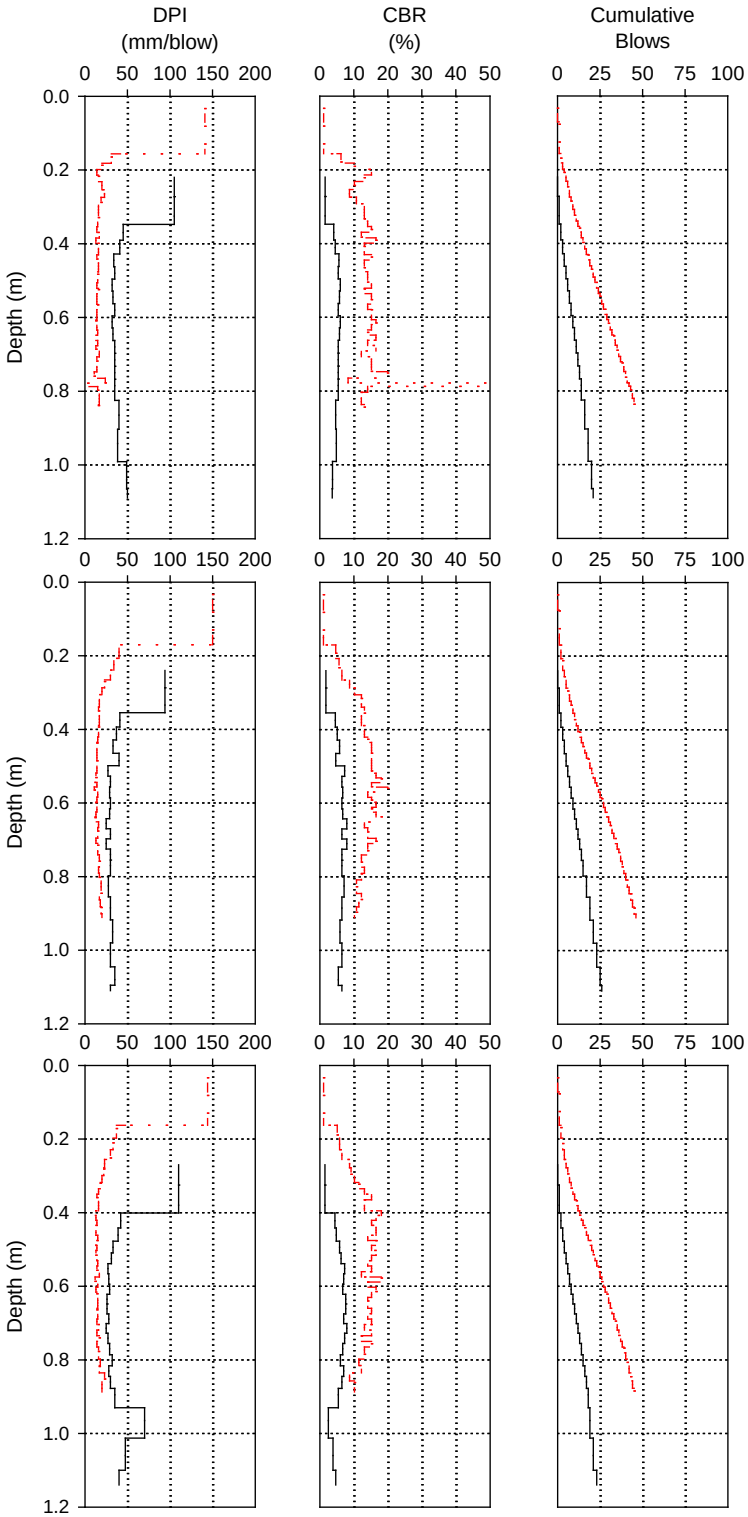


**Figure 55. DCP profiles at three test locations in 1-2(50) GC150 section (solid line represents test on the existing sand base, dashed line represents test after Pass 19) – TB1**

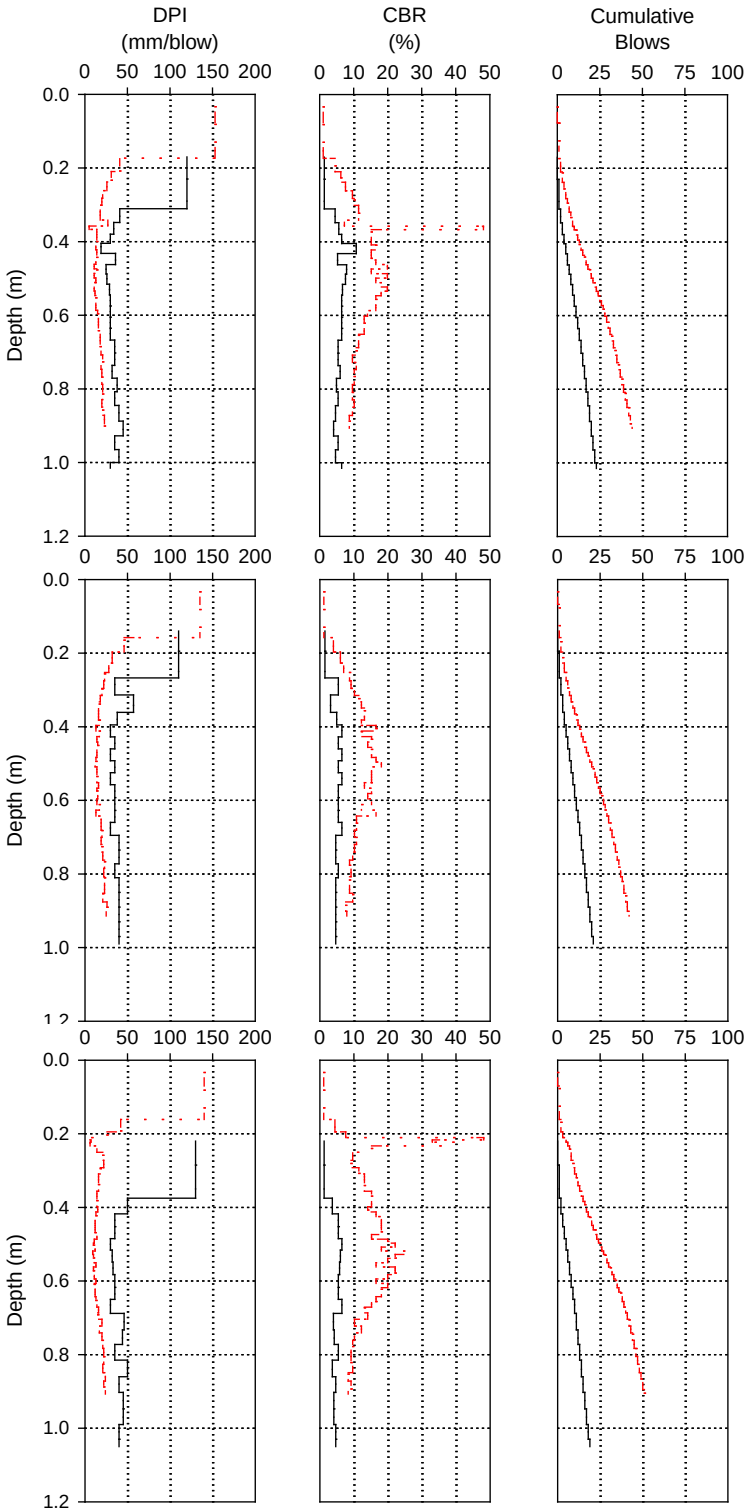


**Figure 56. DCP profiles at three test locations in 1-3(50) GC100 section (solid line represents test on the existing sand base, dashed line represents test after Pass 19) – TB1**

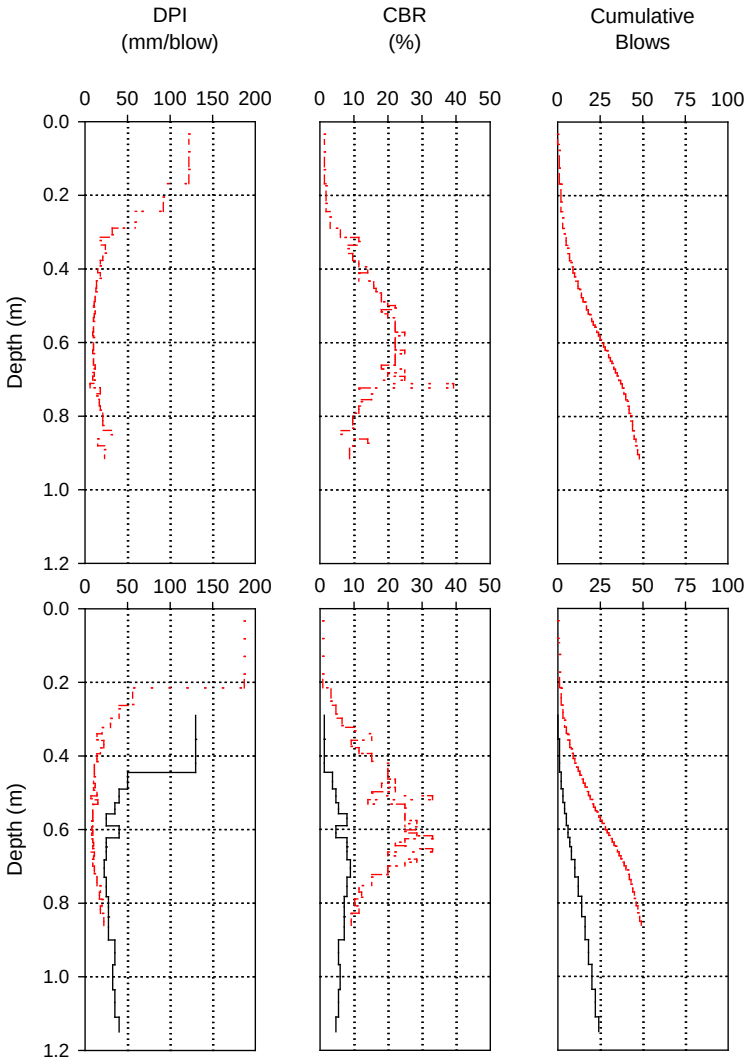


**Figure 57. DCP profiles at two test locations in 1-4(12) C30 section (solid line represents test on the existing sand base, dashed line represents test after Pass 19) – TB1**

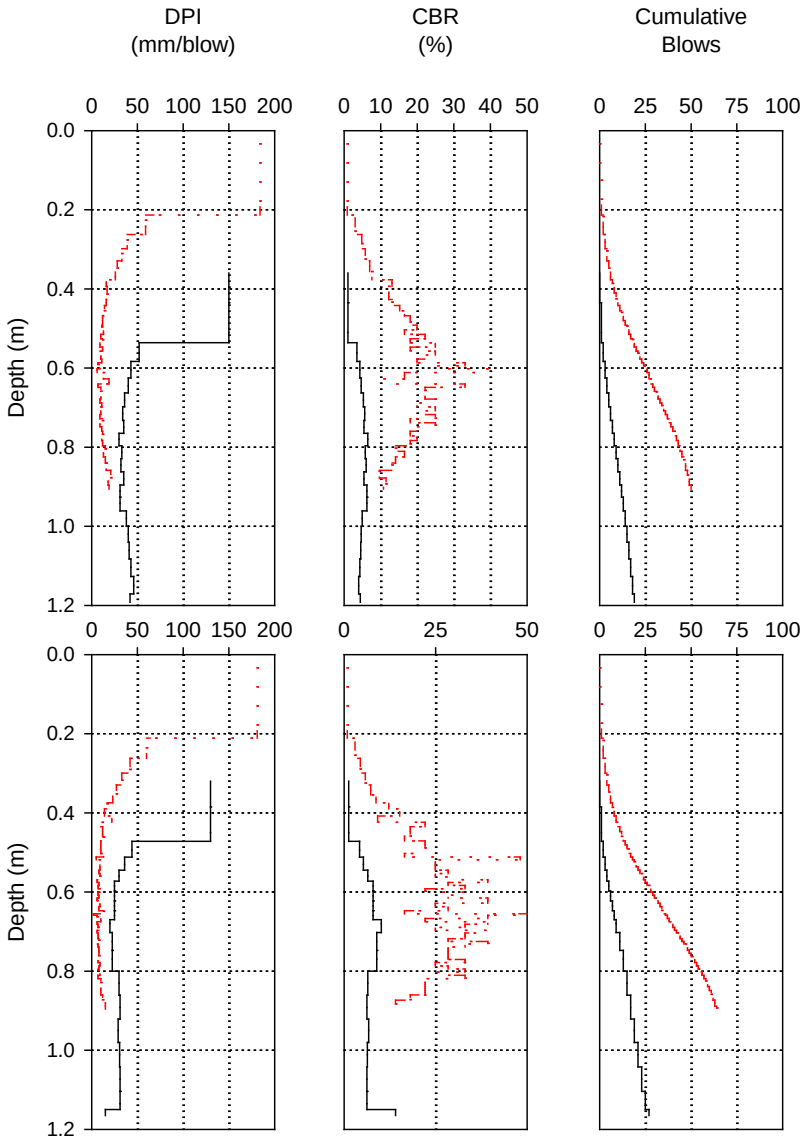


**Figure 58. DCP profiles at two test locations in 1-4(38) PPWF section (solid line represents test on the existing sand base, dashed line represents test after Pass 19) – TB1**

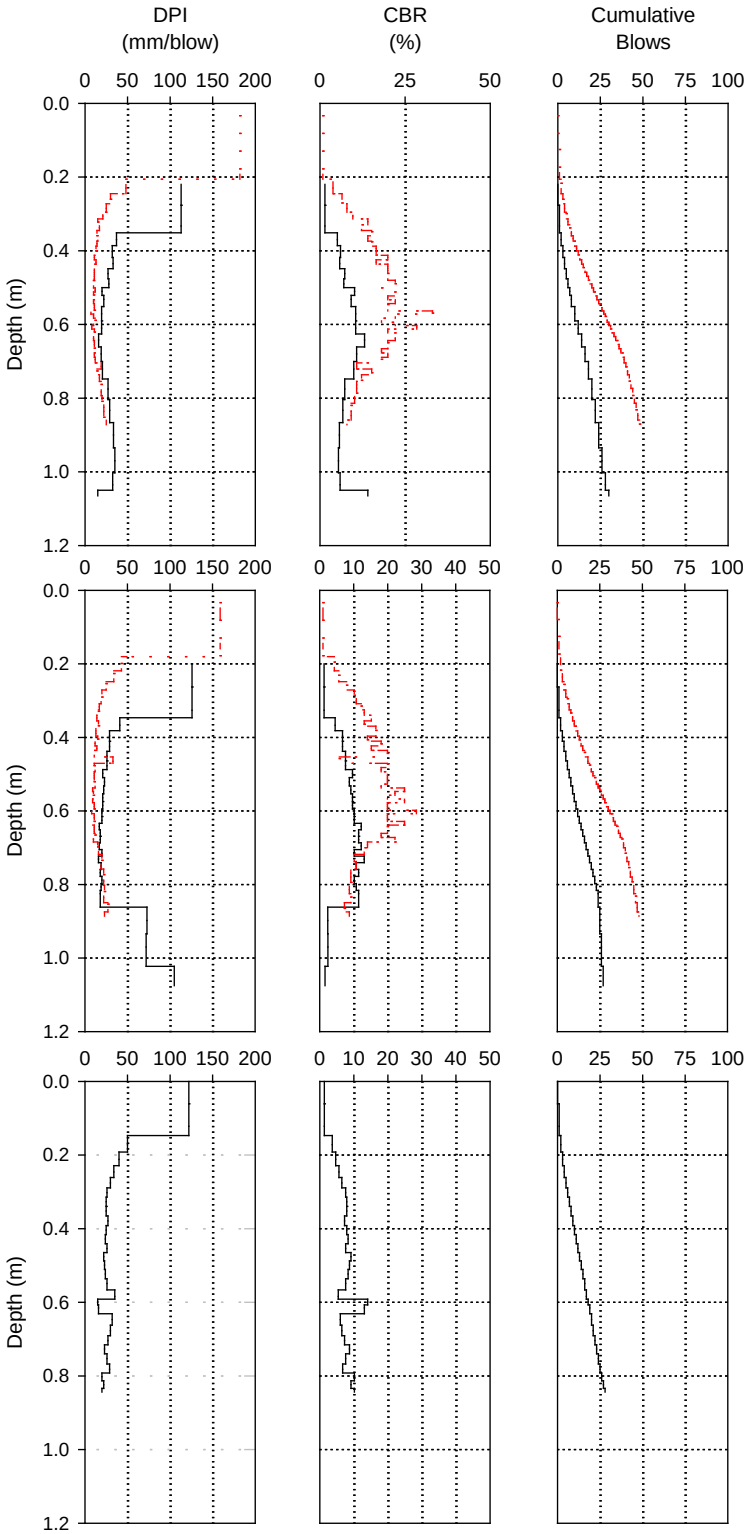


**Figure 59. DCP profiles at three test locations in 1-5(50) control section (solid line represents test on the existing sand base, dashed line represents test after Pass 19) – TB1**

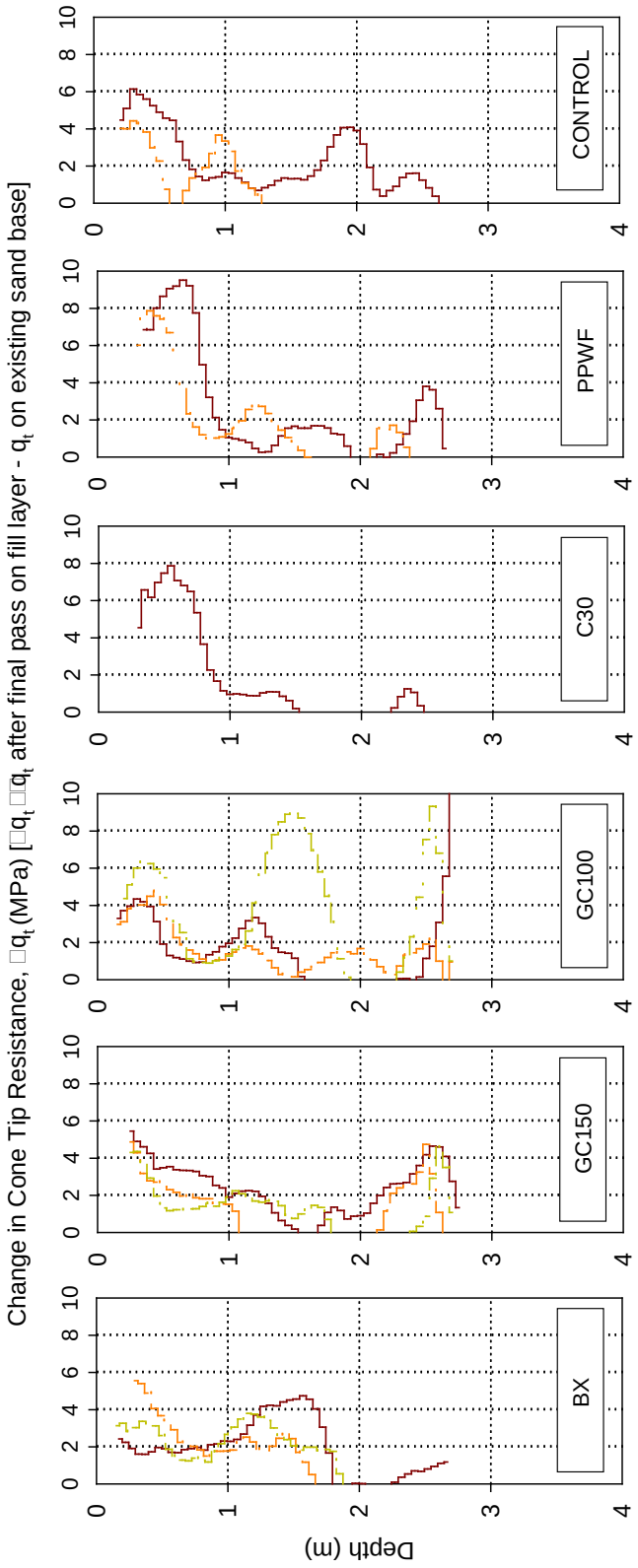


**Figure 60. Change in CPT $q_t$ with depth at test locations in each section – TB1**

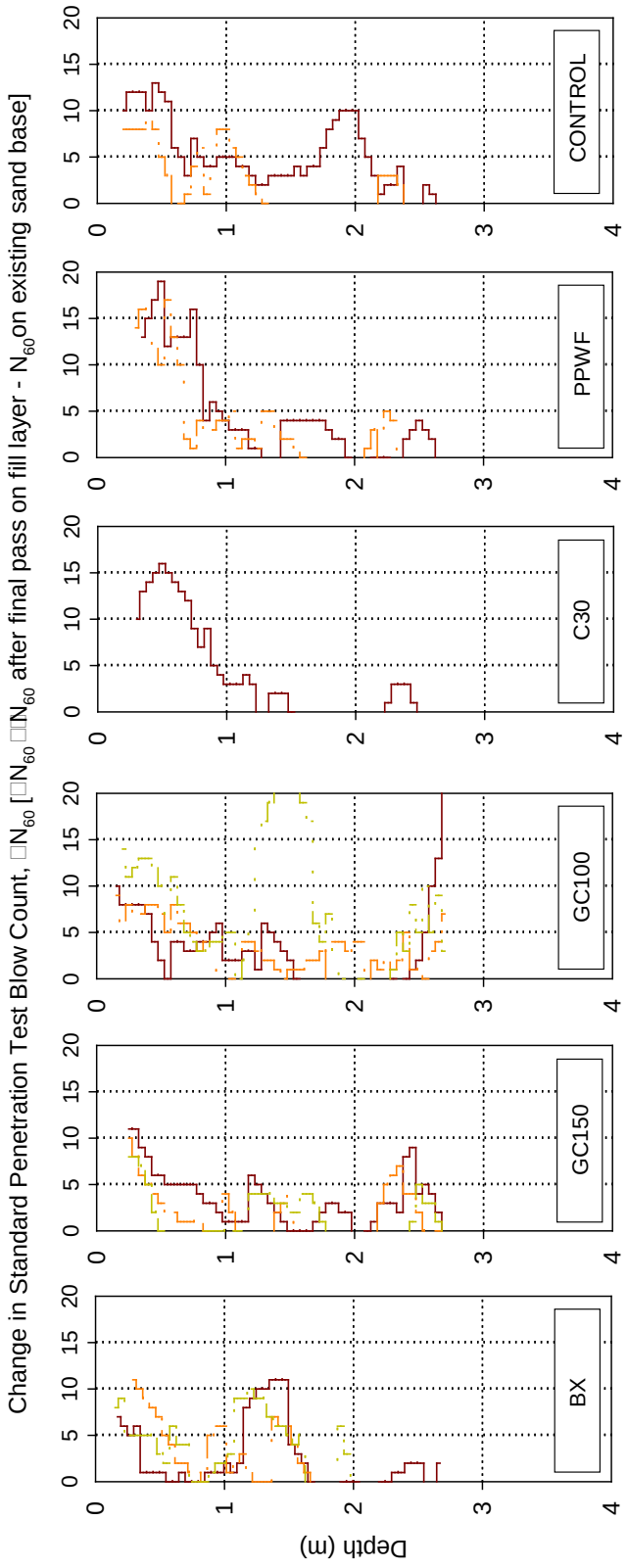


**Figure 61. Change in $N_{60}$ with depth at test locations in each section – TB1**

### 5.2.4 EPC Measurements

Total vertical and horizontal residual stresses and a ratio of the total horizontal to vertical residual stresses (referred to as lateral stress ratio, K) with increasing compaction passes are shown in Figure 62. Peak vertical and horizontal stresses under vibratory compaction on layer 1 and after layer 2 was placed are shown in Figure 63 to Figure 65. For a = 0.90 mm vibratory compaction pass on layer 1, the total peak horizontal stress in the Control section was recorded as 89 kPa which was higher than the total peak horizontal stresses recorded in the reinforced sections (49 to 70 kPa). On the other hand, the total peak vertical stress in the Control section sand base layer was about the same (300 kPa) as the total peak vertical stresses in the reinforced sections (280 to 315 kPa). The reduction in total peak horizontal stresses in the reinforced sections is expected and is a result of increased lateral confinement within the reinforced layers.

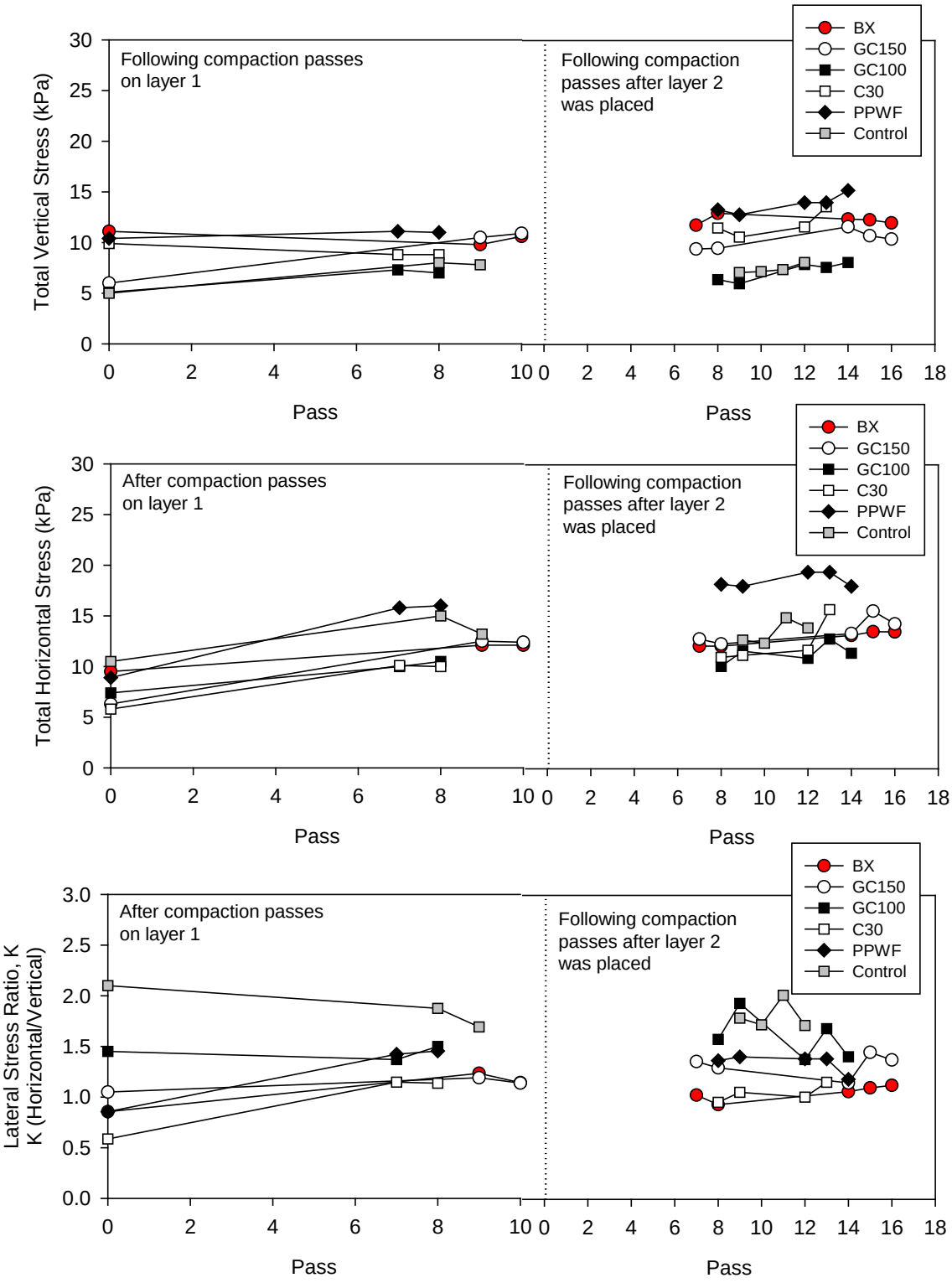


**Figure 62. Total vertical and horizontal stresses, and lateral stress ratio values measured following compaction passes in each section – TB1**

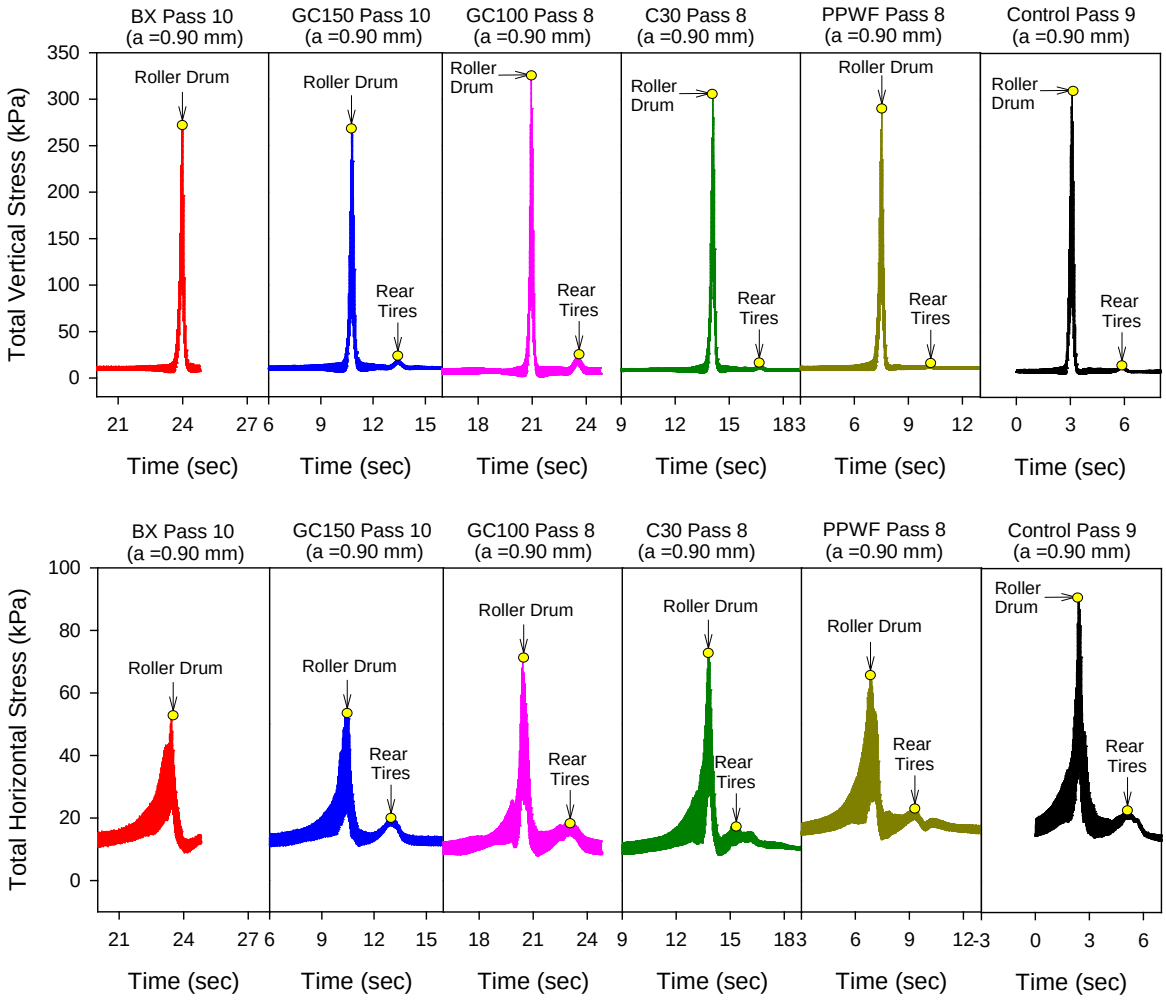


**Figure 63. Total vertical and horizontal stresses under roller vibratory compaction (a = 0.90 mm) on layer 1 – TB1**

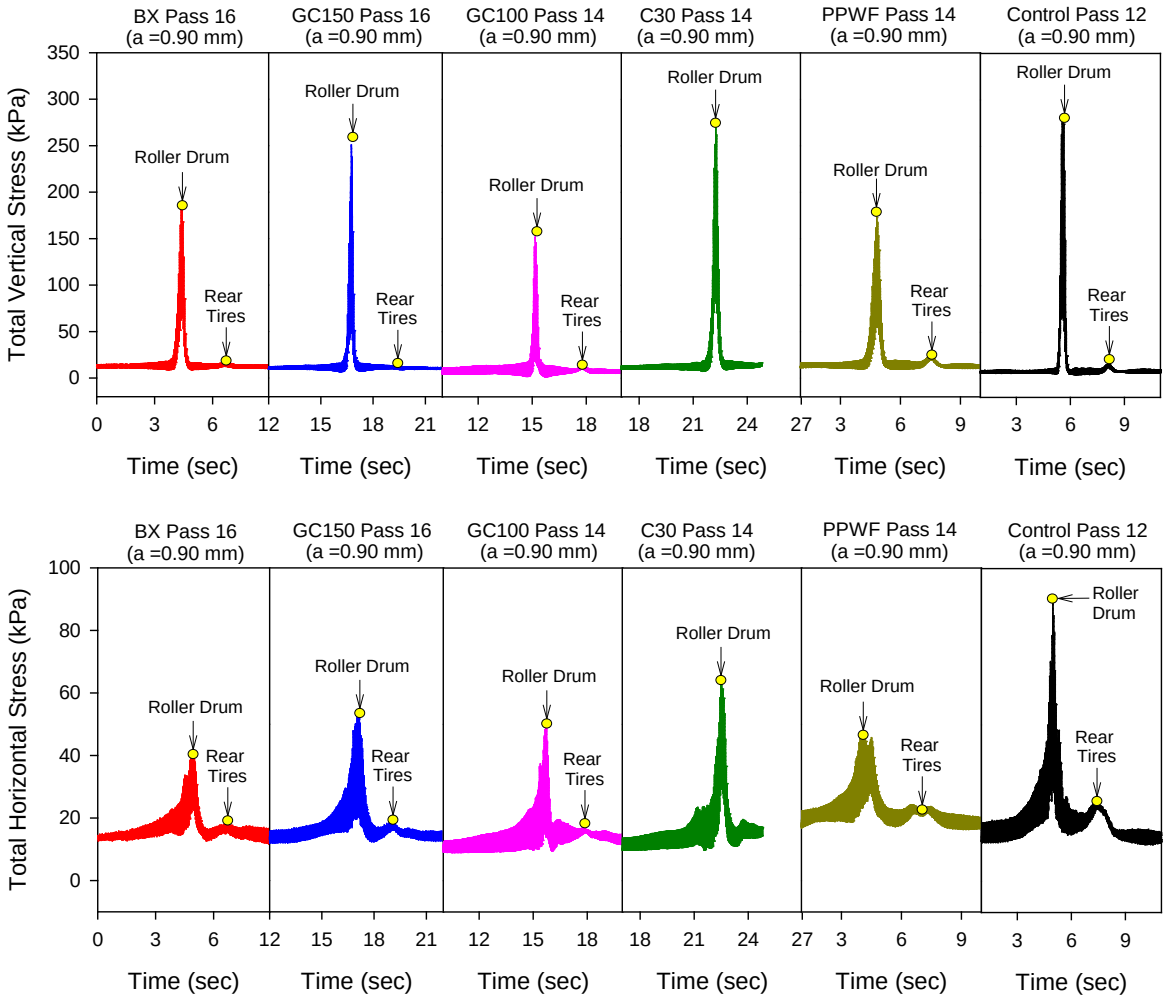


**Figure 64. Total vertical and horizontal stresses under roller vibratory compaction (a = 0.90 mm) after layer 2 was placed – TB1**

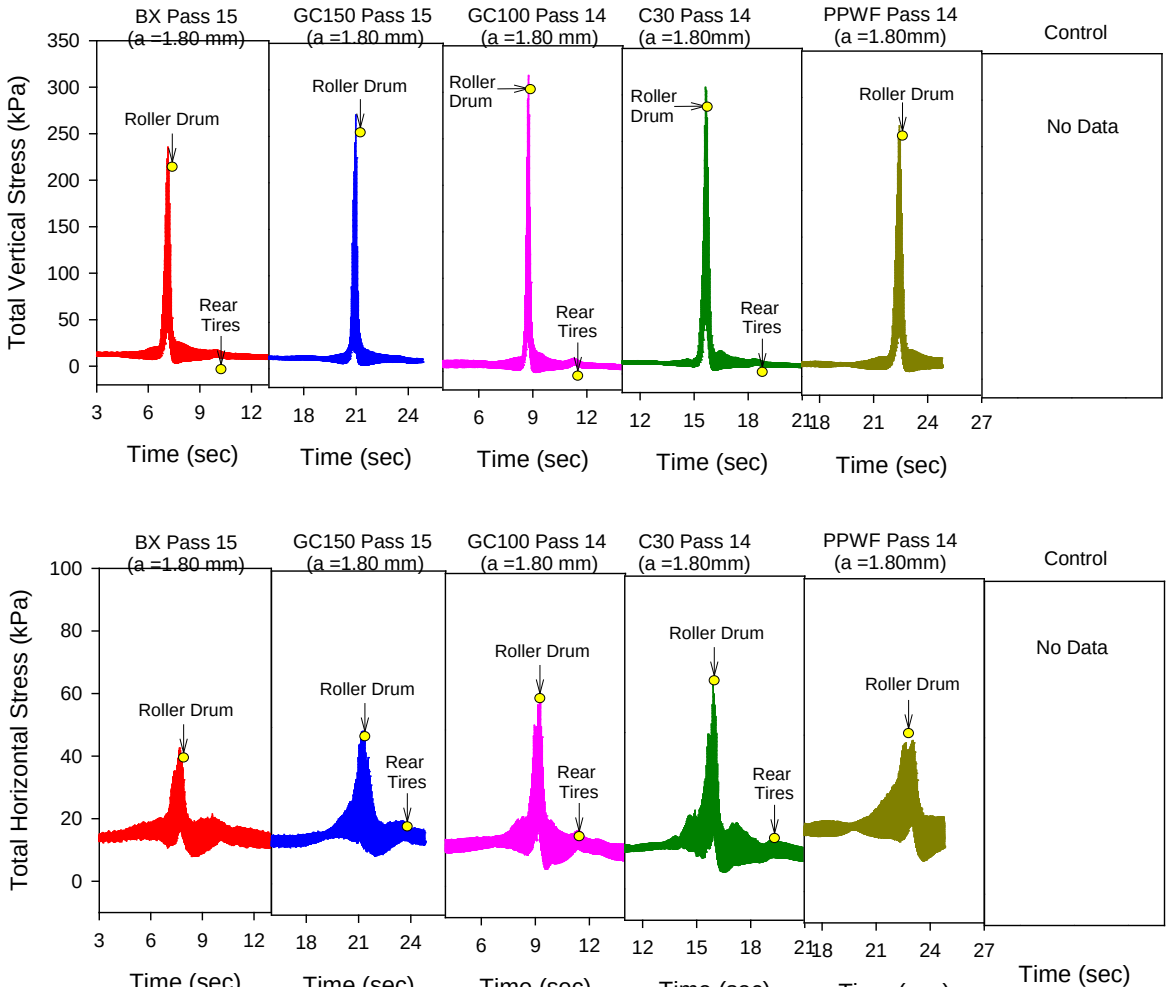


**Figure 65. Total vertical and horizontal stresses under roller vibratory compaction (a = 1.80 mm) after layer 2 was placed – TB1**

### 5.2.5 Vibration Monitoring Measurements

Vibration monitoring results (longitudinal, vertical, and horizontal particle peak velocities (PPV's)) were obtained during vibratory compaction passes using a = 0.90 mm and 1.80 mm settings on TBs 1 and 2. The seismographs were positioned at 7.6 m and 30.5 m away from the center of the GC100 section in TB1 as shown in Figure 66. Particle peak velocities for each pass are shown in Figure 66.

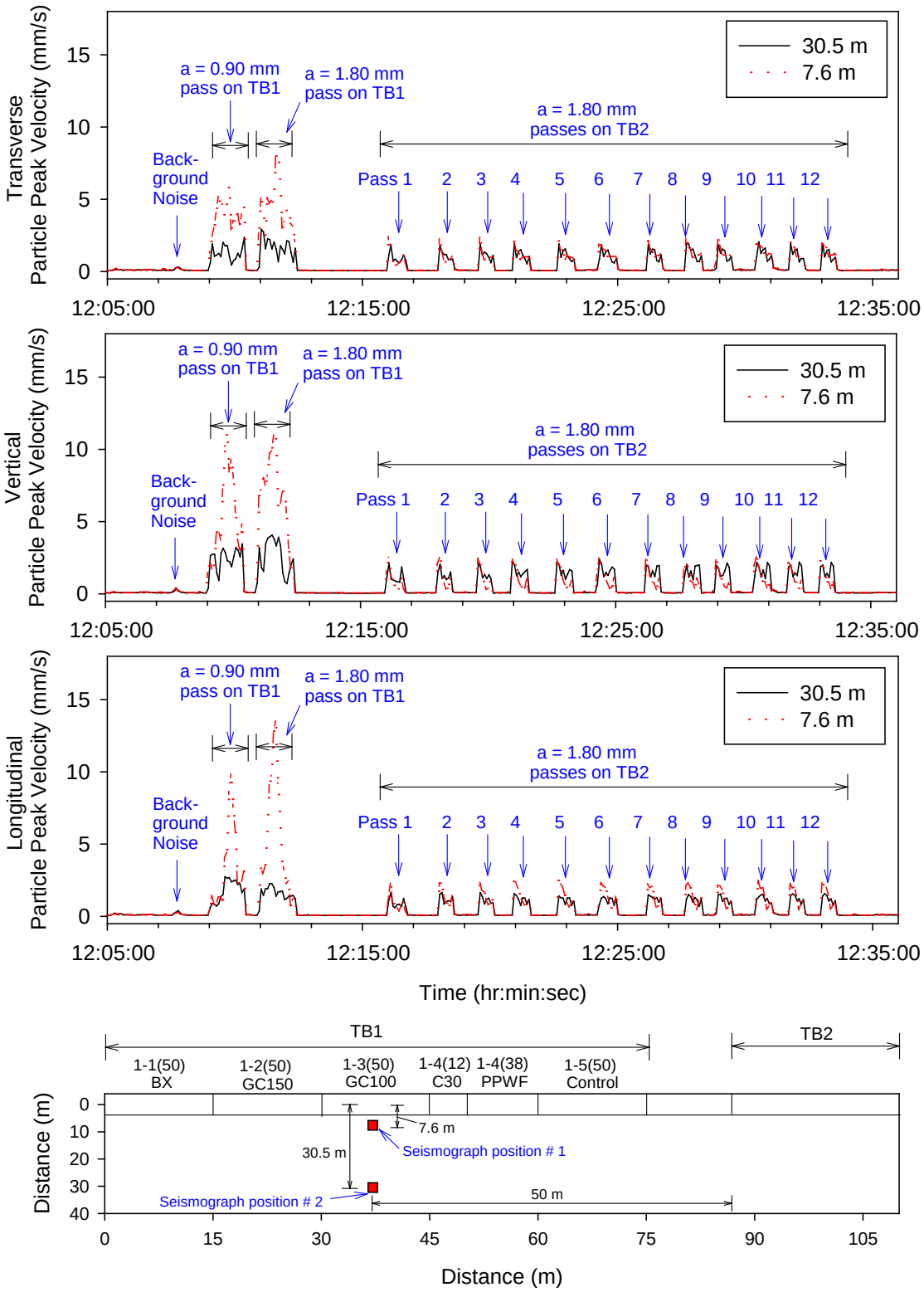


**Figure 66. Peak particle velocity readings from seismograph during compaction passes on TB1 and TB2**

## 5.3 TB2 – CALIBRATION TEST AREA

### 5.3.1 TB Construction and In Situ Testing

The TB consisted of excavating and replacing about 1.2 m thick loose lift (Figure 67) of existing sand layer over a plan area of about 6.2 m x 25 m, just adjacent to TB1. The TB was leveled using a motor grader (Figure 68) and then a BX geogrid was installed on the surface as shown in Figure 69 over a 10 m length of the TB, which is referenced to as BX grid section. About 100 mm thick loose sand layer was installed atop of BX geogrid as shown in Figure 70. No reinforcement was placed in the remaining portion of the TB and therefore is referred to as Control section. The TB was compacted with 12 roller pass using a = 1.80 mm settings (Figure 71). Plan area of the TB with in situ test locations and location of BX grid is shown in Figure 72. Prior to compaction passes, DCP and LWD testing were conducted in the loose lift at one random location to obtain a baseline reference value. After final compaction pass, LWD and DCP tests were conducted at three test locations each in BX grid and Control sections. LWD tests were conducted at surface, at about 100 mm below surface, and at about 450 mm below surface in excavations (Figure 73) to assess the influence of confinement and change in modulus with depth.

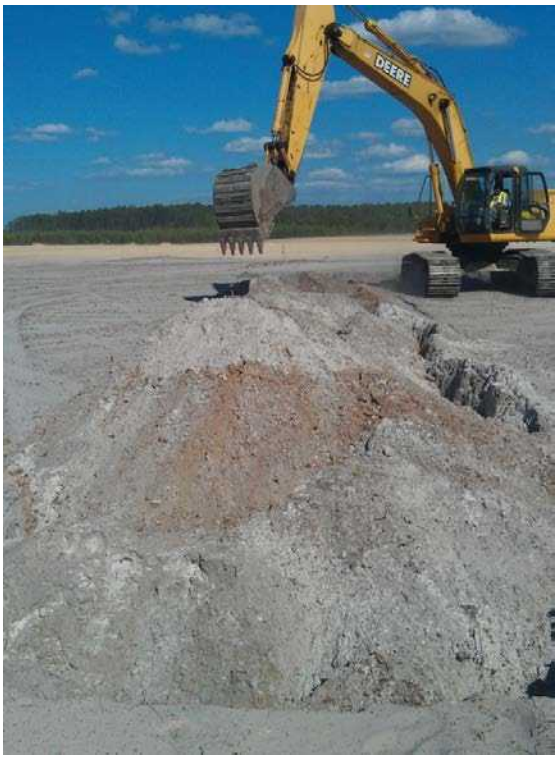


**Figure 67. Excavation and replacement of 1.2 m thick loose lift – TB2**

**Figure 68. Loose lift leveling process – TB2**

**Figure 69. Installation of BX geogrid on TB2**

**Figure 70. Fill placement (~100 mm thick) over BX geogrid – TB2**

**Figure 71. Compaction of test bed using CS74 vibratory smooth drum roller (a = 1.80 mm) – TB2**

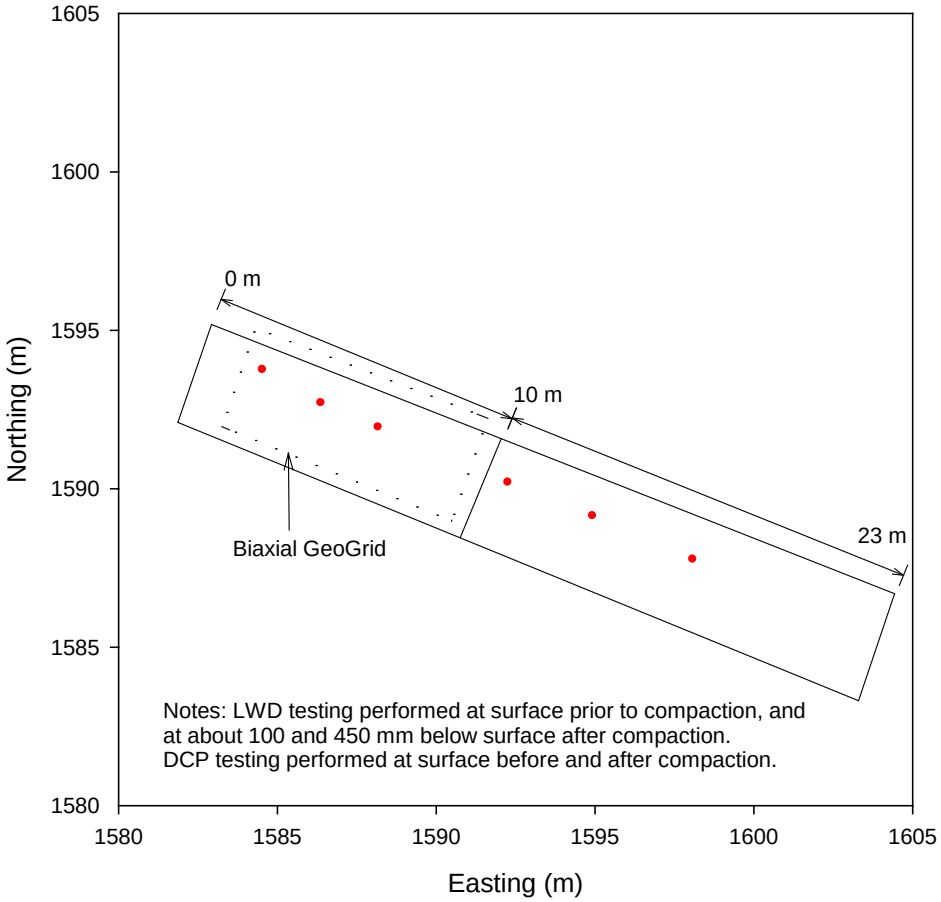


**Figure 72. Plan view and GPS test locations of TB2**

**Figure 73. LWD testing in excavations at about 100 mm and 450 mm below surface – TB2**

### 5.3.2 RICM and In Situ Test Measurements

MDP* and CMV measurements from each compaction pass along the TB are shown in Figure 74 and Figure 75, respectively. Average MDP* and CMV for BX grid and Control sections with increasing pass are shown in Figure 76. Average MDP* in both BX grid and Control sections rapidly increased with increasing pass up to pass 4 and achieved a plateau by pass 6. Average CMV in both BX grid and Control sections increased with increasing passes up to pass 12. Both MDP* and CMV were slightly greater in the BX grid section compared to the Control section.

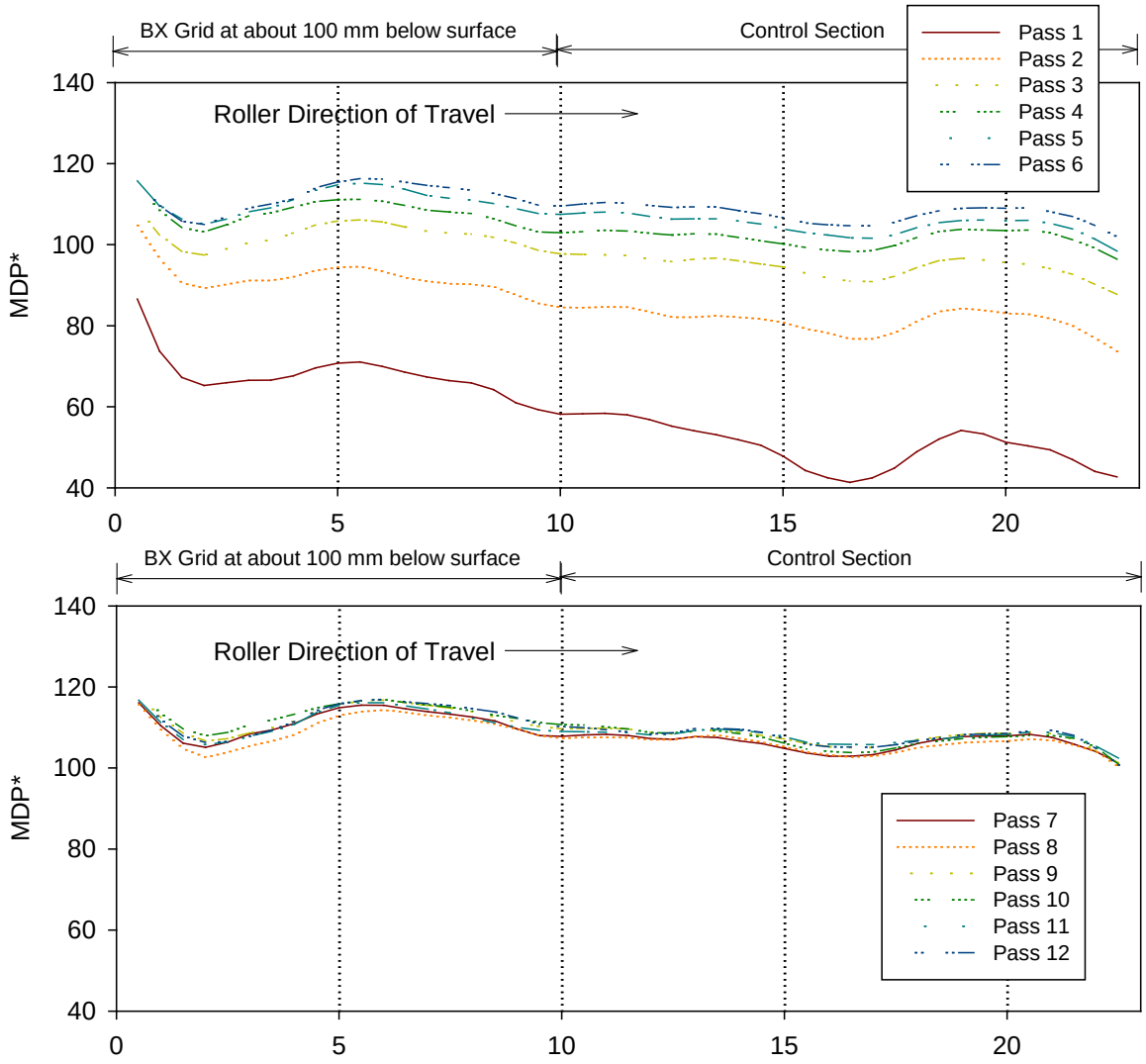


**Figure 74. Roller-integrated MDP* measurements for passes 1 to 12 (a = 1.80 mm) – TB2**

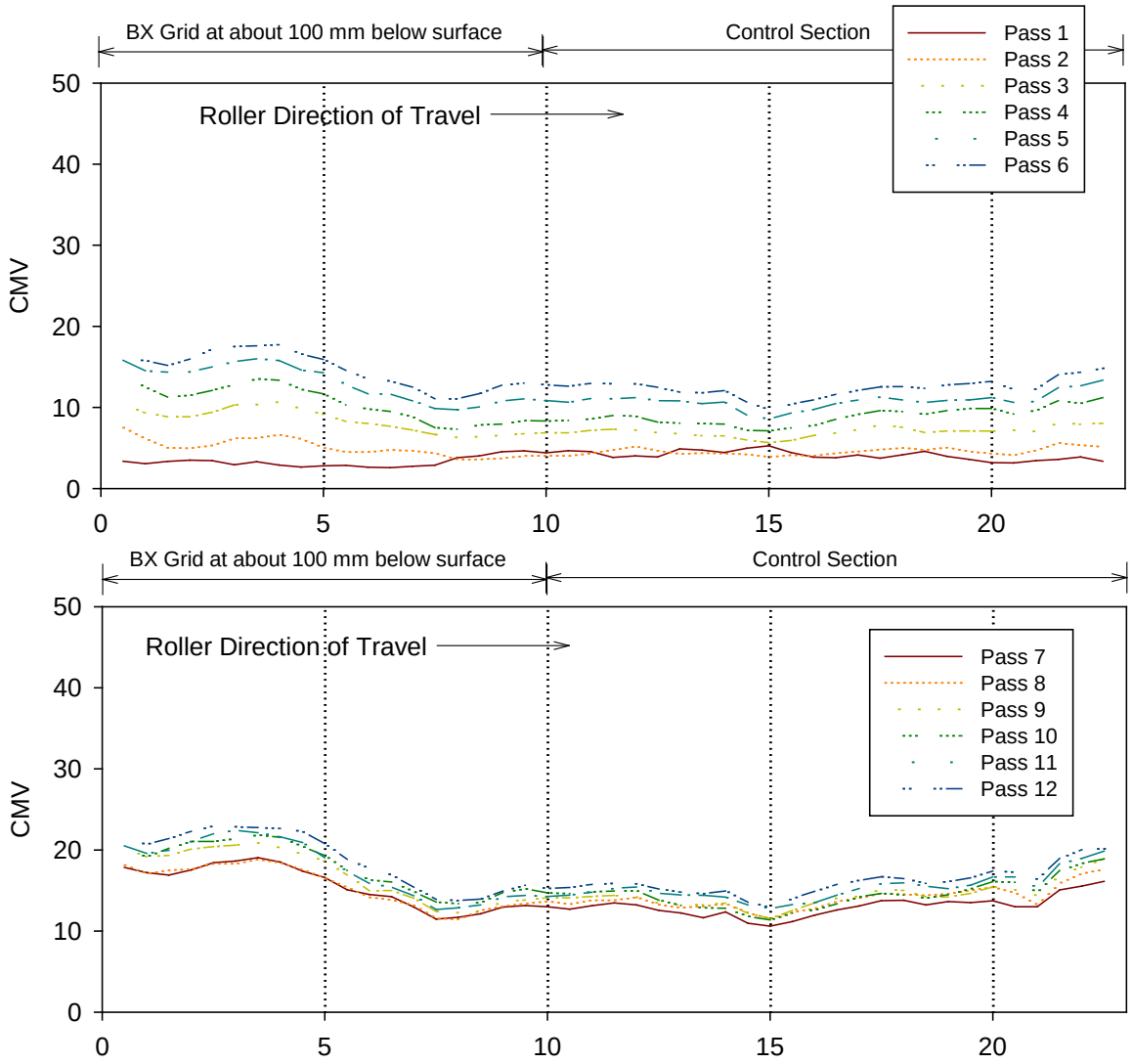


**Figure 75. Roller-integrated CMV measurements for passes 1 to 12 (a = 1.80 mm) – TB2**

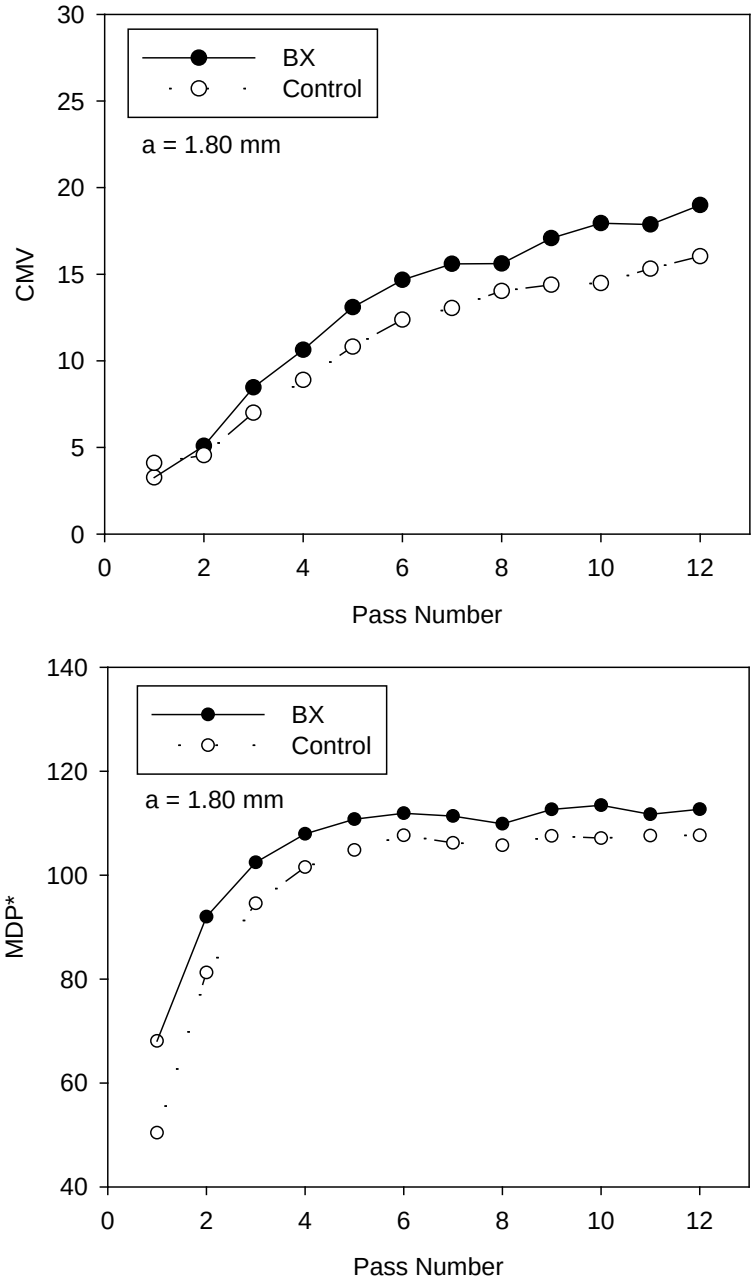


**Figure 76. Average CMV and MDP* measurements with increasing pass – TB2**

LWD modulus results along the TB are presented in Figure 77. Average LWD at surface, at 100 mm, and at 450 mm below surface were about 1.4, 1.1, and 1.1 times higher, respectively, in the BX grid section than in the Control section. The modulus values increased with depth at all test locations. DPI, CBR, and cumulative blow count profiles before and after compaction in the BX grid and Control sections are shown in Figure 78 and Figure 79, respectively. Prior to compaction, CBR values were <0.5 up to the DCP termination depth of about 0.9 m below surface. CBR profile after compaction showed improvements down to the termination depth. Weighted average CBR (up to the termination depth) in the BX section was about 5.2 and in the Control section was about 4.8.

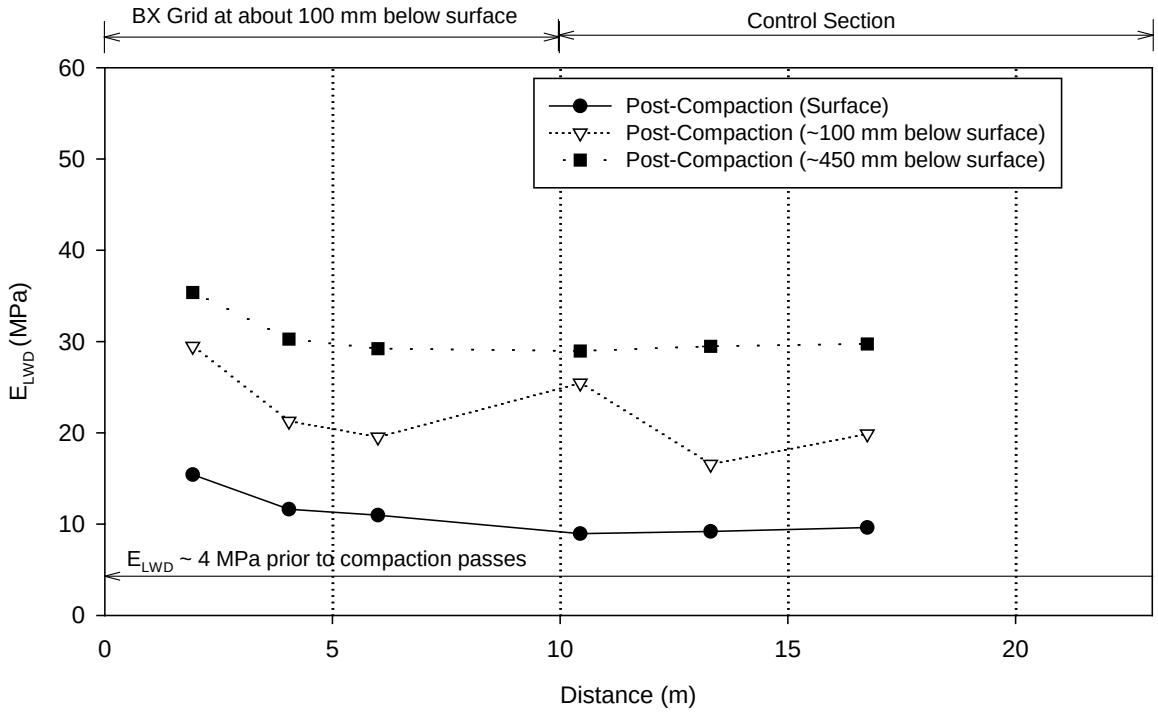


**Figure 77. LWD modulus measurements before and after compaction (at surface, 100 mm, and 450 mm below surface) – TB2**

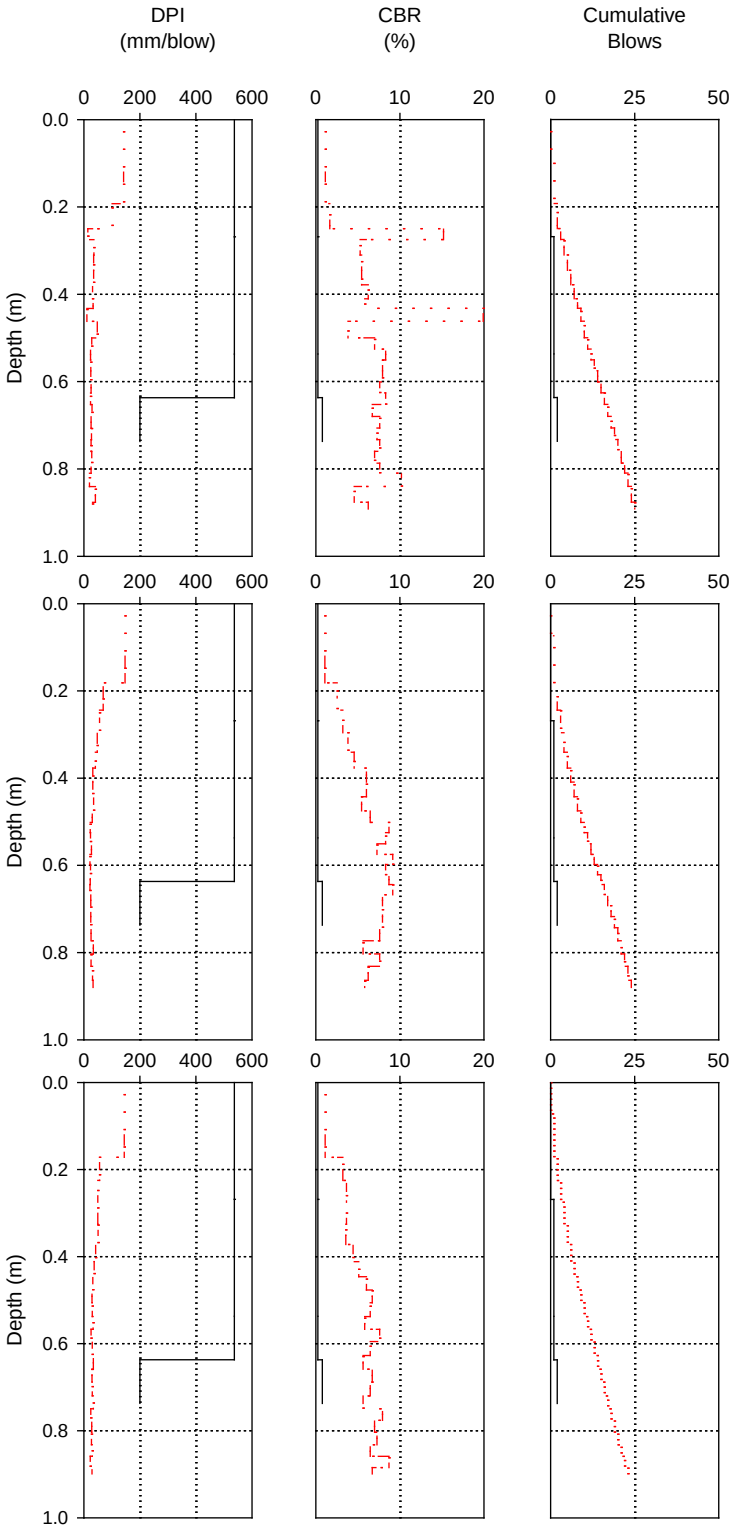


**Figure 78. DCP test results before (solid line) and after (dashed line) compaction at three test locations on BX geogrid section– TB2**

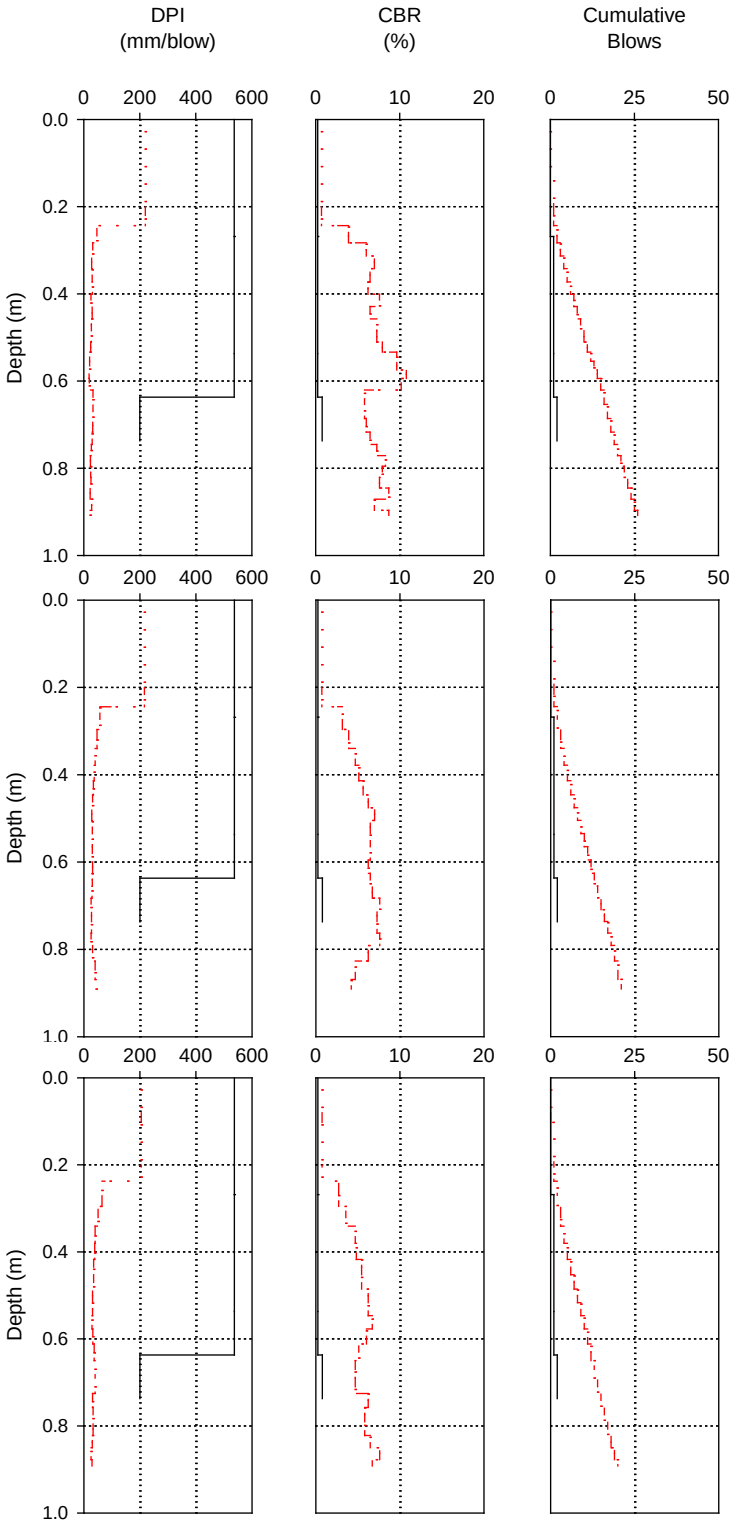


**Figure 79. DCP test results before and after compaction at three test locations control section (solid line represents before compaction and dashed line represents after compaction) – TB2**

## 5.4 TB3 – PRODUCTION AREA

This test bed consisted of a recycled asphalt pavement (RAP) base surfaced over natural sand subgrade layer and was being used as a haul road for construction traffic (Figure 80). The RAP layer was about 30 to 120 mm thick. Plan dimensions of the test bed were about 10 m wide x 95 m long. The area was mapped in four roller lanes using five roller passes with static, a = 0.90 mm, and a = 1.80 mm settings. Details of settings used for each pass are provided in Table 5. Following the final mapping pass, LWD and DCP tests were obtained at 11 to 12 test locations using the CMV and MDP* color-coded maps in the roller (four test locations each in low, medium, and high CMV or MDP* value areas).

Figure 81 shows color-coded CMV and MDP* maps, and a pass coverage map of the TB area. Using pass count coverage maps can be used as an effective QC method. Correlations between in situ point measurements (LWD modulus, weighted average CBR of RAP base layer ($CBR_{Base}$) and weighted average CBR of the natural subgrade layer ($CBR_{Subgrade}$) down to the test termination depth) and CMV and MDP* RICM measurements are presented in Figure 82. The correlations were developed by spatially pairing the in situ point measurements and RICM measurements using GPS measurements. DPI, CBR, and cumulative blow count profiles comparing with RICM and LWD modulus values at each test location are shown in Figure 83 to Figure 88.

Correlations yielded linear regression relationships between point measurements and RICM measurements. The intercept values in the regression relationships were affected by the amplitude settings, while the slope coefficient remained about the same. $CBR_{Base}$ versus MDP* showed the highest $R^2$ values (about 0.9) of all regression relationships. LWD modulus versus both CMV and MDP* RICM measurements yielded similar $R^2$ values (0.6 to 0.7). $CBR_{Subgrade}$ values also correlated well with the RICM measurements yielding $R^2$ values in the range of 0.7 to 0.8. Previous research indicated that CMV measurements have a measurement influence depth in the range of 0.8 m to 1.5 m depending on soil layering, drum mass, and excitation force (ISSMGE 2005, Rinehart and Mooney 2009, Vennapusa et al. 2011), while MDP* measurements have a measurement influence depth in the range of 0.3 to 1.3 m depending on the heterogeneity in subsurface conditions (Vennapusa et al. 2009). Therefore, both CMV and MDP* measurements provide a composite response based on both RAP base and subgrade layer properties. However, the relative influence of the RAP base layer versus the subgrade layer on CMV and MDP* could not be discerned in this case as $CBR_{Base}$ and $CBR_{Subgrade}$ appear to be correlating well with each other.

It must be noted that some level of scatter in relationships between point measurements and RICM measurements is inevitable due to the following reasons (Mooney et al. 2010 and Vennapusa et al. 2011): (a) differences in measurement influence depths between measurements, (b) differences in ground stress states during testing, (c) inherent repeatability measurement errors associated with each measurement type, and (d) uncertainty in spatial pairing of point measurements with RICM measurements. In addition, results obtained from TB1 indicated the influence of direction of travel on RICM measurements, particularly with MDP* measurements. ISSMGE (2005) suggest $R^2 = 0.5$ as suitable for calibration purposes.

**Figure 80. Picture of TB3 recycled asphalt pavement (RAP) surfacing on sand subgrade**

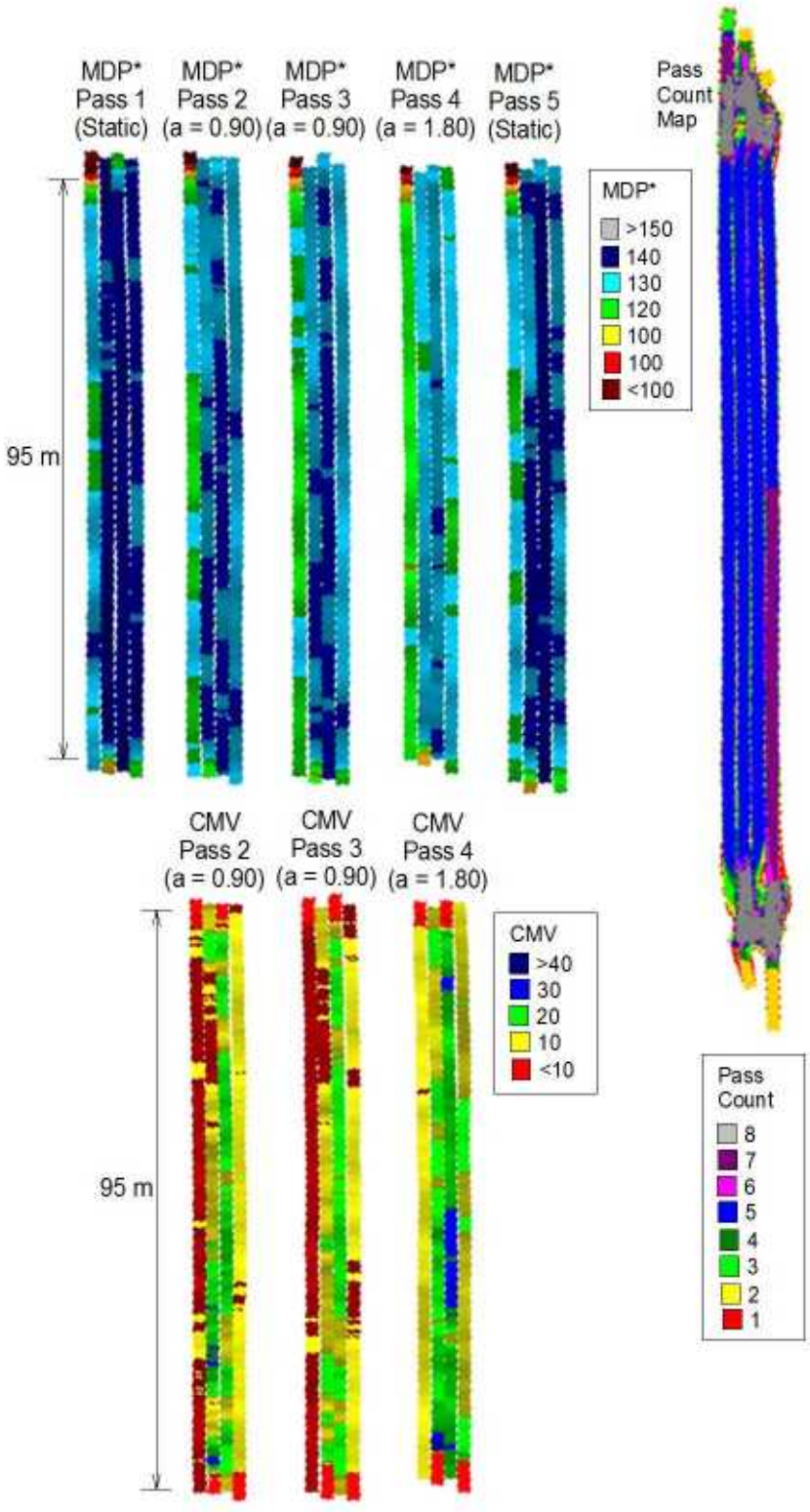


**Figure 81. Roller-integrated CMV, MDP*, and pass count map from mapping passes – TB3**

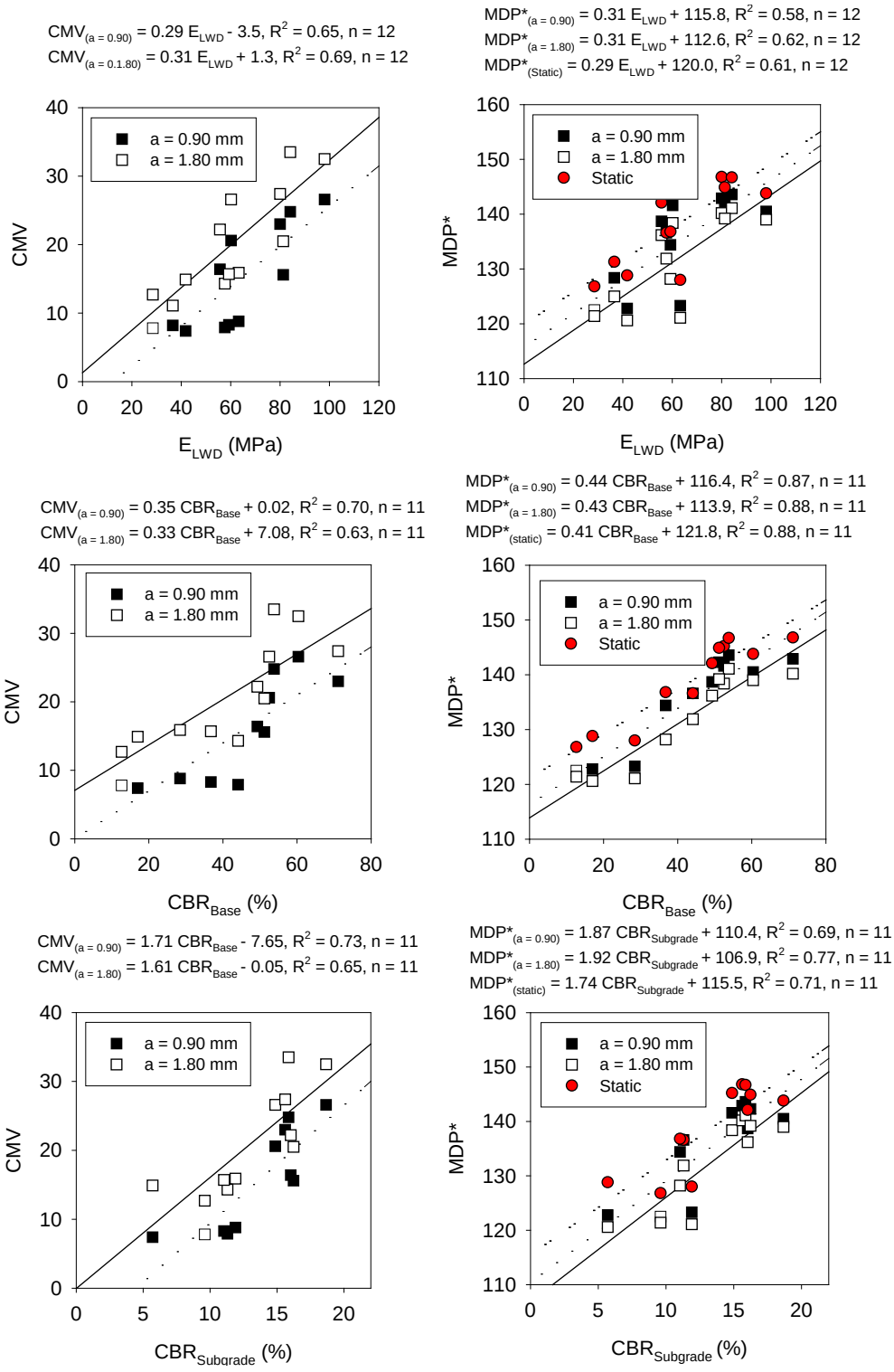


**Figure 82. Correlations between roller-integrated RICM and in situ point measurements – TB3**

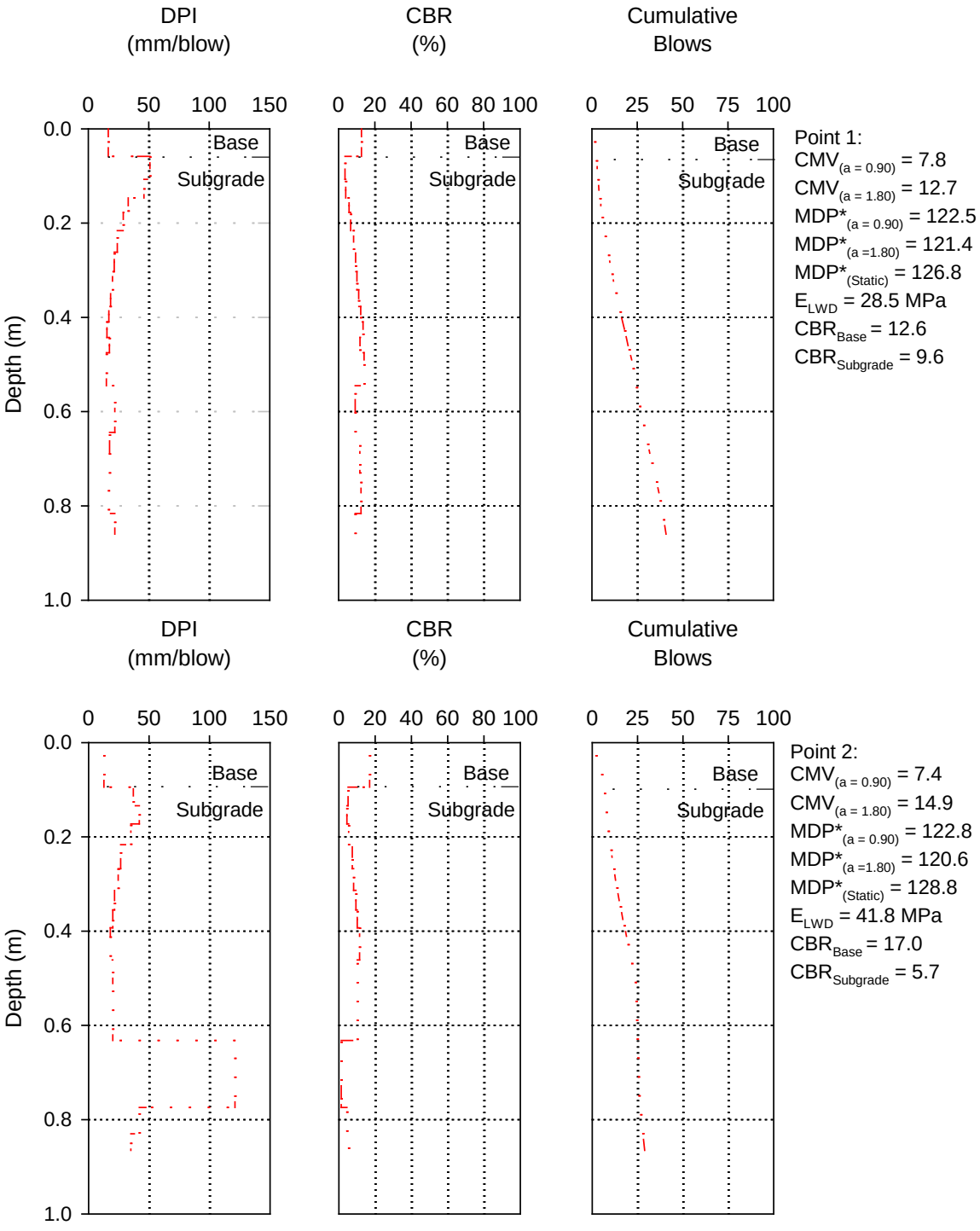


**Figure 83. DPI, CBR, and cumulative blow profiles at points 1 and 2 (CMV, MDP*, $E_{LWD}$ test measurements, and calculated $CBR_{Base}$ and $CBR_{Subgrade}$ are shown in the figure) – TB3**

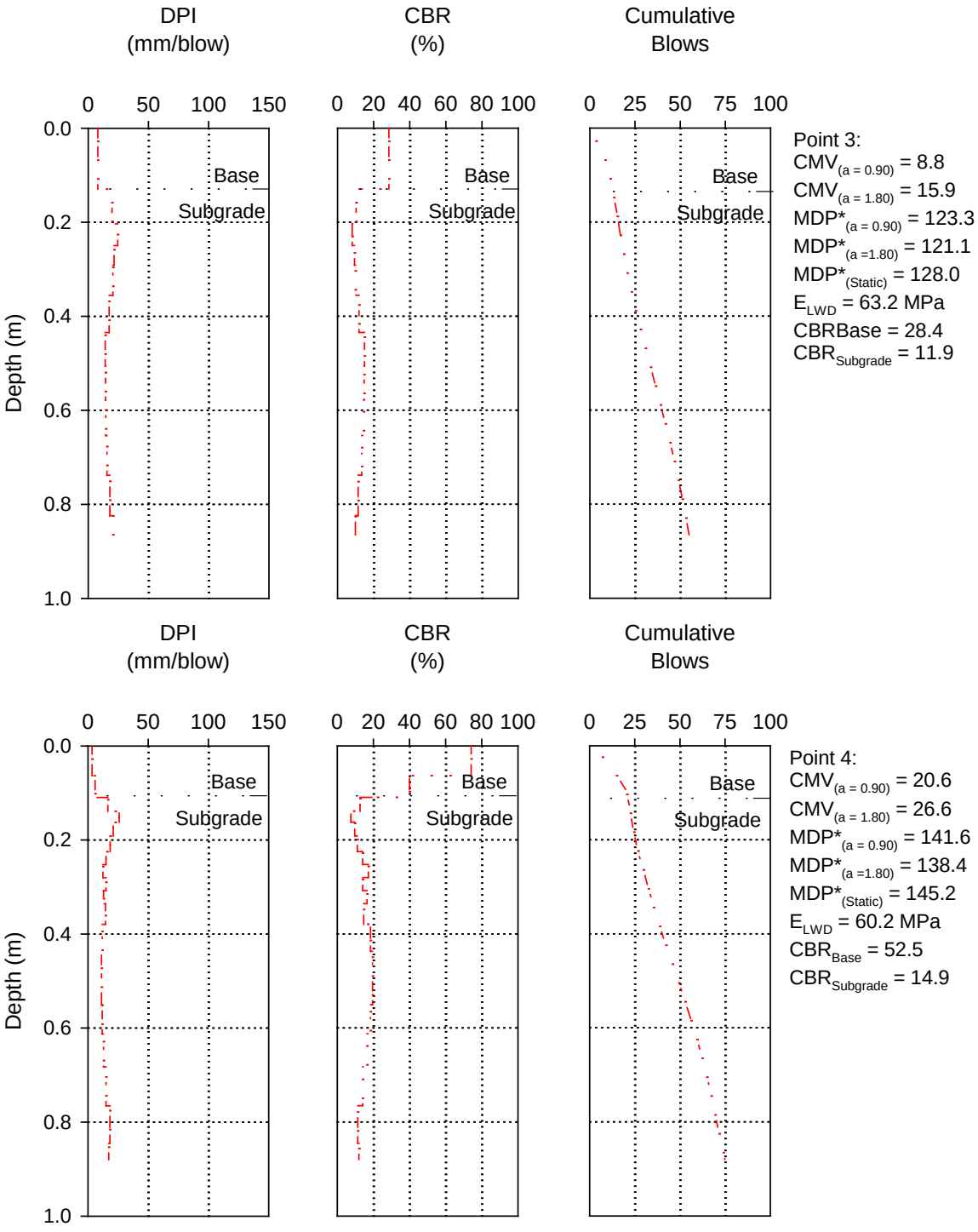


**Figure 84. DPI, CBR, and cumulative blow profiles at points 3 and 4 (CMV, MDP*, $E_{LWD}$ test measurements, and calculated $CBR_{Base}$ and $CBR_{Subgrade}$ are shown in the figure) – TB3**

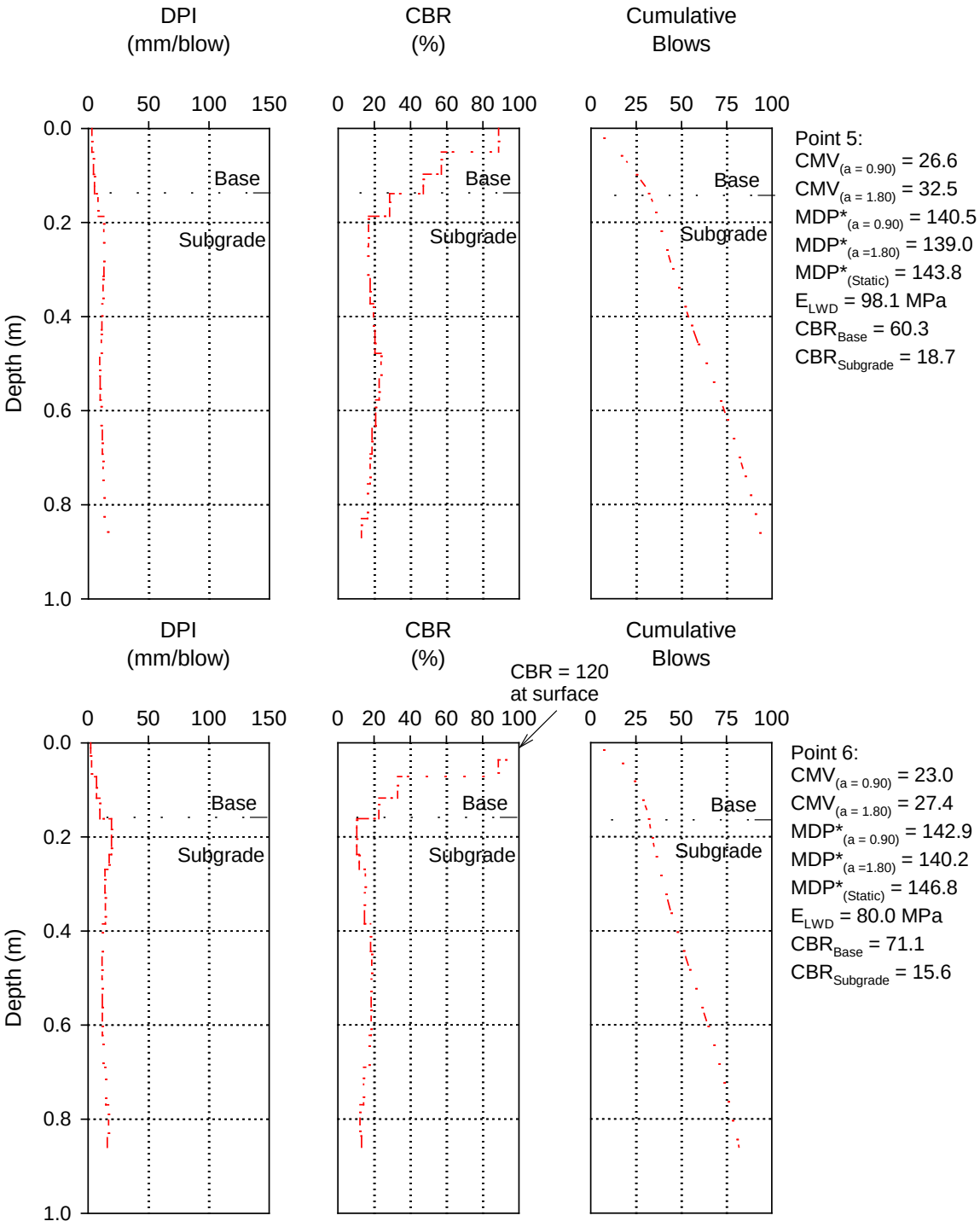


**Figure 85. DPI, CBR, and cumulative blow profiles at points 5 and 6 (CMV, MDP*, $E_{LWD}$ test measurements, and calculated $CBR_{Base}$ and $CBR_{Subgrade}$ are shown in the figure) – TB3**

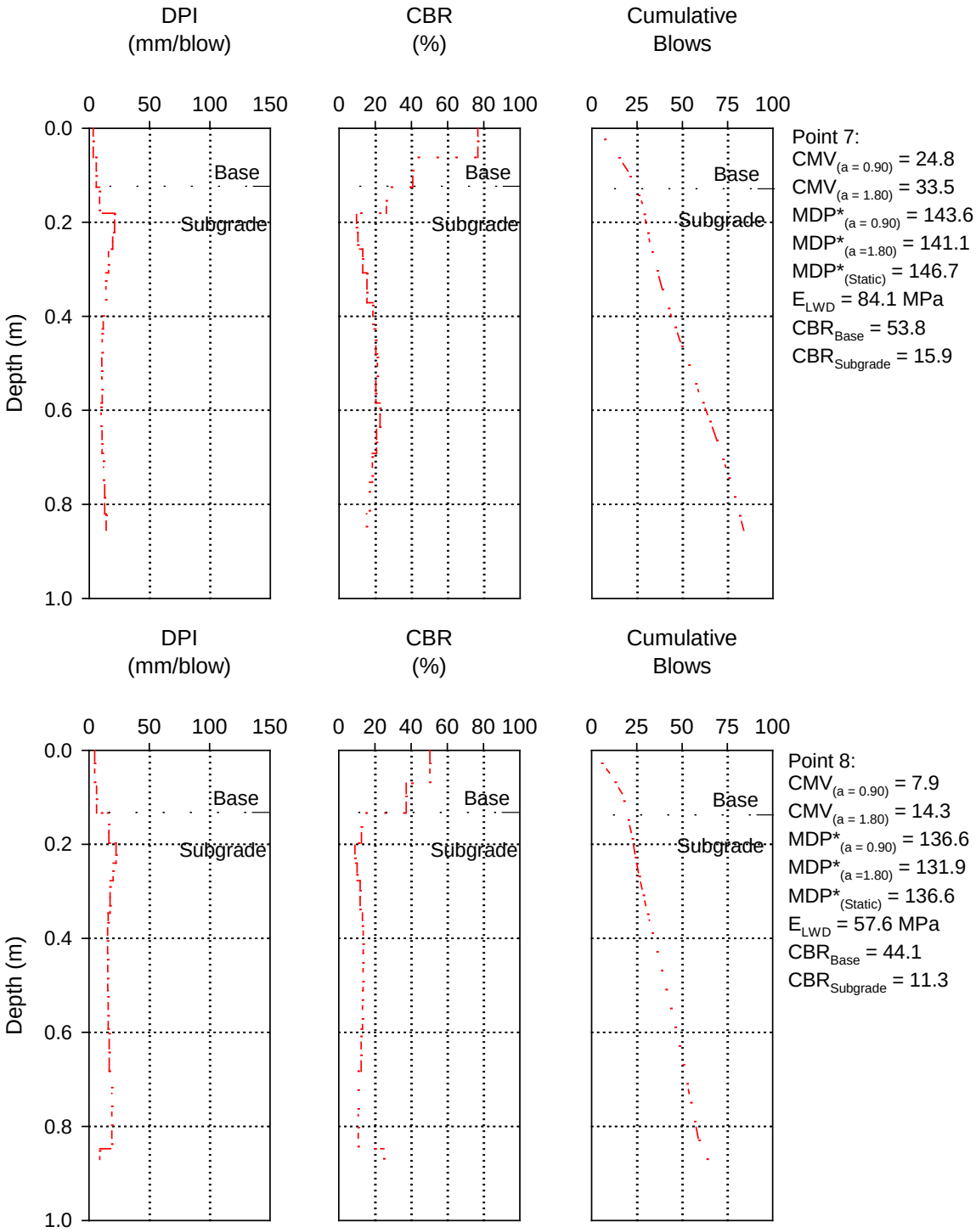


**Figure 86. DPI, CBR, and cumulative blow profiles at points 7 and 8 (CMV, MDP*, $E_{LWD}$ test measurements, and calculated $CBR_{Base}$ and $CBR_{Subgrade}$ are shown in the figure) – TB3**

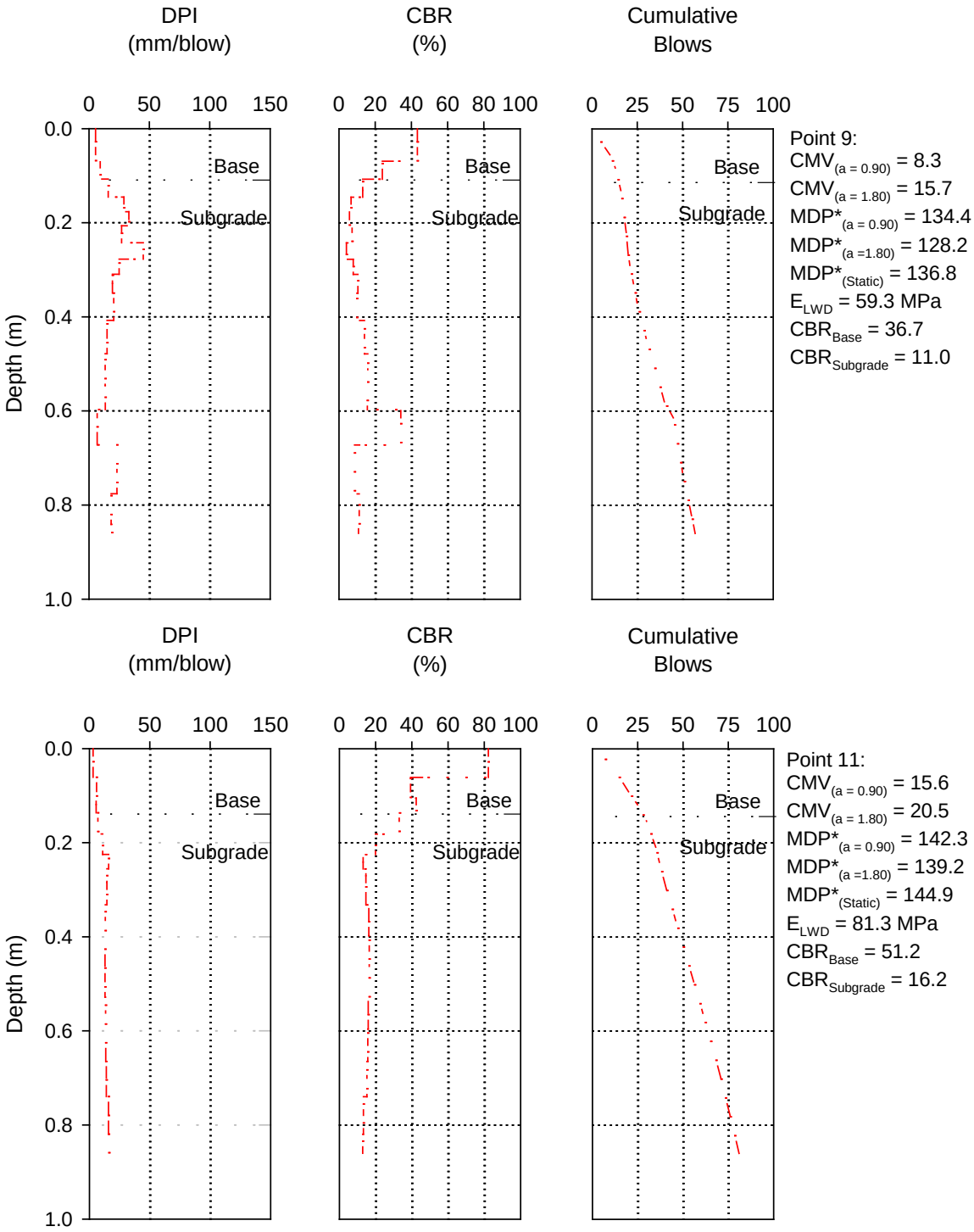


**Figure 87. DPI, CBR, and cumulative blow profiles at points 9 and 11 (CMV, MDP*, $E_{LWD}$ test measurements, and calculated $CBR_{Base}$ and $CBR_{Subgrade}$ are shown in the figure) – TB3**

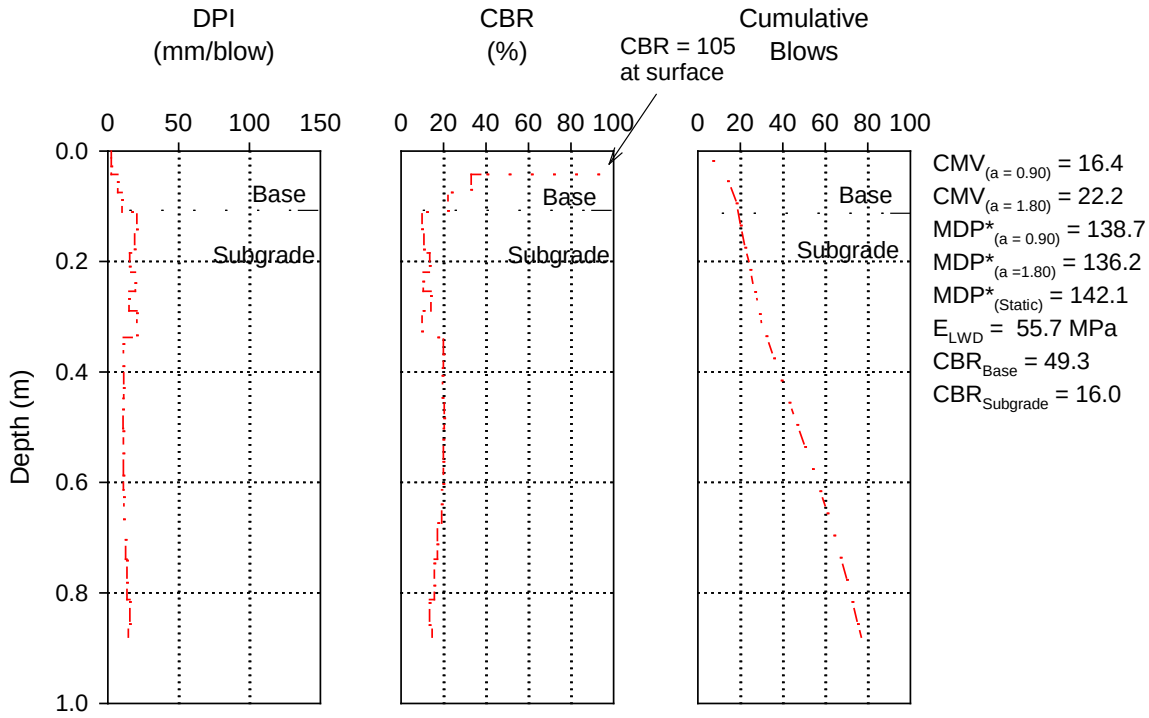


**Figure 88. DPI, CBR, and cumulative blow profiles at point 12 (CMV, MDP*, $E_{LWD}$ test measurements, and calculated $CBR_{Base}$ and $CBR_{Subgrade}$ are shown in the figure) – TB3**

## 5.5 TB4 – PRODUCTION AREA

This test bed consisted of compacted brown sand embankment subgrade layers in a production area along the mainline roadway alignment (Figure 89). Pull behind scrapers were used for hauling fill material (Figure 90) in this area and compaction occurring under scraper tires and other construction traffic was considered acceptable on this project. Plan dimensions of the test bed were about 12.5 m wide x 65 m long. The area was divided into five roller lanes as shown in Figure 89, and was mapped in only lanes 1, 2, 4, and 5. Lane 3 was left un compacted by the RICM roller to evaluate differences in dry density, CBR, and LWD modulus properties with lanes compacted using the RICM roller. Mapping was conducted using four roller passes with static, a = 0.90 mm, and a = 1.80 mm settings. Details of settings used for each pass are provided in Table 5. Following the final mapping pass, NG, LWD and DCP tests were obtained at 10 test locations in lanes 1, 2, 4, and 5, and two test locations in lane 3. Test locations were selected using the CMV and MDP* color-coded maps in the roller (three to four locations each in low, medium, and high CMV or MDP* value areas).

Figure 89 shows color-coded CMV and MDP* maps, and a pass coverage map of the TB area. Correlations between in situ point measurements (LWD modulus, dry unit weight, and weighted average CBR of the subgrade layer ($CBR_{Subgrade}$) down to the termination depth) and CMV and MDP* RICM measurements are presented in Figure 92. Similar to correlations in TB3 presented earlier, correlations in this TB were also developed by spatially pairing the in situ point measurements and RICM measurements using GPS measurements. DPI, CBR,

and cumulative blow count profiles comparing with RICM, LWD modulus, dry unit weight and moisture content values at 10 test locations from lanes 1, 2, 4, and 5 are shown in Figure 93 to Figure 97. DPI, CBR, and cumulative blow count profiles comparing LWD modulus, dry unit weight and moisture content values at two test locations from lane 3 (un compacted lane) are shown in Figure 98.

Correlations from this TB yielded low $R^2$ values (< 0.3) or with no statistically significant relationship between any of the point measurements and RICM measurements. One possible reason for such poor correlations is narrow range of measurements. For example, CMV in low amplitude mode varied only between 19 and 31 at the test locations. Other factors as discussed above in TB3 such as differences in measurement influence depths and in ground stress states under loading, measurement repeatability errors, spatial pairing errors, and influence of direction of travel, all contribute to scatter in the relationships.

Comparing results obtained from TBs 1, 3, and 4 revealed some interesting differences in average CMV and MDP* measurements, and in situ point measurements (Table 8):

- MDP* measurements were higher in TB3 (RAP base underlain by natural sand) than in TBs 1 and 3 with sand fill. LWD modulus measurements also show a similar trend as MDP* measurements. This indicates that MDP* and LWD measurements show higher values if a thin “stiff” crust exists at the surface.
- CMV measurements were higher in TB4 (production embankment section with sand fill) than in TBs 1 and 3. $CBR_{Subgrade}$ (which is a weighted average of CBR to a depth of about 0.9m below surface) also show a similar trend between the TBs as CMV measurements. This indicates that CMV measurements have a deeper measurement influence depth and is not necessarily affected by a thin “stiff” crust at the surface as MDP* and LWD measurements. The higher CMV measurements and $CBR_{Subgrade}$ in TB4 is likely due compaction caused under construction traffic, while there was virtually no traffic on TB1 and very less traffic on TB3.
- Increasing vibration amplitude from a = 0.90 to 1.80 mm resulted in higher CMV in all TBs. MDP* values were also influenced by the amplitude settings; however, results showed different trends in different TBs. Results from TBs 3 and 4 showed that on average MDP* decreases with increasing vibration amplitude from a = 0 (static) to 1.80 mm, while results from TB1 showed that on average MDP* increases with increasing vibration amplitude.


**Figure 89. Pictures of production area test bed compaction (compaction on the test bed was achieved using contractors' equipment (see next picture); lanes 1, 2, 4, and 5 were mapped using the CS74 roller after compaction and lane 3 was not mapped but tested using DCP, LWD, and NG for comparison between mapped versus unmapped lanes) – TB3**

**Figure 90. Pull behind scrapers used for hauling fill material and also for compaction on site**

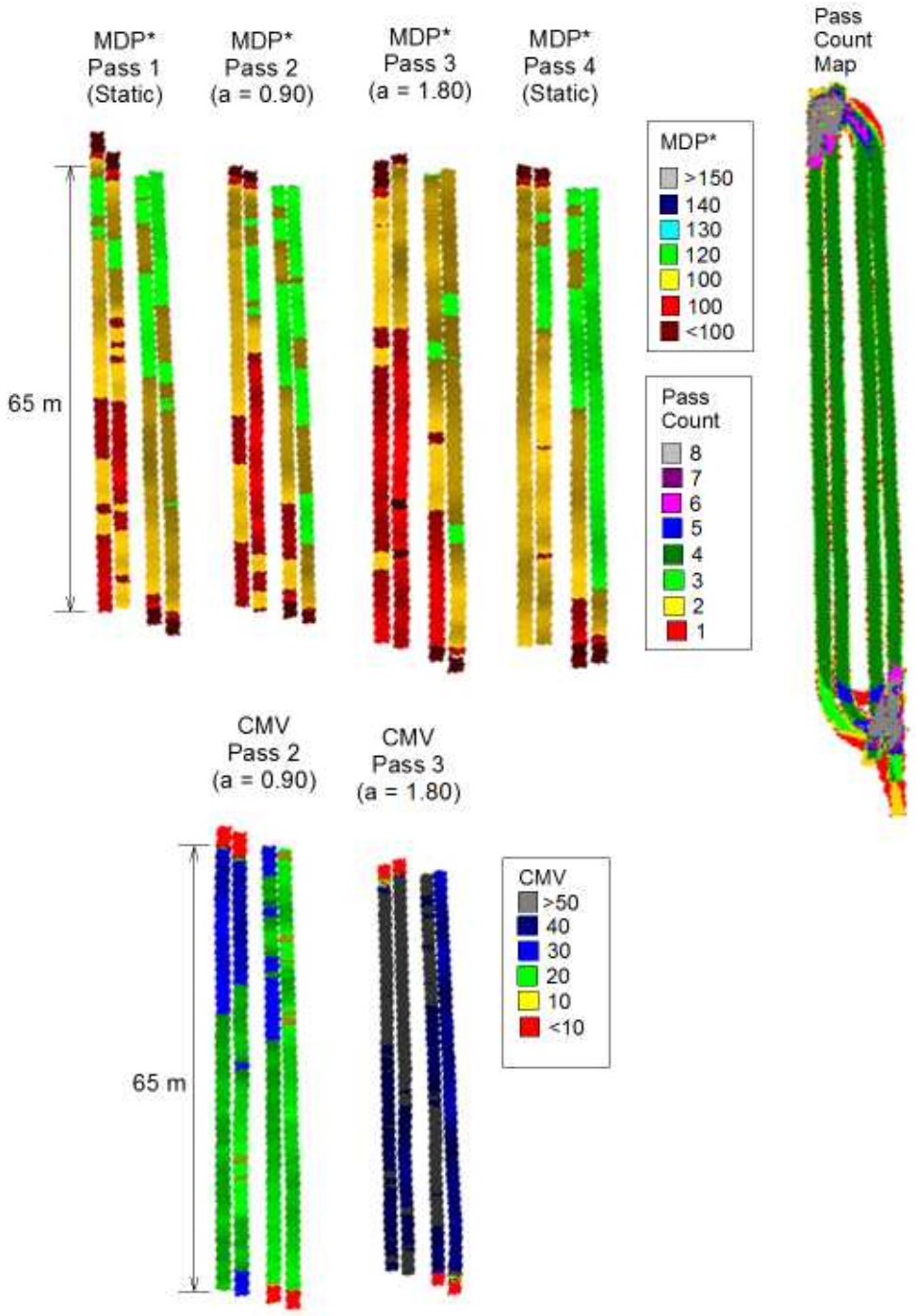


**Figure 91. Roller-integrated CMV, MDP*, and pass count map from mapping passes – TB4**

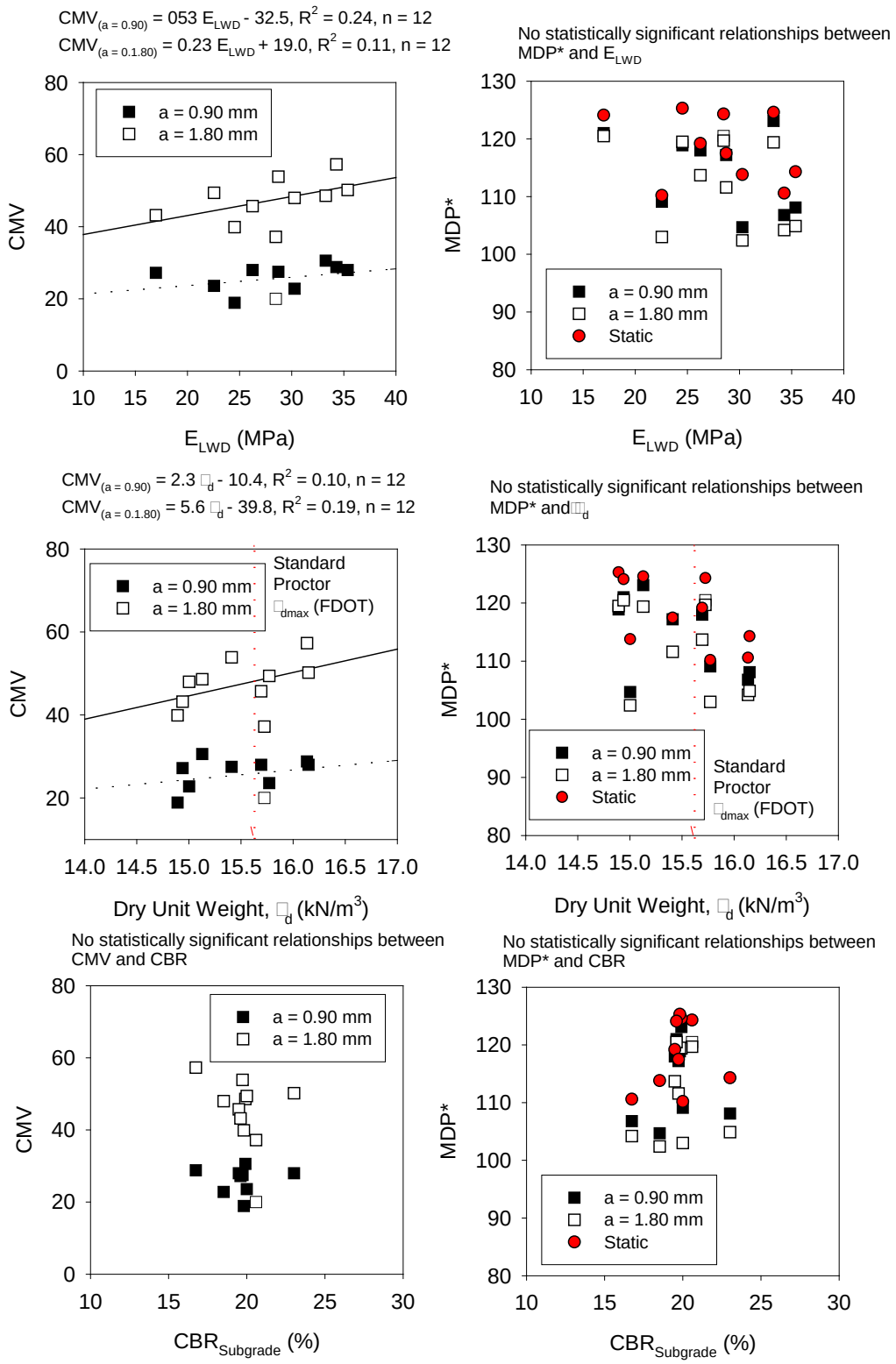


**Figure 92. Correlations between roller-integrated RICM and in situ point measurements – TB4**

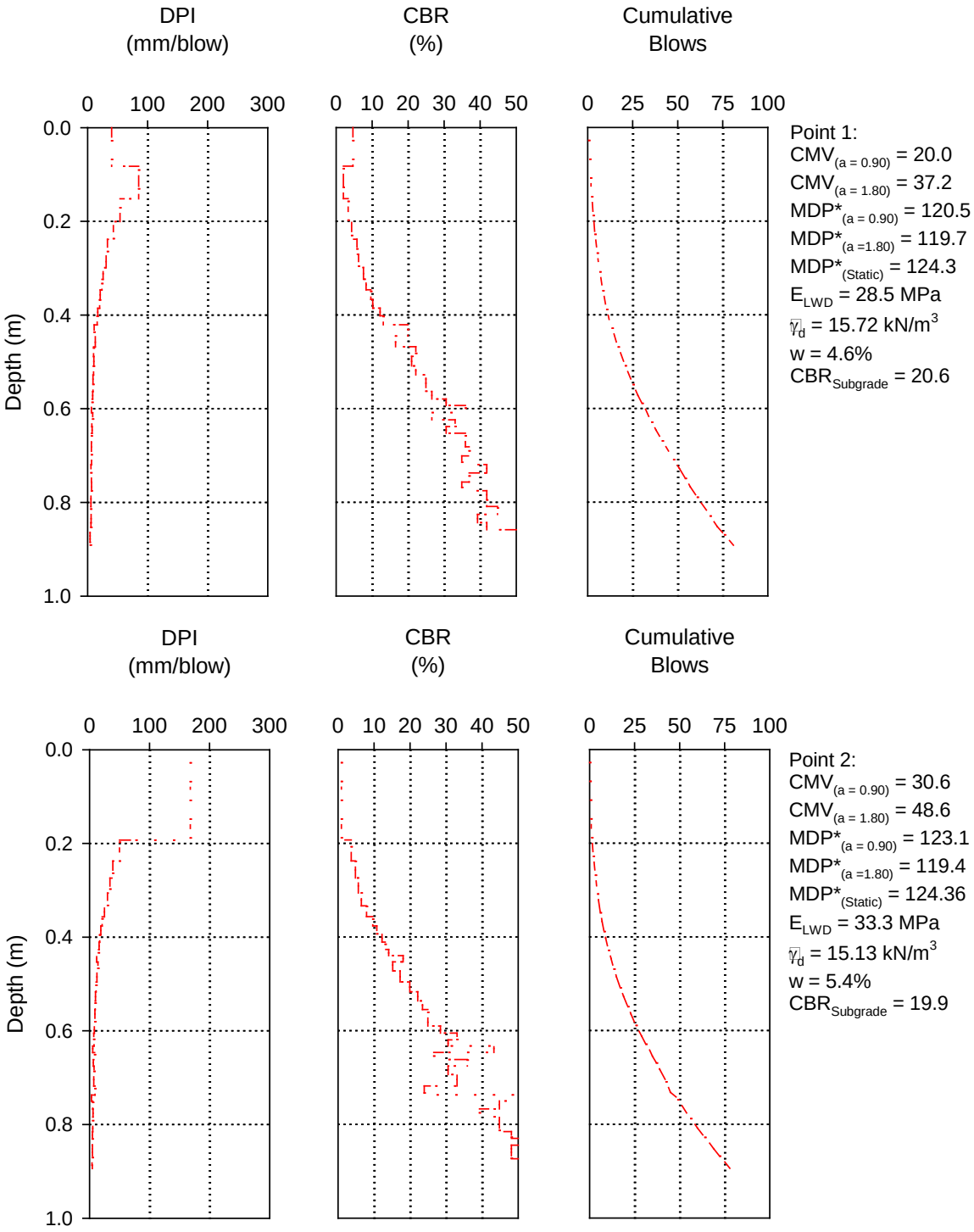


**Figure 93. DCP test locations at points 1 and 2 (CMV, MDP*, $E_{LWD}$, $\gamma_d$, and *w* test measurements at these locations are shown in the figure) – TB3**

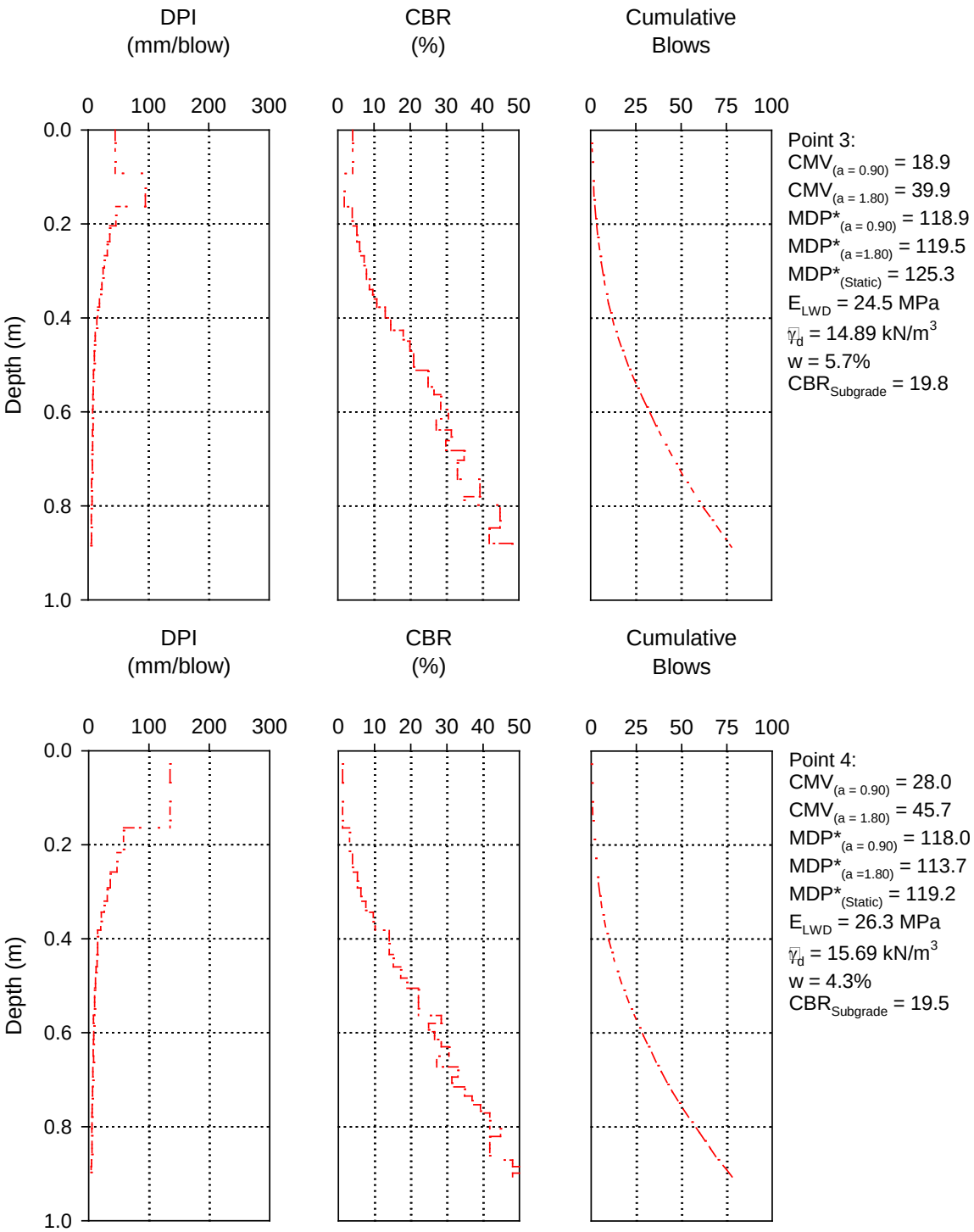


**Figure 94. DCP test locations at points 3 and 4 (CMV, MDP*, $E_{LWD}$, $\gamma_d$, and *w* test measurements at these locations are shown in the figure) – TB3**

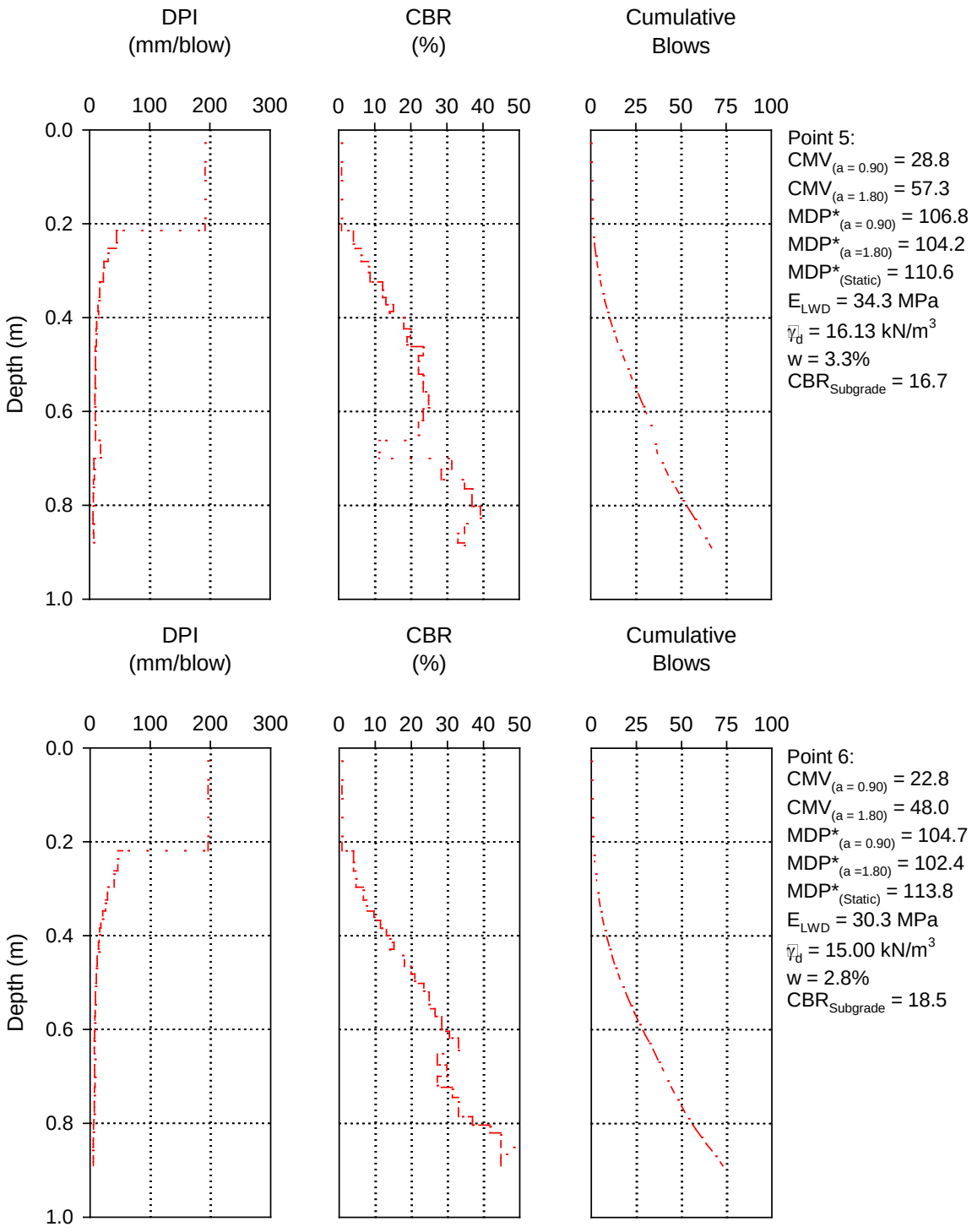


**Figure 95. DCP test locations at points 5 and 6 (CMV, MDP*, $E_{LWD}$, $\gamma_d$, and *w* test measurements at these locations are shown in the figure) – TB3**

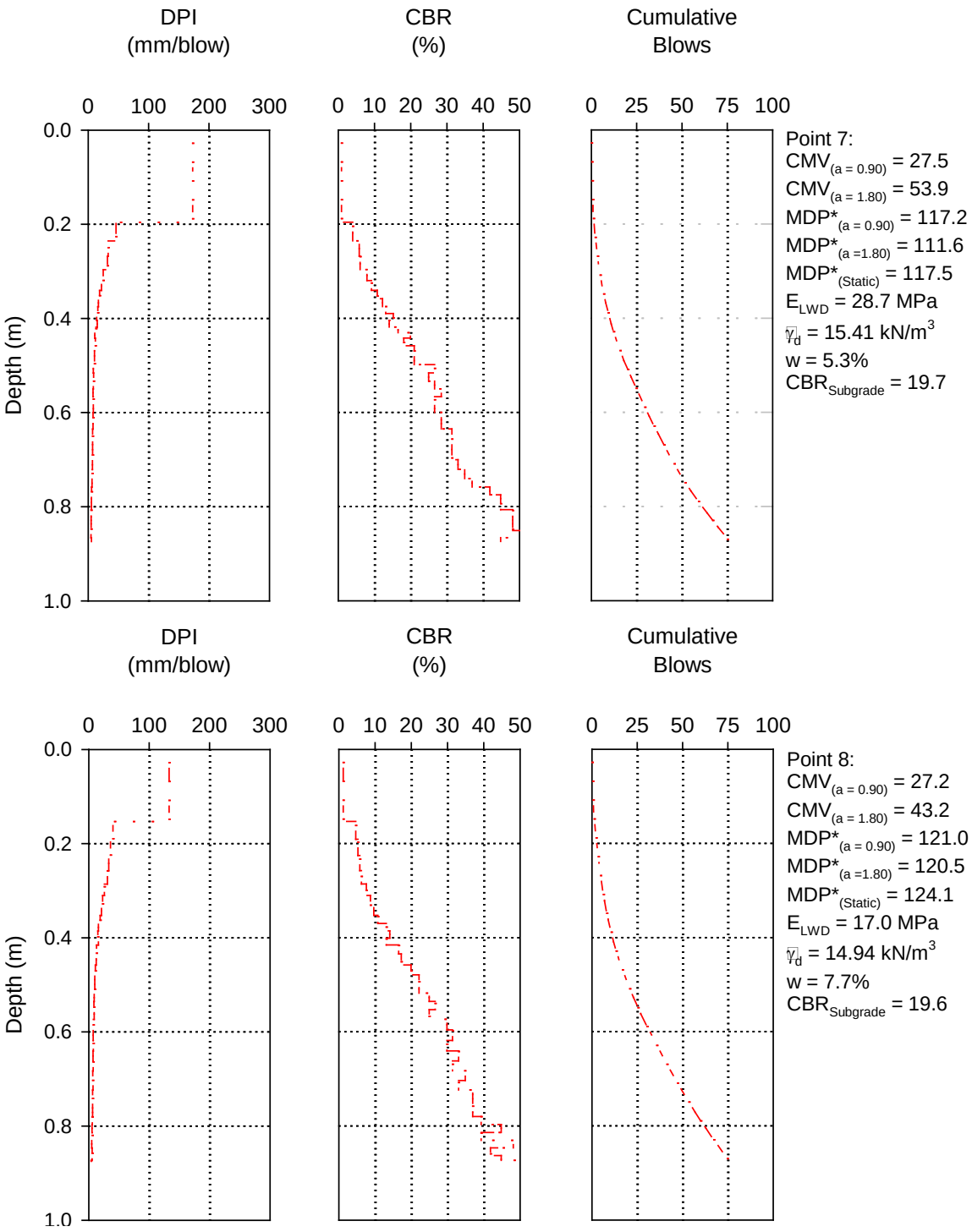


**Figure 96. DCP test locations at points 7 and 8 (CMV, MDP*, $E_{LWD}$, $\gamma_d$, and *w* test measurements at these locations are shown in the figure) – TB3**

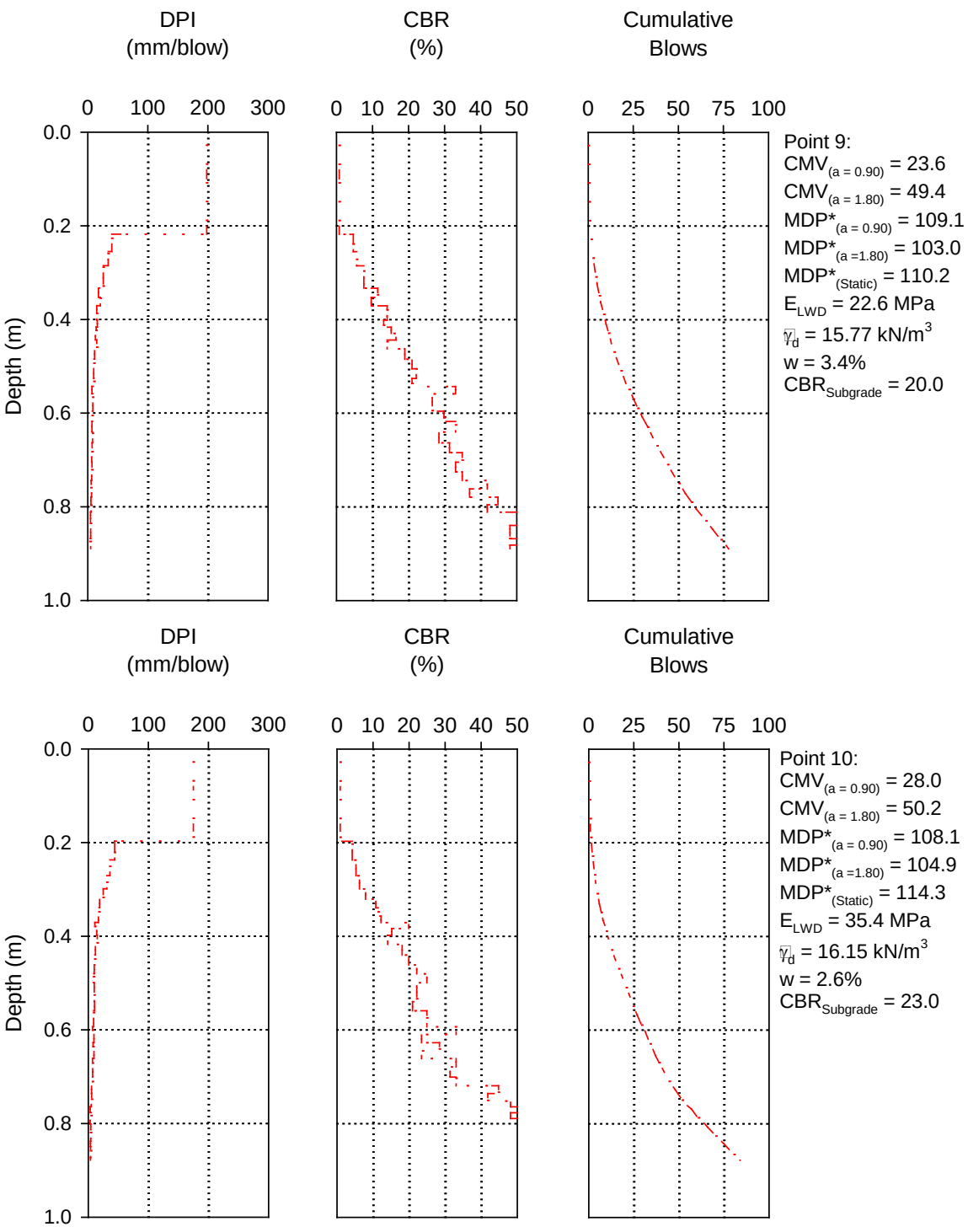


**Figure 97. DCP test locations at points 9 and 10 (CMV, MDP*, $E_{LWD}$, $\gamma_d$, and *w* test measurements at these locations are shown in the figure) – TB3**

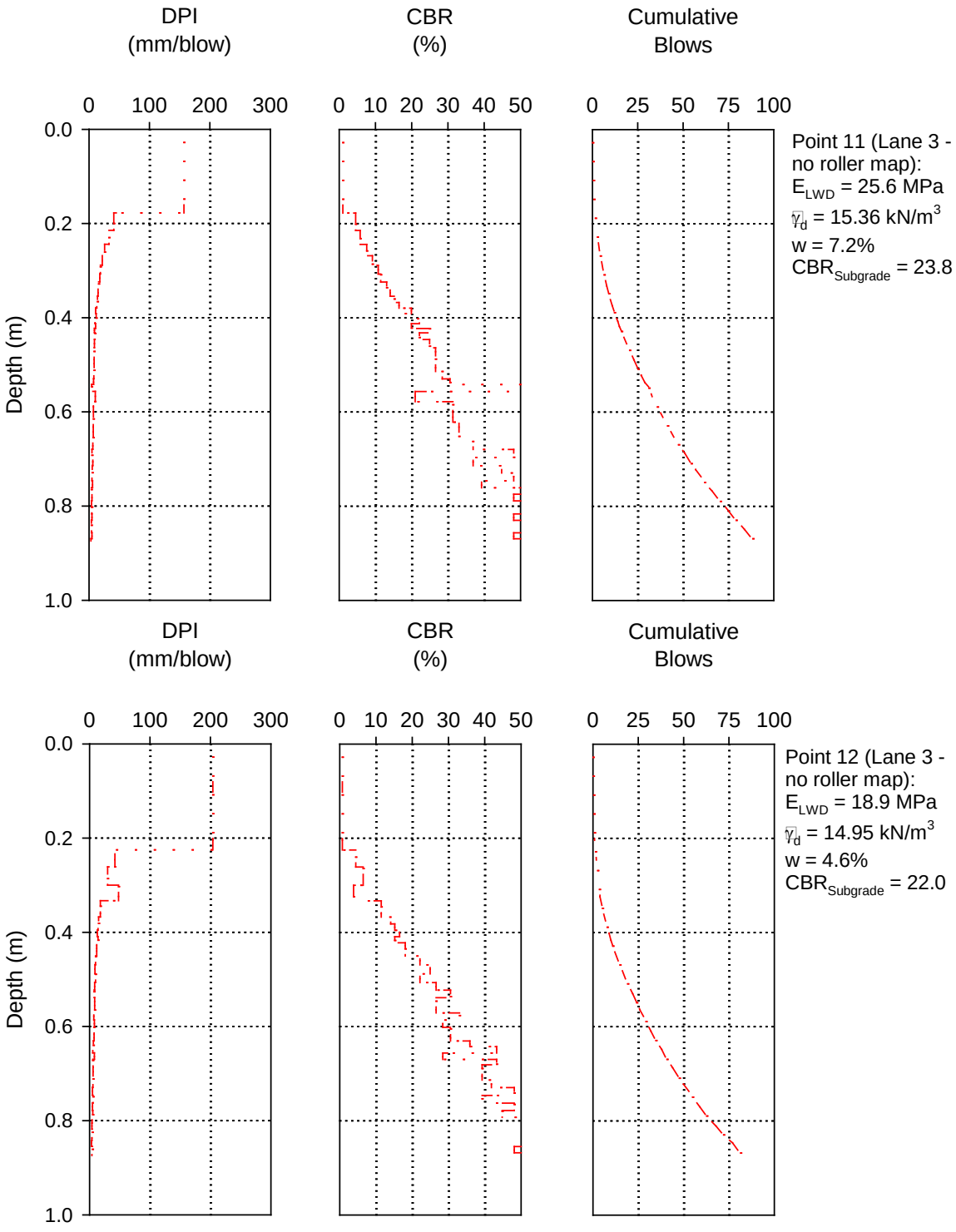


**Figure 98. DCP test locations at points 11 and 12 on lane 3 with no roller mapping passes ($E_{LWD}$, $\gamma_d$, and *w* test measurements at these locations are shown in the figure) – TB3**

**Table 8. Comparison of average RICM and in situ test measurements between TBs 1, 3, and 4**

| Measurement/ Description | TB1 | TB3 | TB4 |
|---|---|---|---|
| Material and Subsurface Conditions | 100 to 200 mm thick sand fill over natural sand subgrade | 30 to 100 mm thick RAP base over natural sand subgrade | Compacted sand embankment fill (production area) |
| MDP* (Static) | 108.9 | 137.6 | 118.4 |
| MDP* (a = 0.90 mm) | 114.1 | 135.7 | 114.7 |
| MDP* (a = 1.80 mm) | 112.7 | 131.9 | 111.9 |
| CMV (a = 0.90 mm) | 16.6 | 13.8 | 25.5 |
| CMV (a = 1.80 mm) | 27.0 | 20.0 | 47.3 |
| $E_{LWD}$ (MPa) at surface | 27.2 | 62.2 | 27.1 |
| $CBR_{Base}$ (%) | No base layer | 43.4 (RAP Base) | No base layer |
| $CBR_{Subgrade}$ (%) | 11.3 | 13.3 | 20.3 |

## 5.6 RICM DEMONSTRATIONS AND GEOTECHNICAL MOBILE LAB OPEN HOUSE

An open house, which included demonstration of the RICM roller, and a tour of the Iowa State University geotechnical mobile lab with several laboratory and in situ testing methods, was conducted on May 18, 2011 as part of this field study. About 25 people attended the open house (Figure 99) including representatives from Florida DOT, National Academy of Sciences, Caterpillar, and the SHRP 2 R02 research team. Photographs from the open house are presented in Figure 100 and Figure 101. Some of the attendees operated the RICM roller and new in situ QC/QA spot testing methods and received hands-on experience.

**Figure 99. Picture of open house attendees in front of ISU Geotechnical Mobile Lab**

**Figure 100. Open house activities on final day of demonstration**

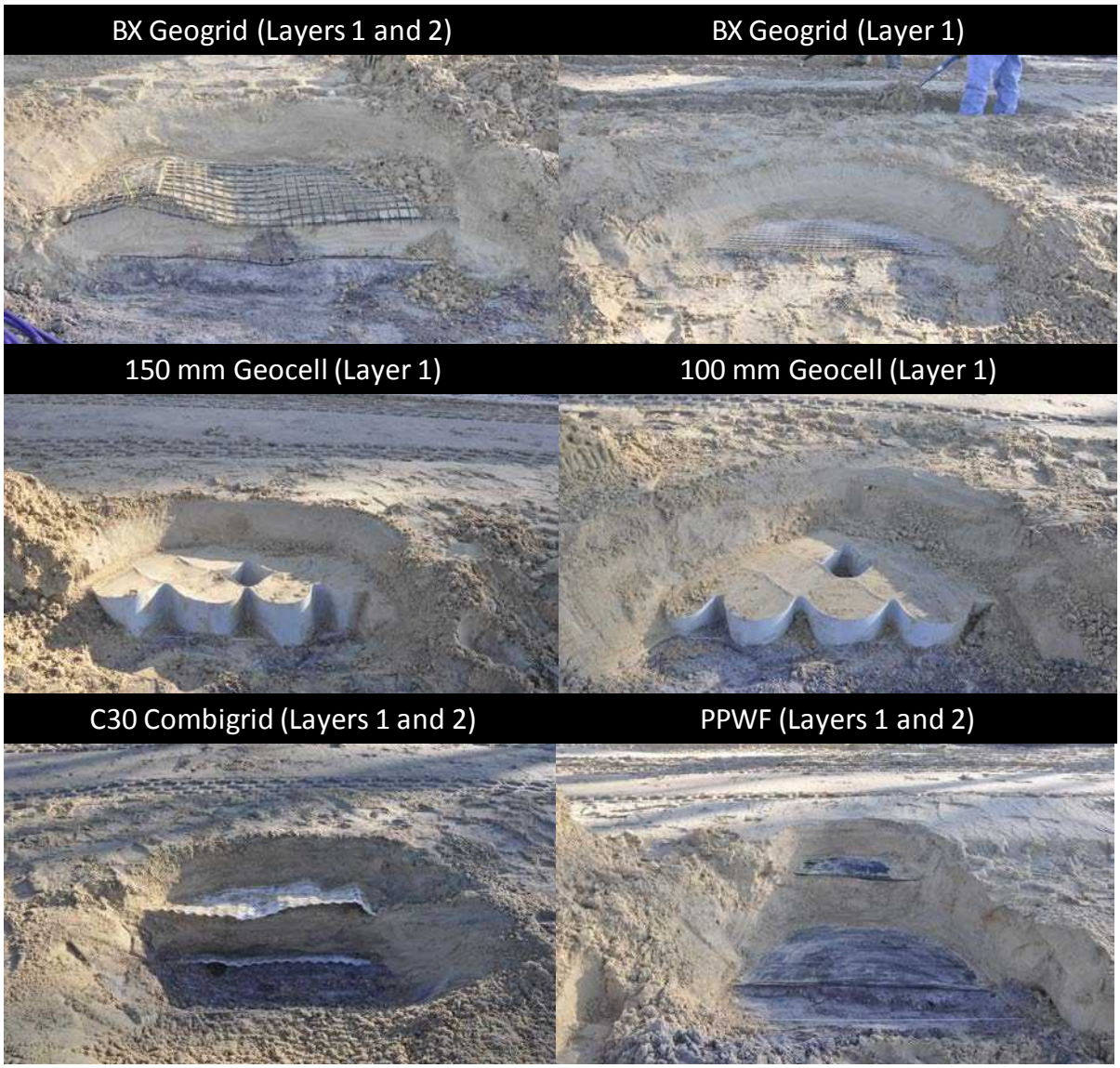


**Figure 101. Pictures of exposed geosynthetics from TB1 displayed for open house**

## CHAPTER 6. SUMMARY OF KEY FINDINGS AND CONCLUSIONS

A summary of key findings and conclusions from this field study are as follows:

- Color-coded display with 100% coverage of compaction area was effective in selecting “soft” and “stiff” areas for spot testing.

- RICM measurements generally were better correlated with LWD and DCP-CBR spot test measurements, than with nuclear gauge density measurements.

- The MDP*-RICM measurements were influenced by the direction of travel. This is because the MDP* measurements represent the mechanical performance of the whole roller, which are affected by the roller-soil interaction at the front drum and the rear tires, and the results are only reported at the center of the drum. The offset distance for MDP* measurements is observed to be about 2.60 m behind the drum center. This is an important aspect to further evaluate because it directly affects how QC/QA test measurements should be obtained to conduct calibration tests and establish target values for acceptance.

- The CMV-RICM measurements were also influenced by the direction of travel. The offsetting occurs because the CMV at a given point indicates an average value over a roller travel length corresponding to a measurement interval of about 0.5 sec.

- TB3 surfaced with RAP over natural sand, and TB4 compacted sand in the road embankment area, revealed some interesting differences in average CMV and MDP* measurements, and in situ point measurements:
    - MDP* measurements were higher in TB3 than in TBs 1 and 3. LWD modulus measurements also showed a similar trend. This indicates that MDP* and LWD measurements show higher values if a thin “stiff” crust exists at the surface.
    - CMV measurements were higher in TB4 than in TBs 1 and 3. $CBR_{Subgrade}$ (which is a weighted average of CBR to a depth of about 0.9m below surface) also show a similar trend between the TBs as CMV measurements. This indicates that CMV measurements have a deeper measurement influence depth and is not necessarily influenced by a thin “stiff” crust at the surface as MDP* and LWD measurements. The higher CMV measurements and $CBR_{Subgrade}$ in TB4 is likely linked to compaction caused under construction traffic, while there was virtually no construction traffic on TB1 and little traffic on TB3.
    - Increasing vibration amplitude from a = 0.90 to 1.80 mm resulted in higher CMV in all TBs. MDP* values were also influenced by the amplitude settings; however, results showed different trends in different TBs. Results from TBs 3 and 4 showed that on average MDP* decreases with increasing vibration amplitude from a = 0 (static) to 1.80 mm, while results from TB1 showed that on average MDP* increases with increasing vibration amplitude.

- Results of in situ spot test measurements and RICM measurements from TB1 constructed with different reinforcements (BX, GC100, GC150, C30, and PPWF) and a control section, revealed the following:
    - MDP* after compaction on layer 1: On average MDP* (a = 0.90 mm) was about 1.07 times higher in the geocell sections compared to the control section. The BX section average MDP*(a = 0.90 mm) was about the same, while the C30 and PPWF sections average MDP* (a = 0.90 mm) were about 0.90 to 0.95 times the control section average MDP* (a = 0.90 mm). Similar trends were observed for MDP* measurements obtained using a = 1.80 mm setting.
    - MDP* after compaction on layer 2 in BX, C30, and PPWF sections (note that BX and PPWF sections were only partially filled with 2 layers): The C30 section average MDP*(a = 0.90 mm) was about the same, while the BX and PPWF sections average MDP* (a = 0.90 mm) were about 0.94 to 0.95 times the control section average MDP* (a = 0.90 mm). Similar trends were observed for MDP* measurements obtained using a = 1.80 mm setting.
    - In contrary to the MDP* measurements, CMV measurements were generally lower in the reinforced sections than in the control section with the exception of measurements in the GC100 section. BX section showed the lowest ratio values compared to all other reinforced sections.
    - On average, the GC100 and GC150 sections resulted in same dry unit weights while the BX, C30, and PPWF sections resulted in slightly lower (about 0.97 to 0.99) dry unit weights than the control section.
    - LWD modulus values in the C30 section were the lowest, while LWD modulus values in the GC150 section were the highest of all test sections. On average, LWD modulus at surface in all reinforced sections (except in C30 section) were about 1.1 to 1.6 times higher than in the control section.
    - LWD modulus values obtained in the excavation were higher (by about 1.2 to 1.4 times) than the measurements obtained at the surface, illustrating the influence of lateral confinement on modulus in sandy soils.
    - Cyclic plate load tests were conducted in GC150, GC100, and BX sections. The test in GC150 section showed the lowest permanent deformation (4.1 mm) and the BX section showed the highest permanent deformation (5.6 mm) at the end of 10 cycles. The test in GC150 section produced the highest modulus (E = 160 MPa) for the $10^{th}$ loading cycle while the test in the GC100 section showed the lowest modulus (E = 125 MPa).
    - CPT and DCP test profiles revealed the compaction influence depth (i.e., the depth up to which there is some change in soil properties after compaction) varied from about 0.9 m to 1.8 m under the CS74 RICM roller. No obvious differences could be discerned in the CPT/DCP profiles between the test sections.

# CHAPTER 7. RECOMMENDATIONS FOR FUTURE WORK

As indicated earlier in Chapter 1 of this report, this field demonstration project was originally intended to evaluate different compaction methods (rapid impact compaction (RIC), impact roller (IR), and RICM, and traditional). However, due to budget limitations and lack of IR and RIC equipment availability at the time of this project, only RICM technology was used in this demonstration. Brief descriptions of RIC and IR technologies are provided in the following sections of this chapter. Future demonstration projects should focus on developing detailed case history information by comparing the RIC, IR, and RICM technologies in terms of their benefits relating to construction cost, time, efficiency, and effectiveness in consistently obtaining design properties, for different material types (granular and non-granular) and subsurface conditions (i.e., lift thicknesses, stable versus unstable foundation layers). Conventional in situ QC/QA testing methods should be used to document soil density, strength, and stiffness properties and obtain detailed field notes (keeping track of time and cost) to develop comparison information. The information obtained from such demonstration projects will also contribute substantially to Elements I/II applications as compaction is a common element in embankment construction. Information obtained from these demonstration projects will also directly contribute to improving the selection and guidance system developed as part of the SHRP 2 R02 project.

## High Energy Impact Roller (IR) Technology

IR technology has seen slow but increasing use over the past 30 years. The IRs are essentially non-circular (three-sided, four-sided, or five-sided) shaped, tow-behind solid steel molds that typically vary in weight from about 8 to 12 tons. The impact compaction energy is transferred to the soil by means of the lifting and falling motion of the non-circular rotating mass. The type of roller depends on the soil type and moisture regime and depth of treatment needed. Currently, IRs are available from at least three manufacturers (Figure 102). These rollers are pulled at relatively high speeds (typically from about 10 to 12 km/h) to generate a high impact force that reportedly can densify material to depths greater than 1 m, which is significantly deeper than conventional static or vibratory rollers. The range of applications for IRs is broad including:

a) In situ densification of existing fill, collapsible sands, landfill waste, mine haul roads, and bulk earthwork.
b) Thick lift compaction.
c) Existing pavement rubblization to create a new subbase.
d) Construction of water storages and channel banks in the agricultural sector.

One recent development in the IR technology is Landpac's Continuous Impact Response (CIR) system. This system involves instrumenting the IR drum with an accelerometer and continuously monitoring the decelerations (in g's) integrated with a global positioning system (GPS) and presenting the results as a map in real-time to the operator. Figure 103 shows an example CIR deceleration map over a 20 hectare site. Application of real-time compaction monitoring technology to earthwork compaction has obvious advantages and ties in with another SHRP 2 technology, Intelligent Compaction.

**Figure 102. Broons (BH-1300) four-sided ("square") impact roller towed using a four wheel drive heavy tractor (top left, Broons 2009); Landpac 25-kJ three-sided impact roller (top right, www.landpac.com/landpac%20apps%20and%20servs.html) ; IRT's Impactor 2000 "square" impact roller (bottom, www.impactor2000.com/soil.html)**

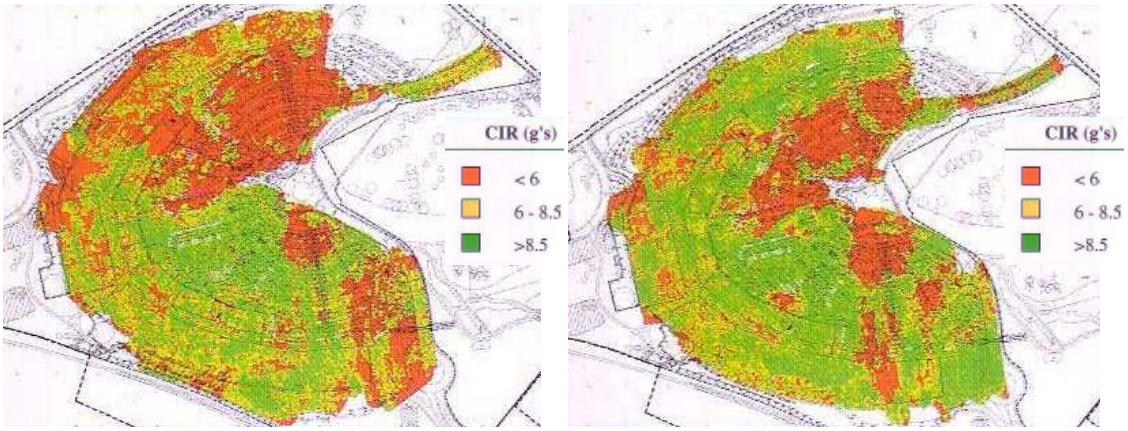


**Figure 103. CIR deceleration data map during the initial IR passes and after 40 IR passes over a 20 hectare site (Landpac 2008)**

### Rapid Impact Compaction (RIC)

RIC is a process that provides controlled impact compaction of the earth using excavator mounted equipment with a 5 to 9 ton (4.5 to 8 ton) weight (7.5 ton/7ton common) which is dropped approximately 1.2 m (4 ft) on to a 1.5 m (5 ft) diameter tamper capable of imparting

40 to 60 blows per minute. The resulting force can densify soils to depths on the order of 3 to 6 m (10 to 20+ ft). The depth of compaction is dependent on the soil properties, groundwater conditions, and compaction energy. Evidence suggests that the higher the energy input, the greater the depth of compaction for some soils. The initial blows in RIC create a dense plug of soil immediately beneath the tamper. Further blows advance the compaction zone. Picture of a typical RIC unit is shown in Figure 104. RIC can be considered an alternative to deep dynamic compaction. Approximately 800 to 2500 $m^2$ (9,000 to 30,000 $ft^2$) can be covered in an average single-shift day (SAICE 2006). Typically, the RIC method is used for the treatment of granular fills in order to improve their geotechnical properties (stiffness and bearing capacity) and to reduce settlement. RIC has been commonly used in sands, silty sands, sandy silts, and miscellaneous fills (personal communication, Cowell 2008). RIC has also been used in collapsible loess soils, ash fill, waste fill, and building waste. The technique is generally not effective in low permeability saturated soils. RIC allows identification of weak zones or "suspect" zones where hard debris fill exists to identify suspect areas that need more treatment (more tamps and/or localized over excavation followed by RIC).

RIC delivers compaction energy to the ground in a relatively controlled manner (e.g., multiple blows with less energy per blow) which allows it to be used closer to existing structures. Peak particle velocities of 50 mm/s (2.0 in/s) at a distance of 9.1 m (30 ft) have been reported (personal communication, O'Malley 2010). Peak noise levels are on the order of 88 dBA (SAICE 2006). In the urban environment, the RIC technique has a number of specific advantages compared to the conventional drop weight dynamic compaction technique including: (1) equipment is relatively small, (2) treatment can be carried out in closer proximity to existing structures and services vulnerable to vibration damage, (3) generally no danger from flying debris, (4) discrete, relatively small foundation areas can be treated, and (5) energy is more efficiently transferred through the compaction foot which remains in contact with the ground.

Quality control is performed by monitoring the compaction energy and deflection of the soil on each blow. An integrated monitoring system can show when optimal compaction is achieved (when additional blows will yield minimal improvement). Preliminary trials are an important aspect at each site to identify optimum compaction operations. Quality assurance can be accomplished by recording the before and after results to see that the average SPT N-value or CPT cone resistance is achieved for the zone needing improvement. Plate bearing tests for different field trials are also used to evaluate bearing characteristics and some in situ geophysical tests have been suggested to overcome potential shortcomings of other in situ tests. For fine-grained soils, piezometers can be used to monitor magnitude and dissipation of excess pore water pressure.


**Figure 104. A typical RIC unit**

**REFERENCES**


Berg, R.B., Christopher, B.R., and Perkins, S. (2000). Geosynthetic Reinforcement of the Aggregate Base/Subbase Courses of Pavement Structures, prepared for American Association of Highway and Transportation Officials Committee 4E, Prepared by the Geosynthetic Materials Association, 2000, 176 p.

Brandl, H., and Adam, D. (1997). "Sophisticated Continuous Compaction Control of Soils and Granular Materials" *Proc., XIVth Intl. Conf. on Soil Mechanics & Foundation Engineering*, Vol. 1, September, Hamburg, Germany.

Broons (2009). *"Square" impact rollers – Specifications Brochure*, Broons Sales, Hire & Engineering, Woodville, South Australia. http://www.broons.com/impact/broons_impact.pdf. (Date Accessed August 2009).

Cleveland, G.S., Button, J.W. and Lytton, R.L. (2002). Geosynthetics in Flexible and Rigid Pavement Overlay Systems to Reduce Reflection Cracking, FHWA/TX-02/1777-1, performed in cooperation with the Texas Department of Transportation and the U.S. Department of Transportation, Federal Highway Administration, Washington DC.

Floss, R., Gruber, N., and Obermayer, J. (1983). "A dynamical test method for continuous compaction control." *Proc. 8th European Conf. on Soil Mechanics and Foundation Engineering*, Rathmayer, H.G., and Saari, K.H.O., Eds., May, Helsinki, 25-30.

Geodynamik ALFA-030. (undated). *Compactometer, Compaction Meter for Vibratory Rollers*, ALFA-030-051E/0203, Geodynamik AB, Stockholm, Sweden.

Holtz, R.D., Christopher, B.R., and Berg, R.R. (2008). "Geosynthetic design and construction guidelines." Report No. FHWA-NHI-07-092, U.S. Department of Transportation, National Highway Institute, Federal Highway Administration, Washington.

ISSMGE. (2005). *Roller-Integrated continuous compaction control (CCC): Technical Contractual Provisions, Recommendations*, TC3: Geotechnics for Pavements in Transportation Infrastructure. International Society for Soil Mechanics and Geotechnical Engineering.

Landpac (2008). *Brochure on Impact Compaction Technology*, LAND PAC, Nigel, South Africa. <http://www.landpac.co.za/Videos&Other/Landpac%20brochure.pdf> (Date Accessed: June 2009 – page updated October 2008).

Mooney, M.A., Rinehart, R.A., White, D.J., Vennapusa, P., Facas, N., Musimbi, O.M. (2010). *Intelligent soil compaction systems*, NCHRP Report 676, National Cooperative Highway Research Program, Transportation Research Board, Washington, D.C.

Pokharel, S.K. (2010). *Experimental Study on Geocell-Reinforced Bases under Static and Dynamic Loading*. Ph.D. Dissertation, Dept. of Civil, Environmental, and Architectural Engineering, The University of Kansas, Lawrence, KS.

Rinehart, R.V. and Mooney, M.A. (2009). "Measurement Depth of Vibratory Roller-Measured Soil Stiffness." *Géotechnique*, 59(7), 609-619.

Samaras, A., Lamm, R., and Treiterer, J. (1991). "Application of continuous dynamic compaction control for earthworks in railroad construction." *Transportation Research Record No. 1309, Journal of the Transportation Research Board*, National Academy Press, 42-46.

SAICE (2006). "Innovative new ground improvement method uses controlled dynamic compaction." Civil Engineering, 14(5), 3–6

Sandström, Å. (1994). *Numerical simulation of a vibratory roller on cohesionless soil*, Internal Report, Geodynamik, Stockholm, Sweden.

Sandström A.J., and Pettersson, C.B. (2004). "Intelligent systems for QA/QC in soil compaction", *Proc., 83rd Annual Transportation Research Board Meeting*, January 11-14. Washington, D.C.

Thompson, M., and White, D. (2008). "Estimating compaction of cohesive soils from machine drive power." *J.of Geotech. and Geoenviron. Engg*, ASCE, 134(12), 1771-1777.

Vennapusa, P., and White, D.J. (2009). "Comparison of Light Weight Deflectometer Measurements for Pavement Foundation Materials". *Geotechnical Testing Journal*, 32(3), 2009, pp. 239-251.

Vennapusa, P., White, D.J., Gieselman, H. (2009). "Influence of support conditions on roller-integrated machine drive power measurements for granular base." *Intl. Foundation Congress and Equipment Expo (IFCEE) 2009*, 15-19 March, Orlando, Florida.

Vennapusa, P., White, D.J., Morris, M. (2010). "Geostatistical analysis of spatial referenced roller-integrated compaction measurements." *J. Geotech. Geoenviron. Engrg.*, ASCE, ASCE, Vol. 135, No. 6, 813-822.

Vennapusa, P., White, D. J., Siekmeier, J., Embacher, R., (2011). "In situ mechanistic characterizations of granular pavement foundation layers." *Intl. J. of Pavement Engineering*, First published on: 15 April 2011 (iFirst).

White D.J., (2008). *Report of the Workshop on Intelligent Compaction for Soils and HMA*, ER08-01, Earthworks Engineering Research Center, Iowa State University, Ames, Iowa.

White, D., and Thompson, M. (2008). "Relationships between in situ and roller-integrated compaction measurements for granular soils." *J.of Geotech. and Geoenviron. Engrg*, ASCE, 134(12), 1763-1770.

White, D.J., Vennapusa, P. (2009). *Report of the Workshop on Intelligent Technologies for Earthworks*, ER09-02, 2nd Annual Workshop organized by the Iowa DOT and the Earthworks Engineering Research Center at Iowa State University, April 14-16, Sheraton West Des Moines Hotel, West Des Moines, Iowa, USA.

White, D.J., Vennapusa, P. (2010a). *Report of the Webinar Workshop on Intelligent Compaction for Earthworks and HMA*, ER10-02, 3rd Annual Workshop Organized by the Earthworks Engineering Research Center at Iowa State University and the Iowa DOT, March 1-2, Ames, Iowa, USA.

White, D.J. Vennapusa, P. (2010b). *Report of the 1st Workshop for Technology Transfer for Intelligent Compaction Consortium (TTICC)*, Transportation Pooled Fund Study Number TPF-5(233), December 14-15, West Des Moines, Iowa, USA.

White, D.J, Jaselskis, E., Schaefer, V., and Cackler, E. (2005). "Real-time compaction monitoring in cohesive soils from machine response." *Transportation Research Record No. 1936*, National Academy Press, 173-180.

White, D. J., Vennapusa, P., Gieselman, H. (2008). *Investigation of Dual Roller-Integrated MDP/CMV Compaction Monitoring Technologies and Measurement Influence Depth*, Center of Transportation Research and Education, Iowa State University, Ames, Iowa, August.

Zorn, G. (2003). *Operating manual: Light drop-weight tester ZFG2000*, Zorn Stendal, Germany.